Interactions and Hofstadter sub-bands in twisted bilayer graphene

Oskar Vafek

National High Magnetic Field Laboratory

and

Department of Physics, Florida State University, Tallahassee, FL

Outline

- *Introduction to twisted bilayer graphene*
  single particle and many-body effects

- *Effects of finite magnetic field:*
  1. *New approach to the Hofstadter problem regardless of the topology of the band*
  2. *Application to TBG at strong coupling*
  3. *Application to the topological heavy fermions in finite B-field*

**Beyond the minimal continuum model: towards a more accurate description of electronic struc.*

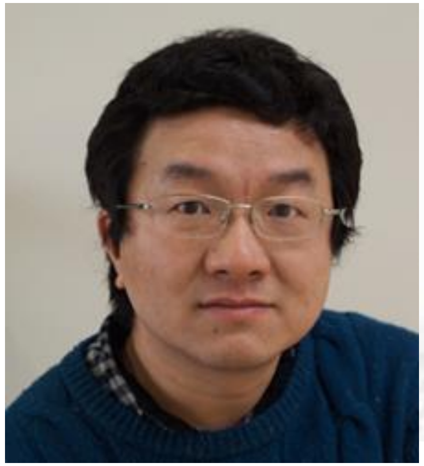

Jian Kang

Xiaoyu Wang

Keshav Singh

Andrei Bernevig

Aaron Chew

Jonah Herzog-Arbeitman

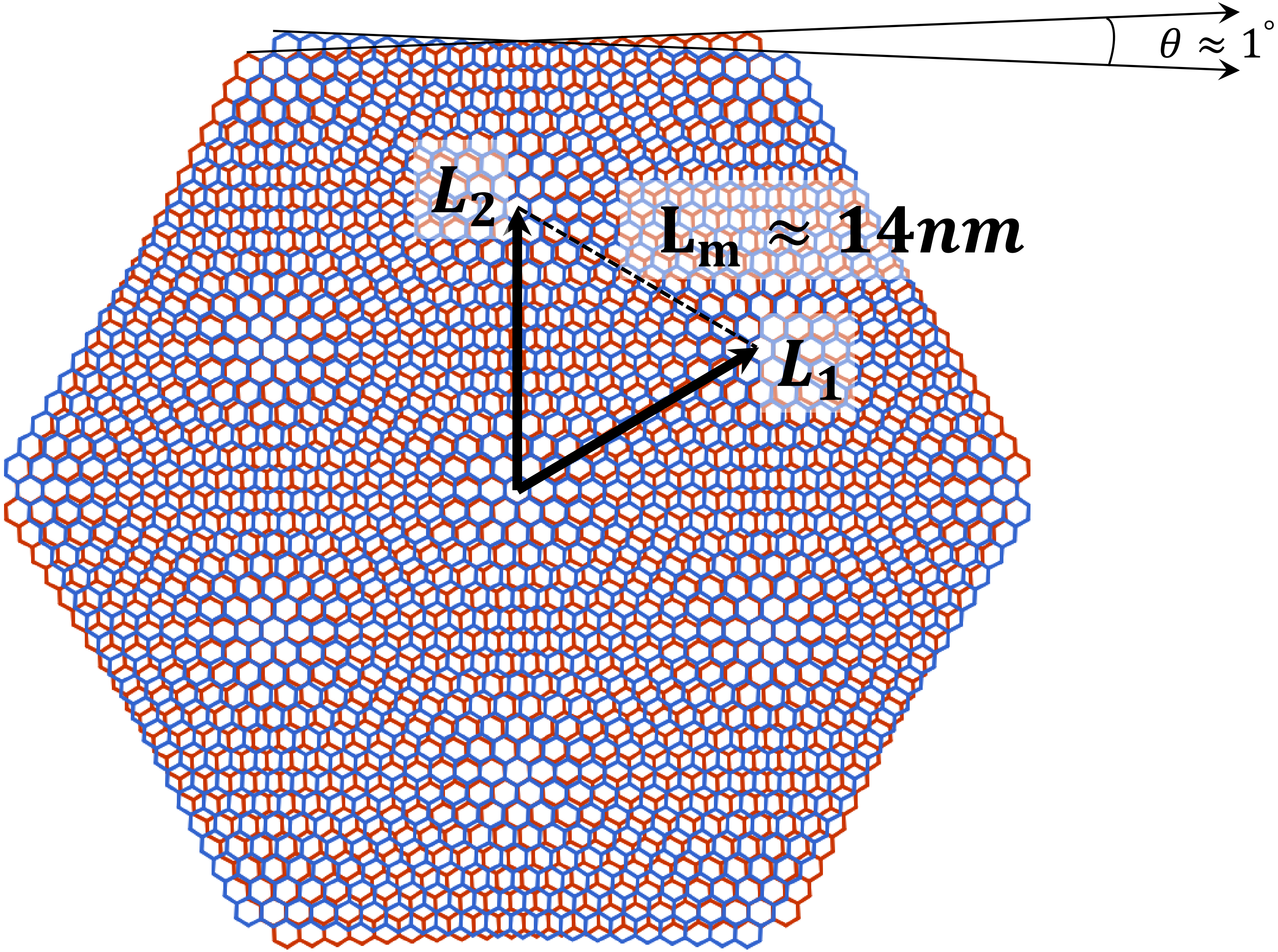

schematic (not to scale)

$$\frac{2w}{v_F\,\delta K}$$

$2w$ ← controlled by pressure

$v_F\,\delta K$ ← controlled by angle

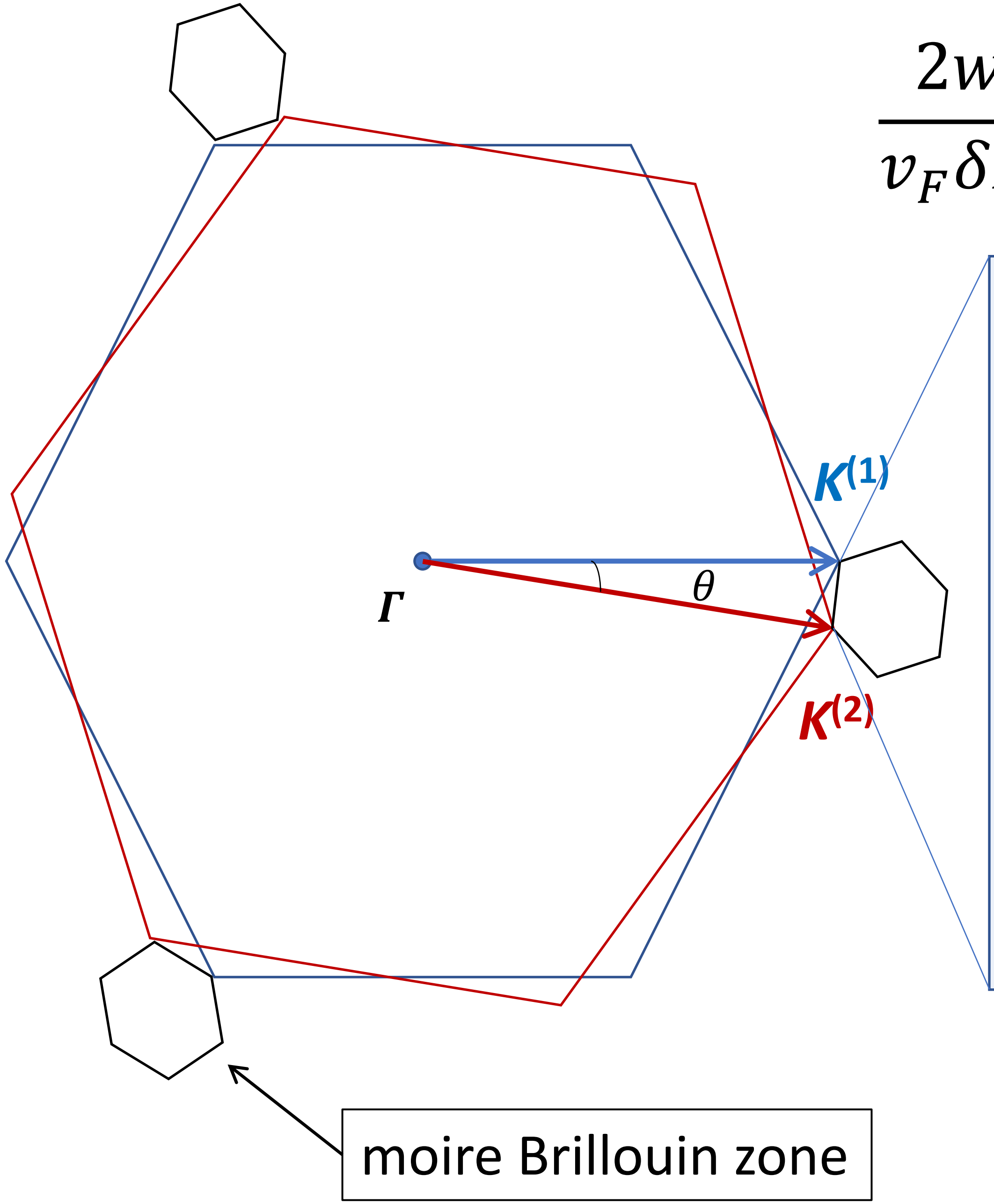

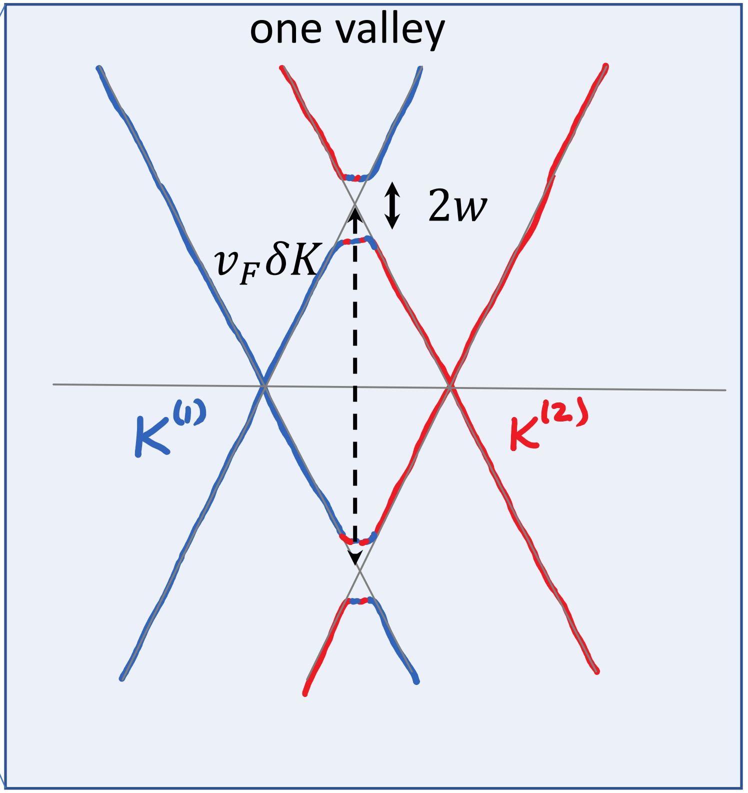

Lopes dos Santos et al PRL (2007)
Li et al Nature Phys (2010)
Shallcross et al PRB (2010)
Mele PRB (2010), (2011)
Bistritzer&MacDonald PNAS (2011)

Minimal continuum model

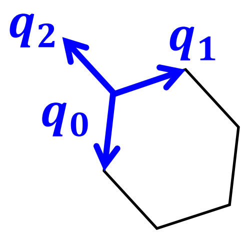

$$H_{BM} = \begin{pmatrix} \hbar v_F \boldsymbol{p} \cdot \sigma_\theta & T(\boldsymbol{r}) \\ T^\dagger(\boldsymbol{r}) & \hbar v_F \boldsymbol{p} \cdot \sigma \end{pmatrix}; \quad \begin{pmatrix} A_{top} \\ B_{top} \\ A_{bot} \\ B_{bot} \end{pmatrix}$$

AA region interlayer tunneling

$$T(\boldsymbol{r}) = \begin{pmatrix} w_0 \sum_{j=0}^{2} e^{-i\boldsymbol{q}_j \cdot \boldsymbol{r}} & w_1\left(e^{-i\boldsymbol{q}_0 \cdot \boldsymbol{r}} + e^{-i\phi} e^{-i\boldsymbol{q}_1 \cdot \boldsymbol{r}} + e^{i\phi} e^{-i\boldsymbol{q}_2 \cdot \boldsymbol{r}}\right) \\ \phi \to -\phi & w_0 \sum_{j=0}^{2} e^{-i\boldsymbol{q}_j \cdot \boldsymbol{r}} \end{pmatrix}$$

$\phi = 2\pi/3$

AB region interlayer tunneling

Lopes dos Santos, Peres and Castro Neto PRL (2007)
Bistritzer and MacDonald PNAS (2011)

Energy

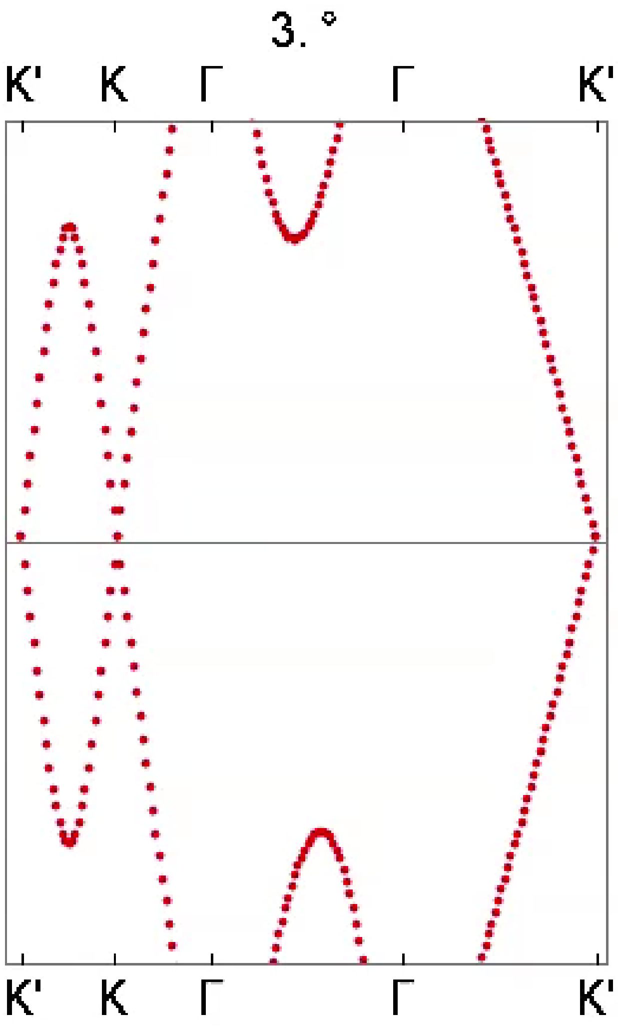

moire Brillouin zone

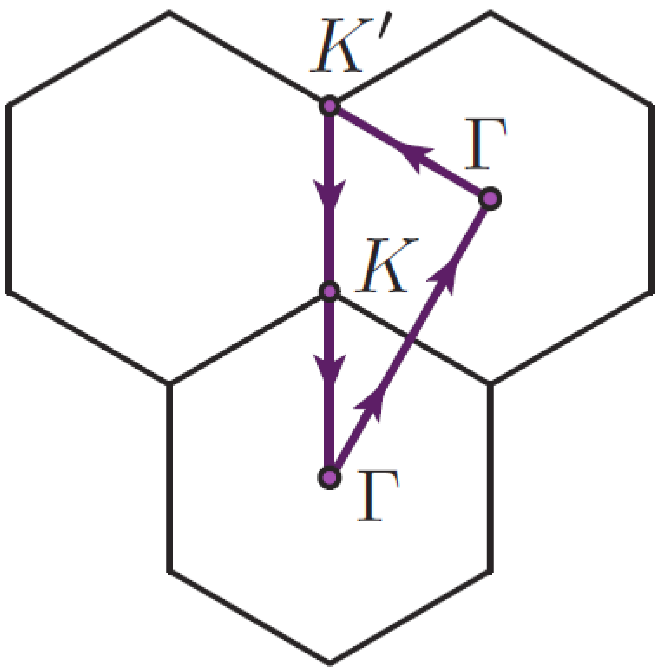

Bistritzer&MacDonald PNAS (2011)

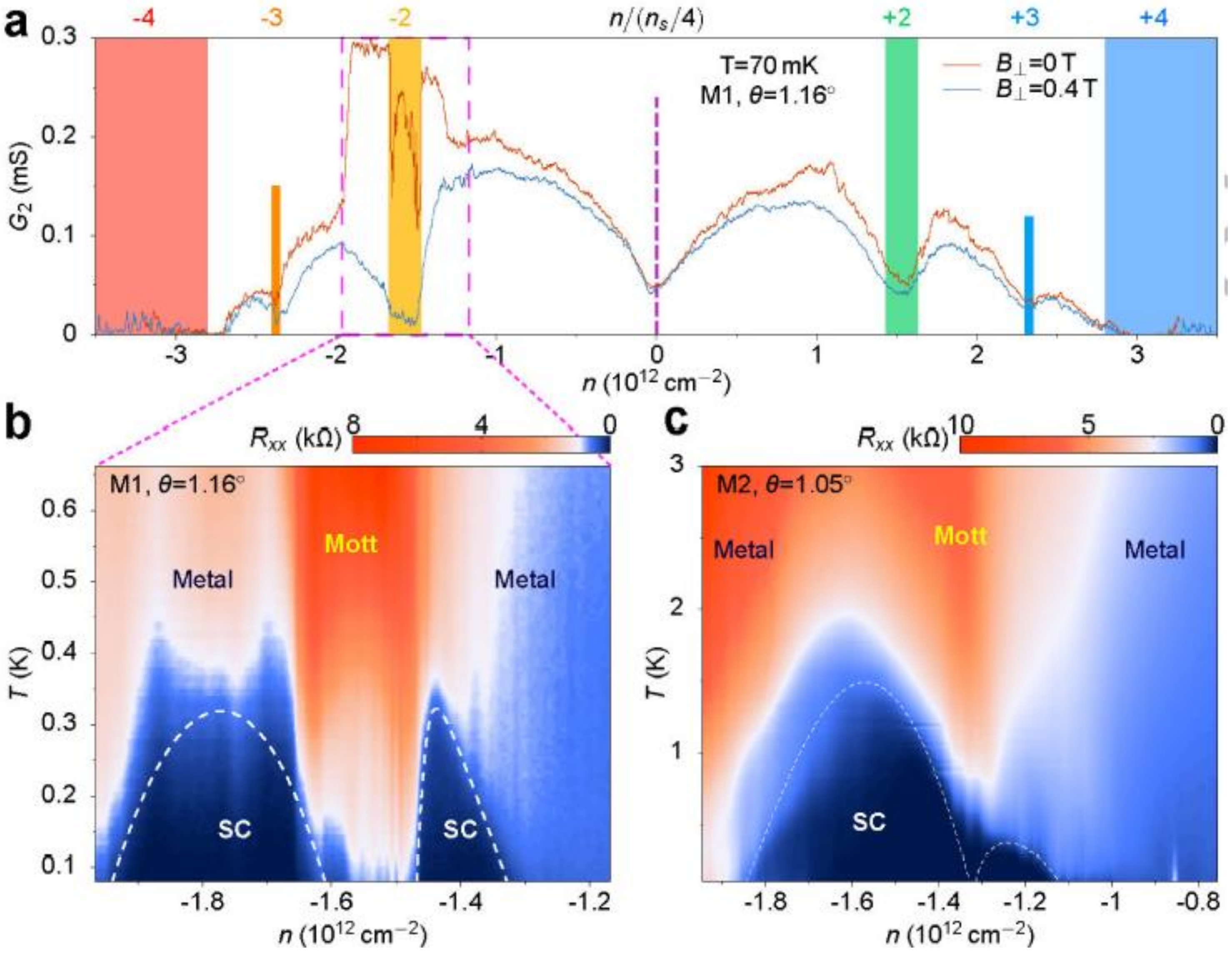

Yuan Cao *et al. Nature* **556**, 80 (2018)
Yuan Cao *et al. Nature* **556**, 43 (2018)

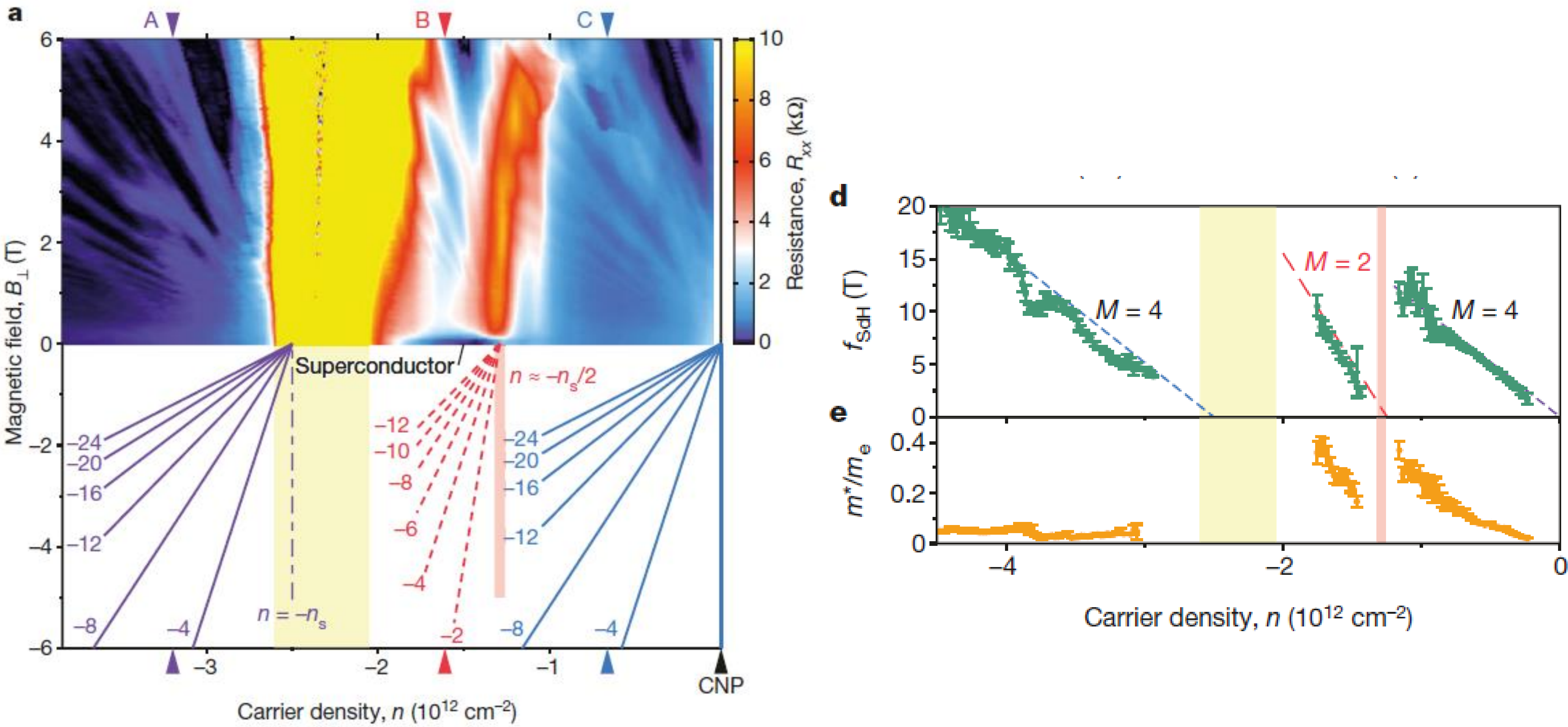

Cao et al, Pablo Jarillo-Herrero Nature 2018

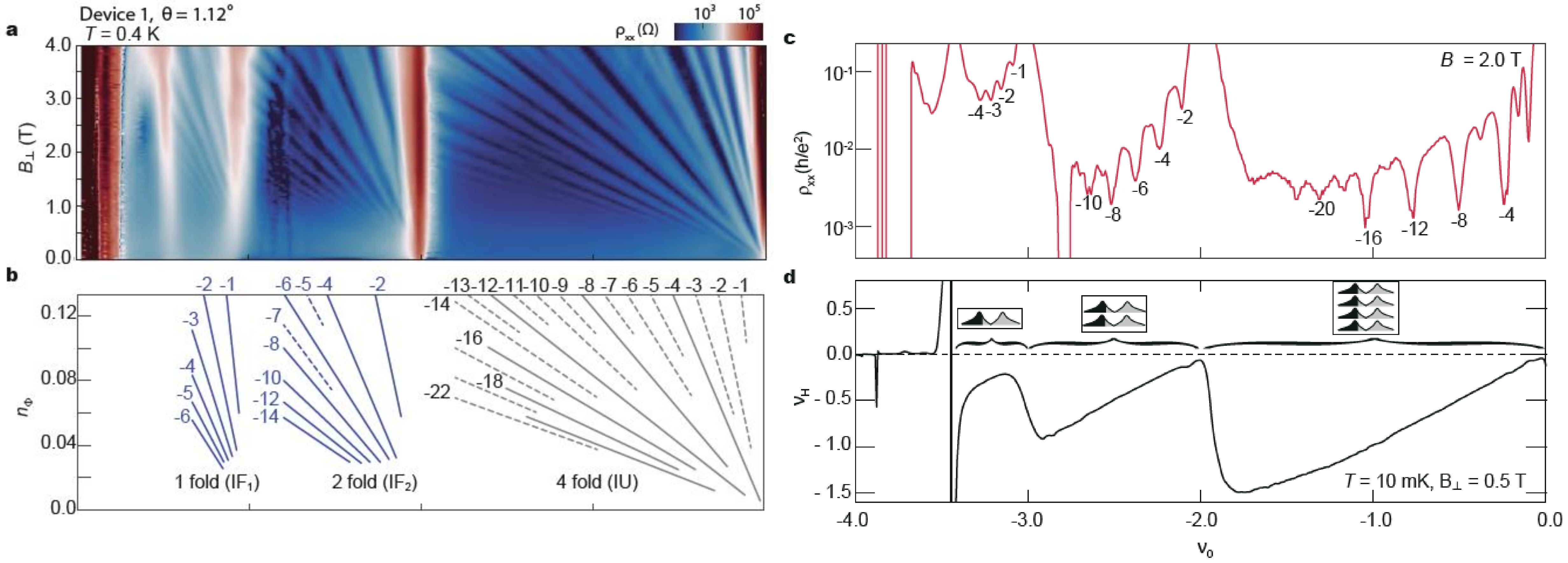

Saito et al, Andrea Young Nature 2021

Band topology and hybrid Wannier states

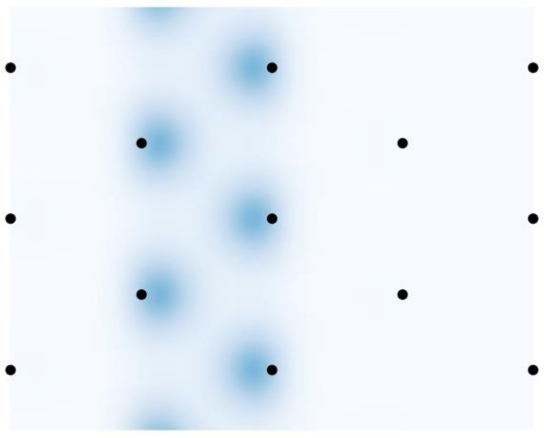

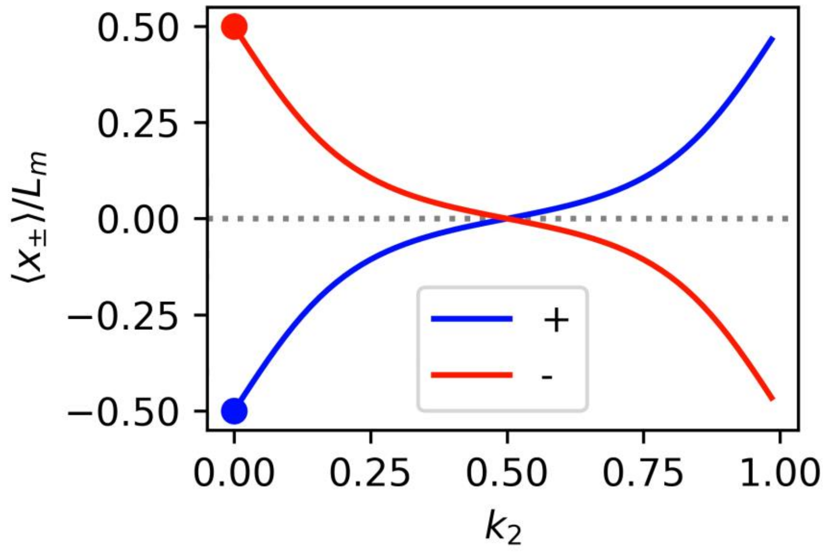

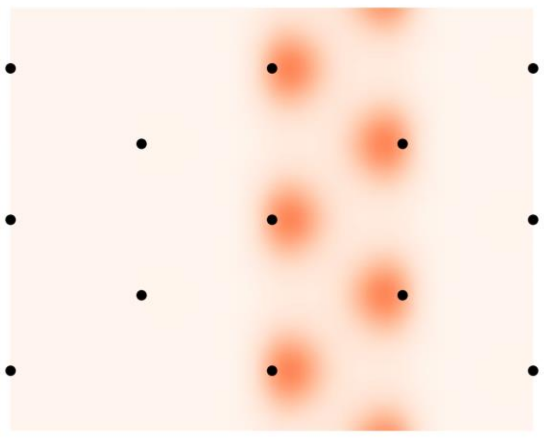

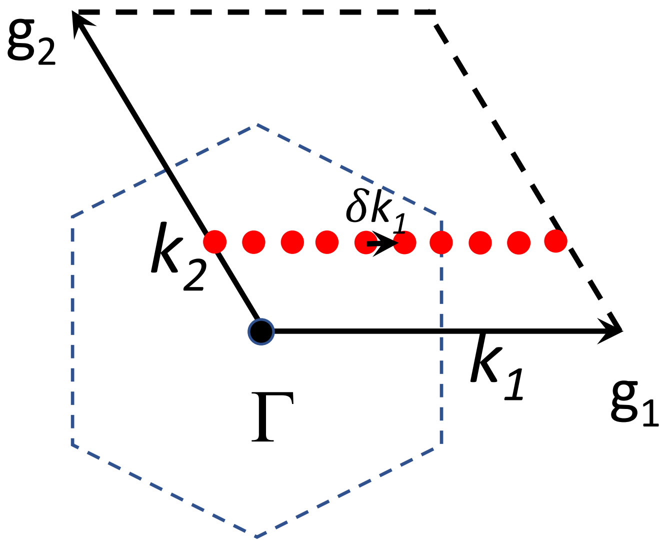

video courtesy Xiaoyu Wang (NHMFL)

Z. Song et al, PRL 123, 036401 (2019); J. Kang and OV PRB 2020

Coulomb interaction is non-perturbative within the narrow bands: strong coupling

(renormalized) $H_{kin} \ll V_{int} = \frac{1}{2}\int d\boldsymbol{r}d\boldsymbol{r}'\, V(\boldsymbol{r}-\boldsymbol{r}')\delta\rho(\boldsymbol{r})\delta\rho(\boldsymbol{r}')$

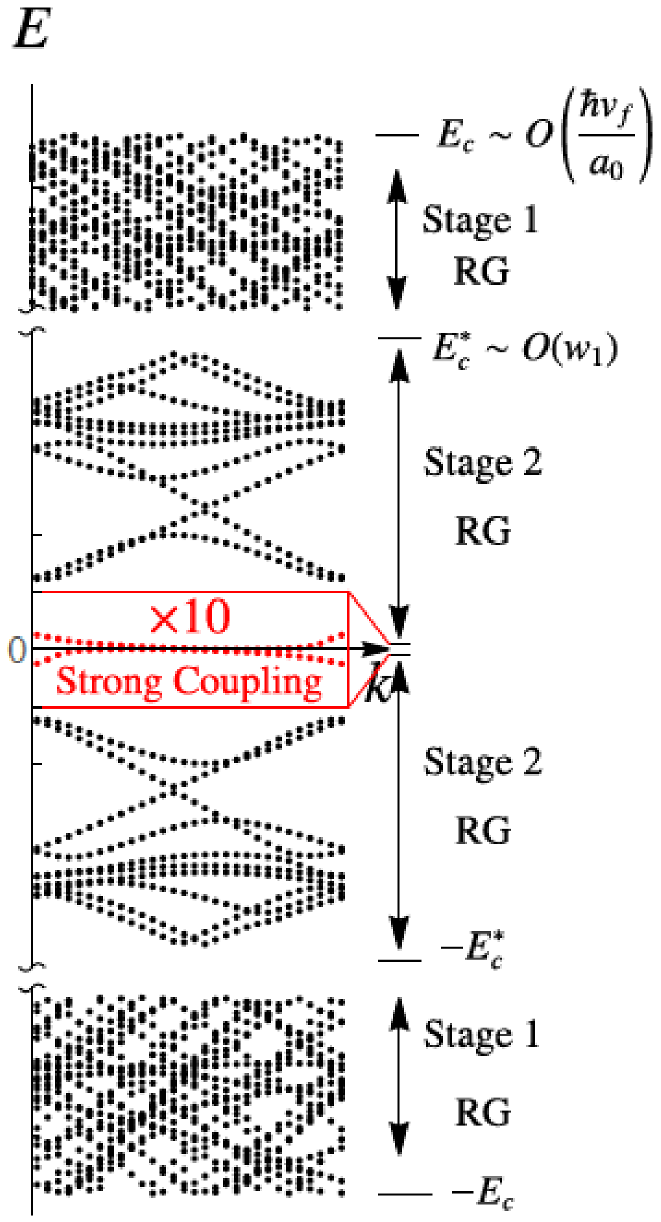

OV and Jian Kang PRL2020

Spin-valley U(4) symmetry in the strong coupling limit

Particle-hole symmetry:
(Z.Song et.al. PRL2019; Hejazi et.al. PRB2019)

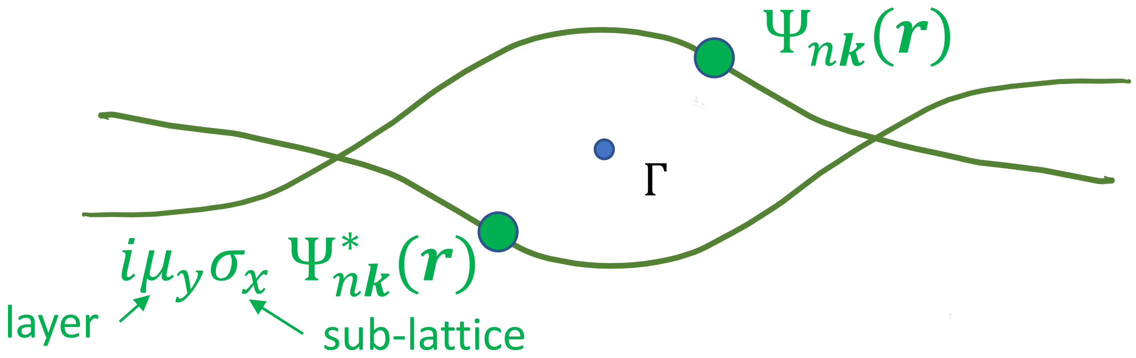

$$\rho(\boldsymbol{r}) = \sum_{\sigma,\boldsymbol{k}\boldsymbol{k}'} \left(d^\dagger_{\sigma,\boldsymbol{K},+,\boldsymbol{k}}\ , d^\dagger_{\sigma,\boldsymbol{K},-,\boldsymbol{k}}\ , d^\dagger_{\sigma,\boldsymbol{K}',+,\boldsymbol{k}}\ , d^\dagger_{\sigma,\boldsymbol{K}',-,\boldsymbol{k}}\right) \begin{pmatrix} A_{\boldsymbol{k}\boldsymbol{k}'}(\boldsymbol{r}) & B_{\boldsymbol{k}\boldsymbol{k}'}(\boldsymbol{r}) & 0 & 0 \\ C_{\boldsymbol{k}\boldsymbol{k}'}(\boldsymbol{r}) & D_{\boldsymbol{k}\boldsymbol{k}'}(\boldsymbol{r}) & 0 & 0 \\ 0 & 0 & D_{\boldsymbol{k}\boldsymbol{k}'}(\boldsymbol{r}) & -C_{\boldsymbol{k}\boldsymbol{k}'}(\boldsymbol{r}) \\ 0 & 0 & -B_{\boldsymbol{k}\boldsymbol{k}'}(\boldsymbol{r}) & A_{\boldsymbol{k}\boldsymbol{k}'}(\boldsymbol{r}) \end{pmatrix} \begin{pmatrix} d_{\sigma,\boldsymbol{K},+,\boldsymbol{k}'} \\ d_{\sigma,\boldsymbol{K},-,\boldsymbol{k}'} \\ d_{\sigma,\boldsymbol{K}',+,\boldsymbol{k}'} \\ d_{\sigma,\boldsymbol{K}',-,\boldsymbol{k}'} \end{pmatrix}$$

commutes with $1,\ \tau_z 1,\ \tau_y\tilde{\sigma}_y,\ \tau_x\tilde{\sigma}_y$

independent spin rotations within each valley

rotations between the valleys!

In the chiral limit B and C vanish and
$U(4) \rightarrow U(4) \times U(4)$

Bultinck et al PRX 2020, Bernevig et al 2020 TBG series
J. Kang and OV, PRL2019 and OV and J.Kang PRL2020

Coulomb interaction is non-perturbative within the narrow bands: strong coupling

(renormalized) $H_{kin} \quad \ll \quad V_{int} = \frac{1}{2}\int d\boldsymbol{r}d\boldsymbol{r}'\, V(\boldsymbol{r}-\boldsymbol{r}')\delta\rho(\boldsymbol{r})\delta\rho(\boldsymbol{r}')$

Charge neutrality point: any many-body state that is annihilated by $\delta\rho(\boldsymbol{r})$ is a ground state

Even integer filling: ground states are many-body eigenstates of $\delta\rho(\boldsymbol{r})$

Odd integer filling: if sublattice is perfectly polarized (i.e. chiral limit) Chern states are ground states

Generalized (gapped) spin-valley ferromagnets are favored by the projected Coulomb interactions

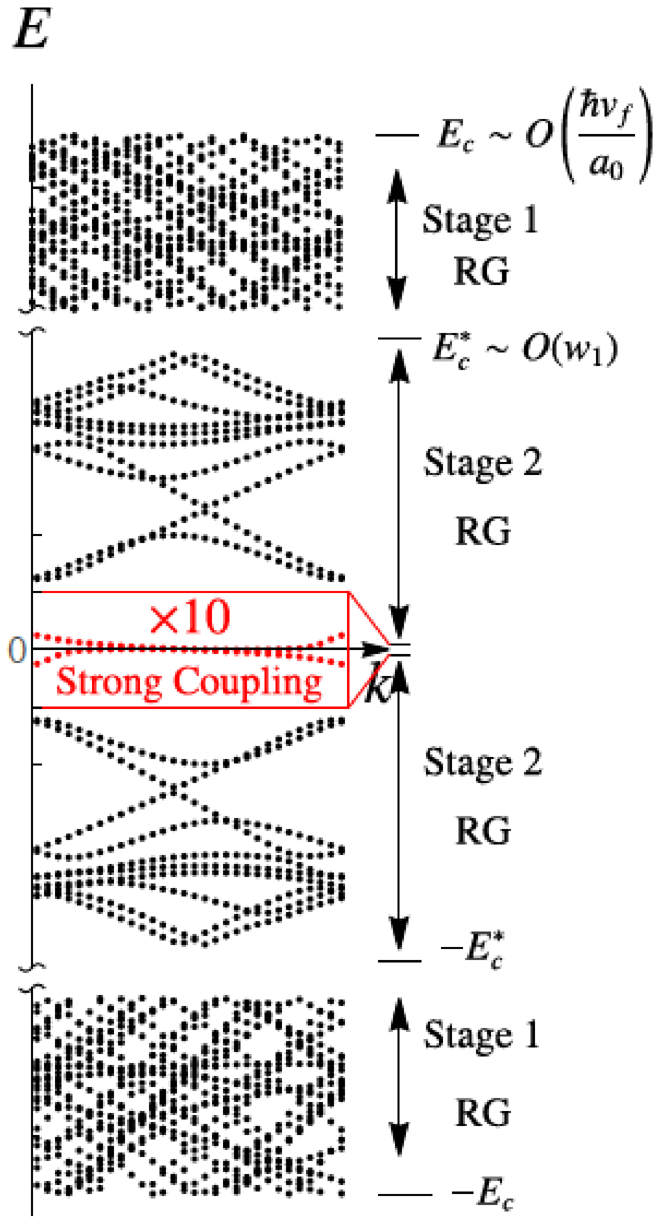

Kang and OV PRL2019; Bultinck et al PRX2020, Bernevig et al 2020TBG series

OV and Jian Kang PRL2020

STM reveals a gap at the charge neutrality point without hBN substrate alignment in the ultra-low strain device regions

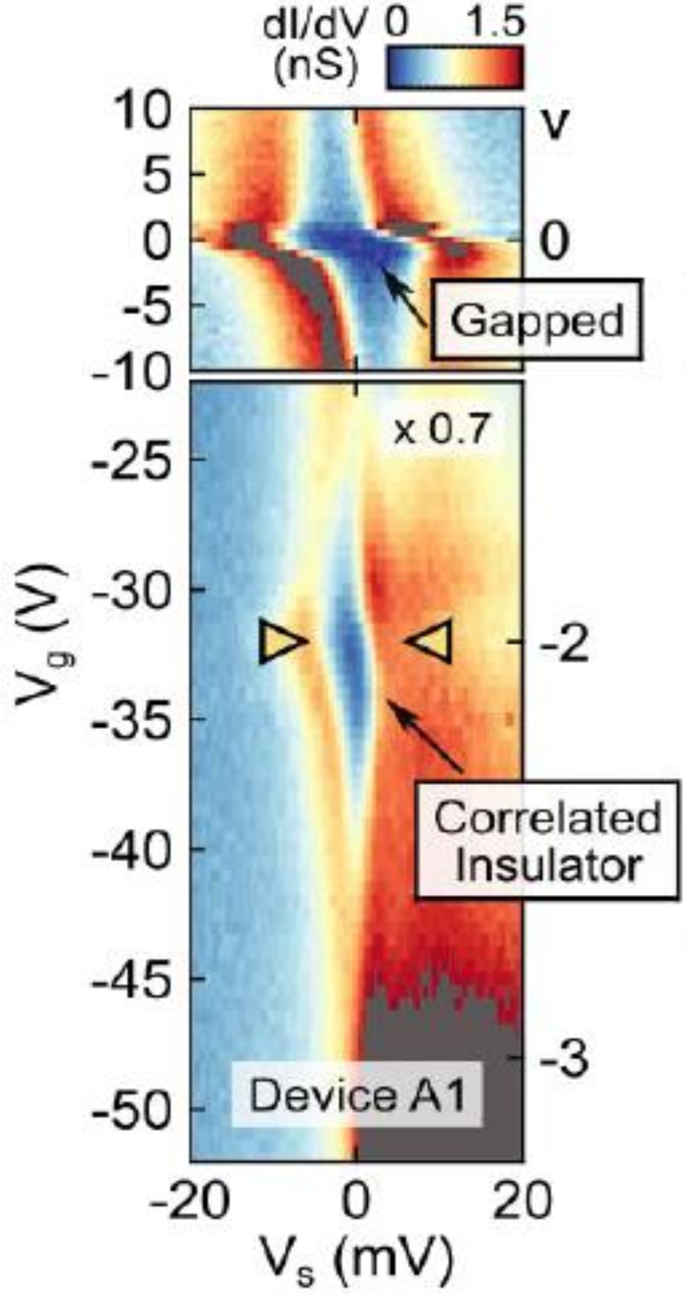

Nuckolls et al, Yazdani 2303.00024

Itineracy at strong coupling

Exact single particle excitation spectrum at CNP in the strong coupling limit

$$EX|\Omega\rangle = \frac{1}{2}\int dr\, dr' V(r-r')\big[\delta\varrho(r), [\delta\varrho(r'), X]\big]|\Omega\rangle$$

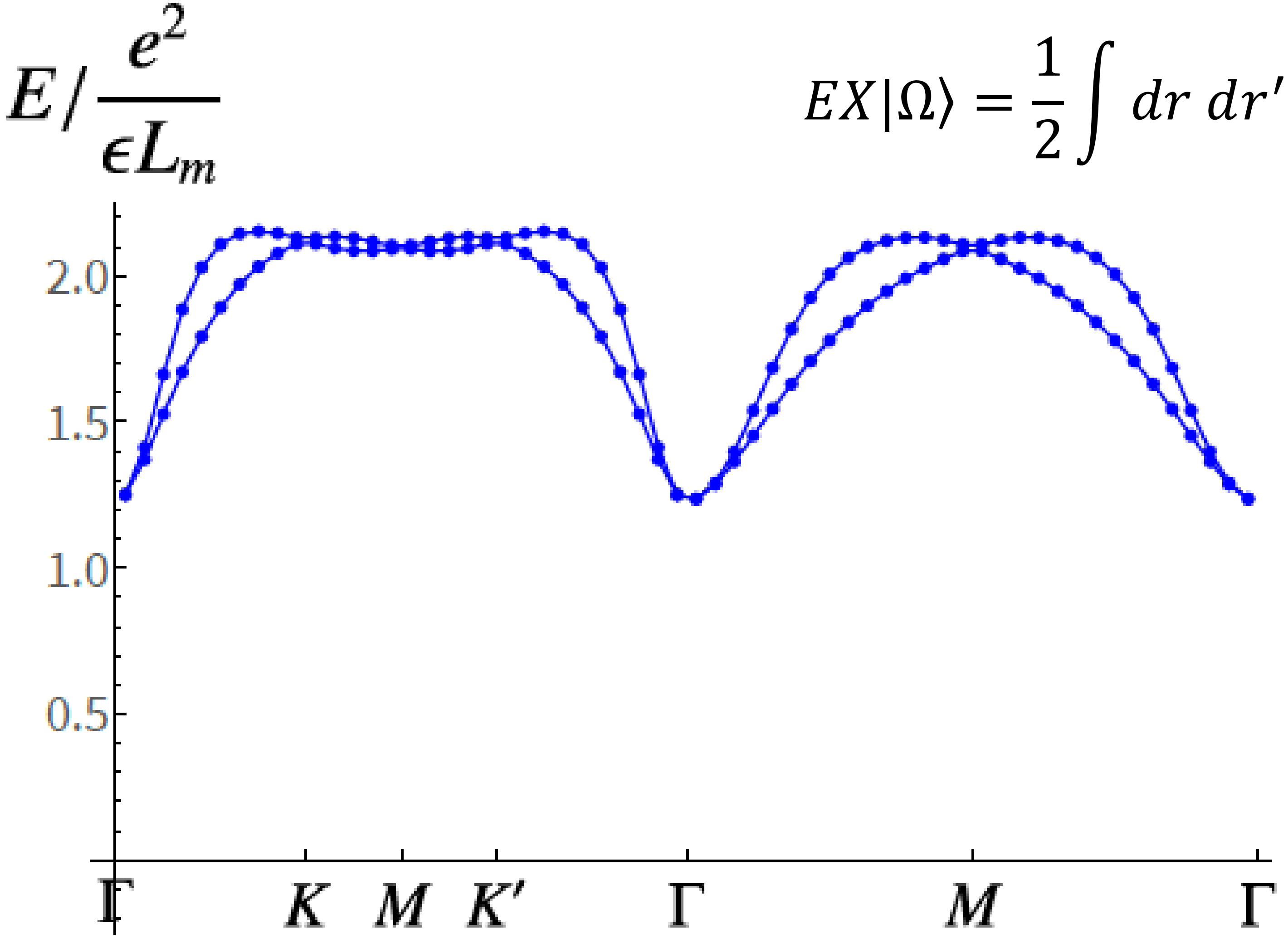

OV and Jian Kang, PRL 2020; Bernevig, Biao Lian, Regnault et al 2020TBG series

Exact single particle excitation spectrum at integer filling in the strong coupling

$$\left(E - E_\upsilon^{(0)}\right) X|\Omega_\upsilon\rangle$$

$$= \frac{1}{2}\int d\boldsymbol{r}\, d\boldsymbol{r}' V(\boldsymbol{r}-\boldsymbol{r}')\big[\delta\varrho(\boldsymbol{r}),[\delta\varrho(\boldsymbol{r}'),X]\big]|\Omega_\upsilon\rangle + \int dr\, dr' V(\boldsymbol{r}-\boldsymbol{r}')[\delta\varrho(\boldsymbol{r}),X\,]\delta\bar{\varrho}_\upsilon(\boldsymbol{r}')|\Omega_\upsilon\rangle$$

$$\mathcal{E}^{(F)}(\boldsymbol{k}) \qquad\qquad \pm\mathcal{E}_\nu^{(H)}(\boldsymbol{k})$$

Exact single particle excitation spectrum at integer filling in the strong coupling: chiral limit ${}^{w_0}/_{w_1} = 0$

$$\mathcal{E}^{hole}(\boldsymbol{k}) = \mathcal{E}^{(F)}(\boldsymbol{k}) - \mathcal{E}_{\nu}^{(H)}(\boldsymbol{k}) \qquad \mathcal{E}^{particle}(\boldsymbol{k}) = \mathcal{E}^{(F)}(\boldsymbol{k}) + \mathcal{E}_{\nu}^{(H)}(\boldsymbol{k})$$

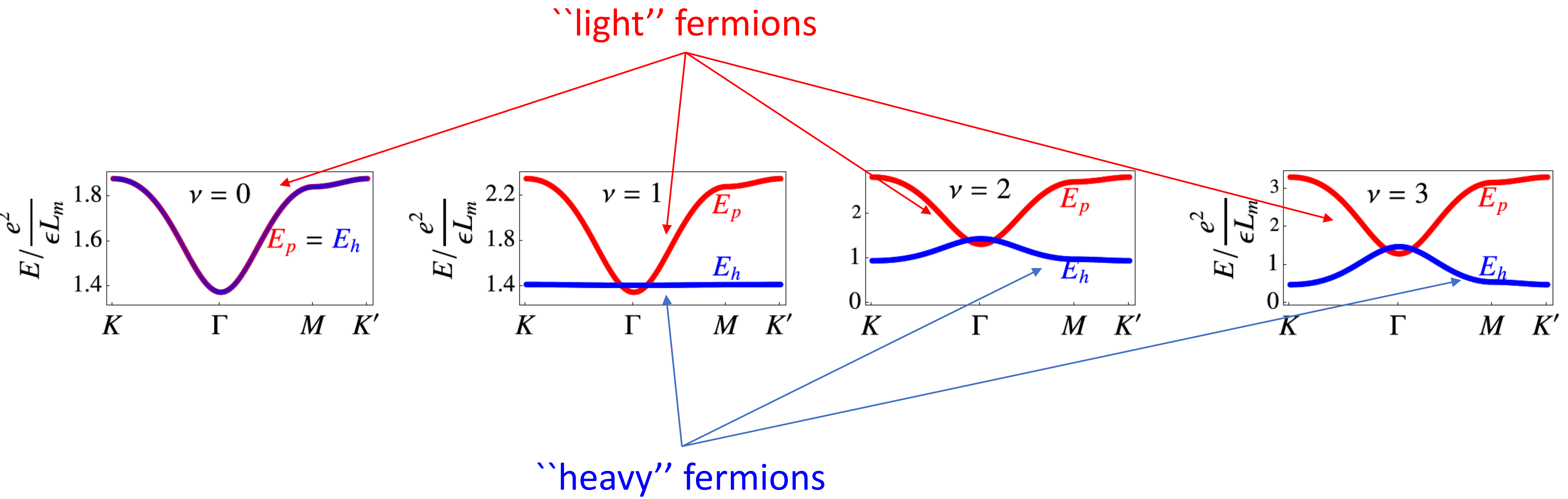

J Kang, BA Bernevig, and OV PRL 127, 266402 (2021), OV and J Kang PRB 104, 075143 (2021)

How do the strong coupling excitations Landau quantize?

(the density operator is charge neutral, therefore it is not immediately clear how the vector potential enters)

(non-interacting) minimal continuum model in magnetic field B

$$H_{BM}(\boldsymbol{p}) \to H_{BM}(\boldsymbol{p} - \frac{e}{c}\boldsymbol{A})$$

existing strategy: minimally substitute and expand in LLs

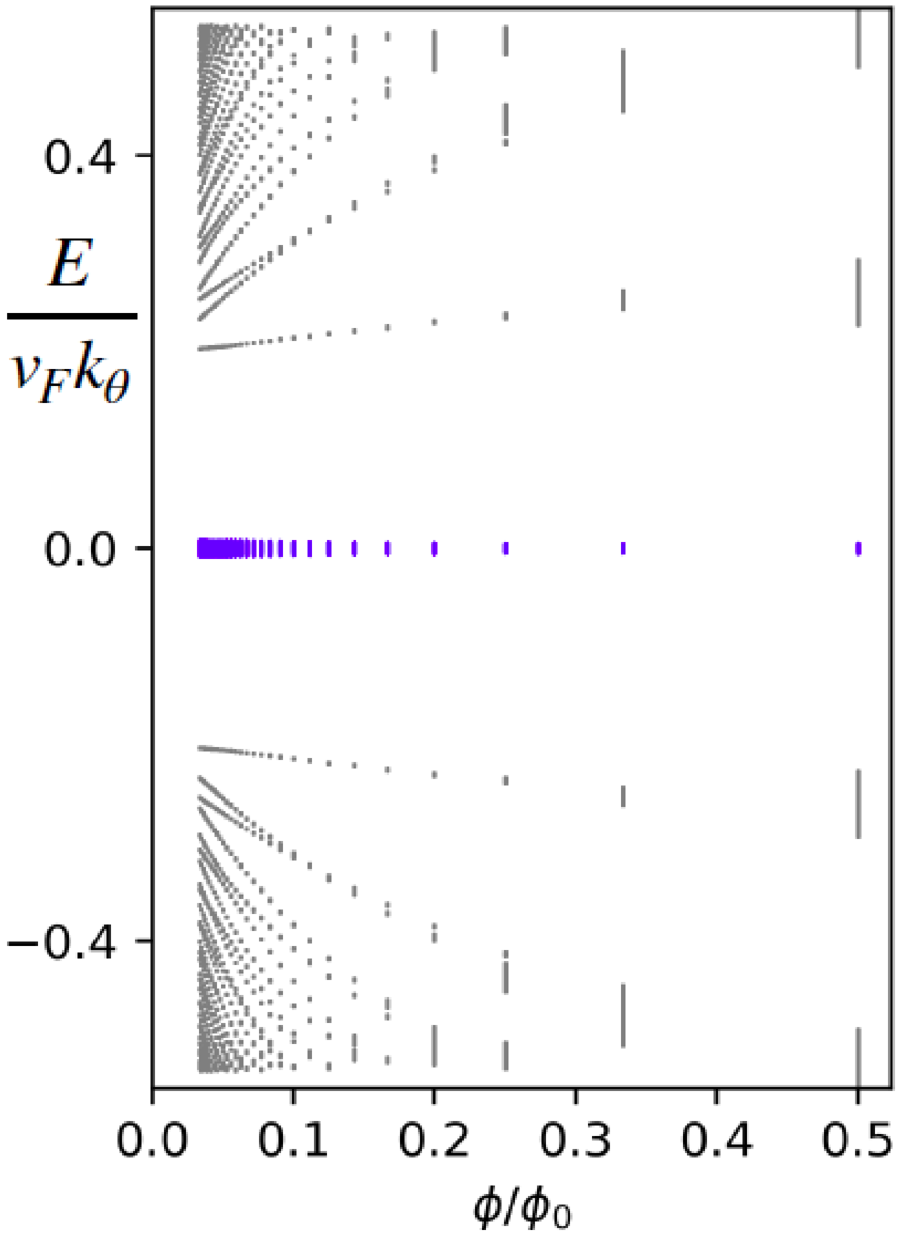

Bistritzer and MacDonald PRB 84, 035440 (2011)
Hejazi, Liu, Balents PRB 100, 035115 (2019)

We need to find a projector onto the narrow bands at finite B-field

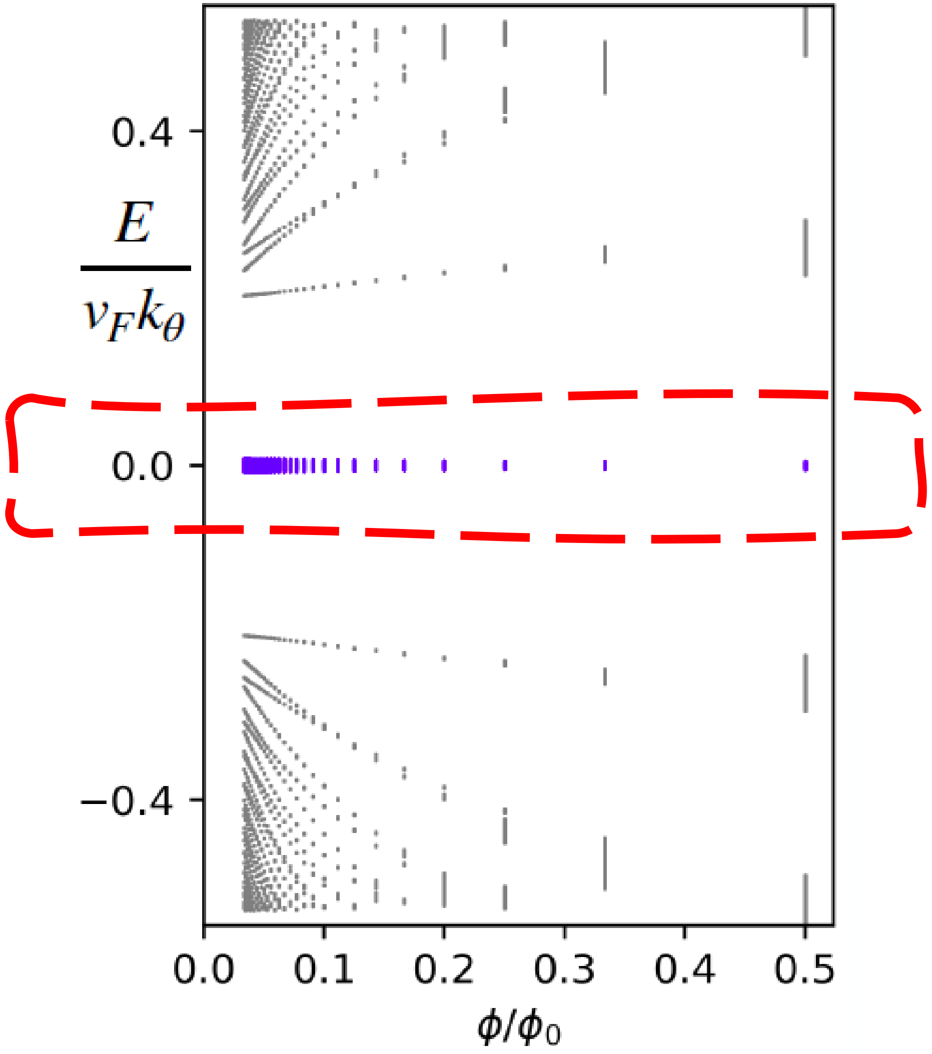

$$V_{int} = \frac{1}{2}\int d\boldsymbol{r}d\boldsymbol{r}'\, V(\boldsymbol{r}-\boldsymbol{r}')\delta\rho(\boldsymbol{r})\delta\rho(\boldsymbol{r}')$$

- Solving the BM model in LL basis is a bit problematic at low **B** because of the high number of LLs that needs to be kept

- Need a new method (that works even if the narrow bands are topological at **B**=0)

Bistritzer and MacDonald PRB 84, 035440 (2011)
Hejazi, Liu, Balents PRB 100, 035115 (2019)

X. Wang and OV PRB 106, L121111 (2022)

Key insight: use B=0 hybrid Wannier states to generate the finite B basis

- for the hybrid Wannier state centered at and near the origin, the Landau gauge vector potential $\boldsymbol{A} = (0, Bx)$ can be treated perturbatively, because the region in real space where $\boldsymbol{A}$ is large gets suppressed by the exponential localization of the hybrid Wannier state.

- the discrete translation symmetry along the y −direction used in constructing the hybrid Wannier state is preserved by such $\boldsymbol{A}$

- Generate the entire basis from the **B**=0 hybrid WS centered near origin by projecting onto irreps of MTG

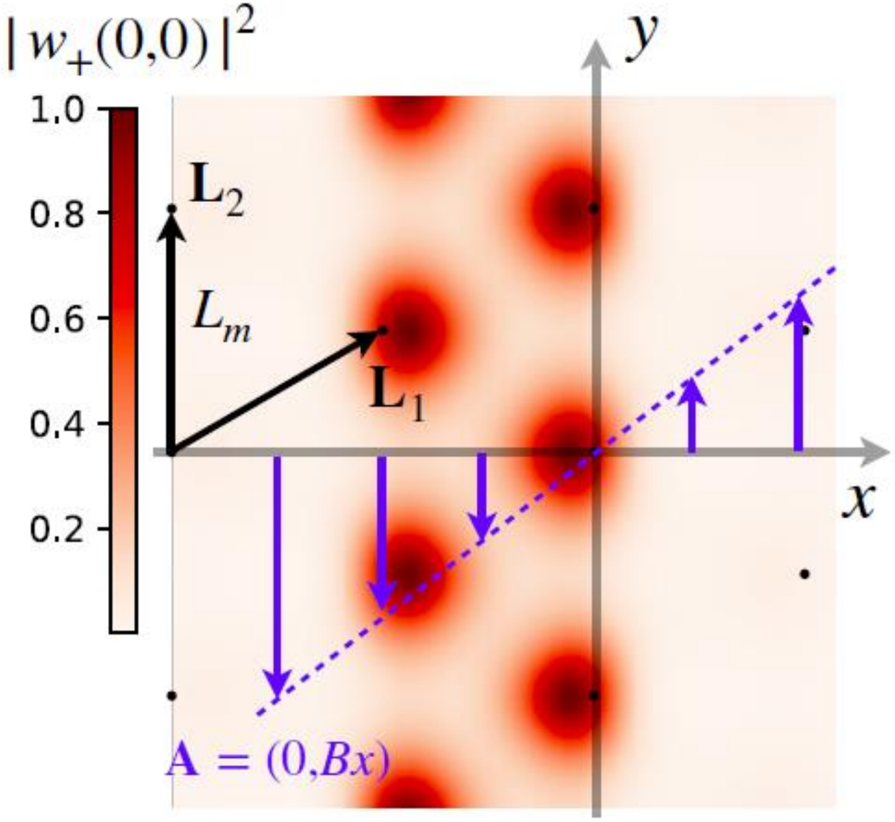

X. Wang and OV PRB 106, L121111 (2022)

Magnetic translation group and projection onto its irreps

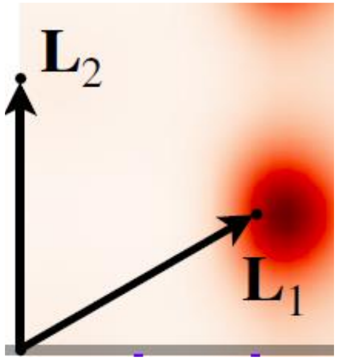

$$t_{\boldsymbol{L}_2}\psi(\boldsymbol{r}) = \psi(\boldsymbol{r}-\boldsymbol{L}_2)$$

$$t_{\boldsymbol{L}_1}\psi(\boldsymbol{r}) = e^{i\frac{eB}{\hbar c}L_{1x}y}\psi(\boldsymbol{r}-\boldsymbol{L}_1)$$

$$\frac{\phi}{\phi_0} = \frac{p}{q}$$

$$\left[t_{\boldsymbol{L}_2}, H_{BM}\left(p_x, p_y - \frac{e}{c}Bx\right)\right] = 0$$

$$\left[t_{\boldsymbol{L}_1}, H_{BM}\left(p_x, p_y - \frac{e}{c}Bx\right)\right] = 0$$

$$\left[t_{\boldsymbol{L}_2}^{q}, t_{\boldsymbol{L}_1}\right] = 0$$

$$\boxed{W_\pm(k_1,k_2;n_0)\rangle \sim \sum_{s=-\infty}^{\infty} e^{2\pi i s k_1} t_{\boldsymbol{L}_1}^{s}\,|w_\pm(n_0,k_2\boldsymbol{g}_2)\rangle}$$

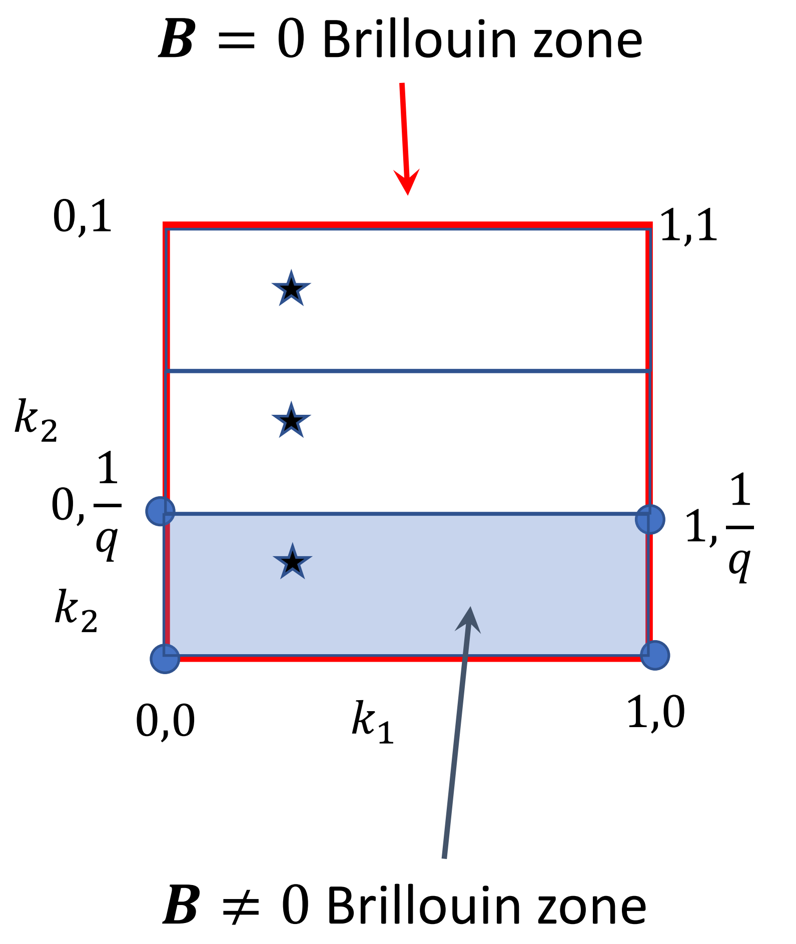

X. Wang and OV PRB 106, L121111 (2022)

TBG band topology and hybrid Wannier states

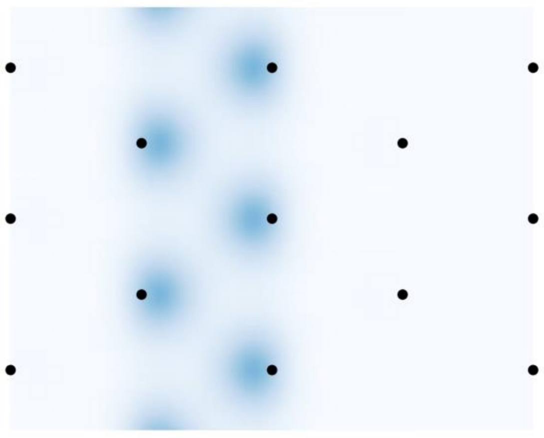

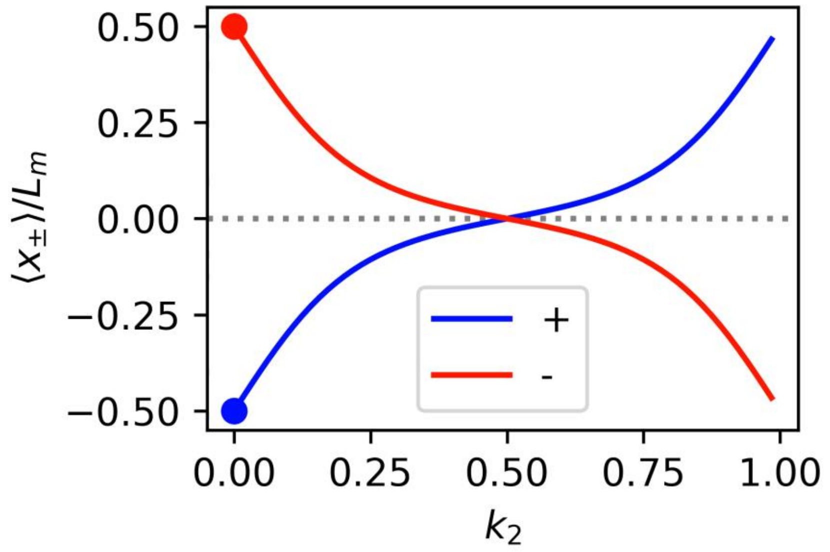

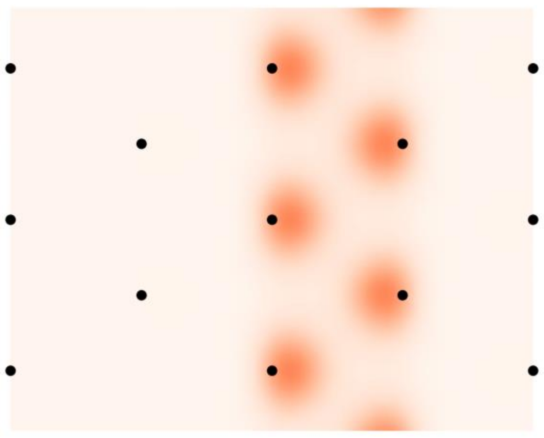

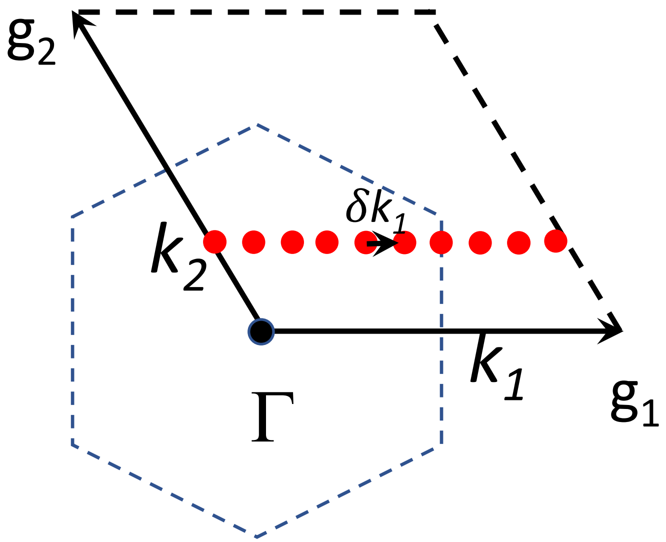

video courtesy Xiaoyu Wang (NHMFL)

Z. Song et al, PRL 123, 036401 (2019); J. Kang and OV PRB 2020

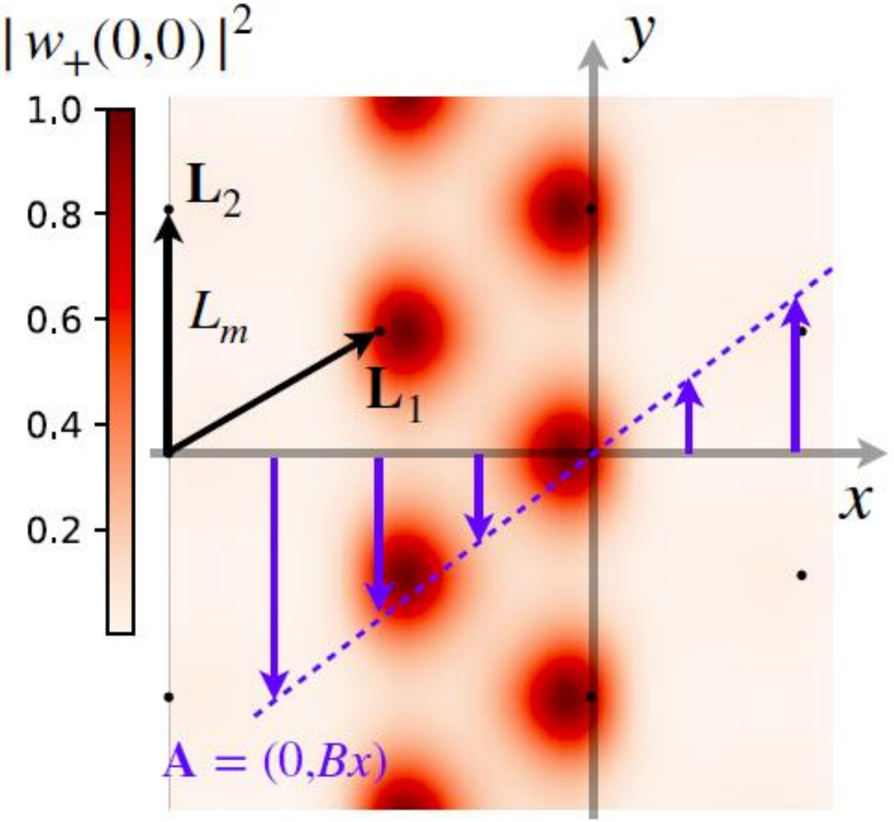

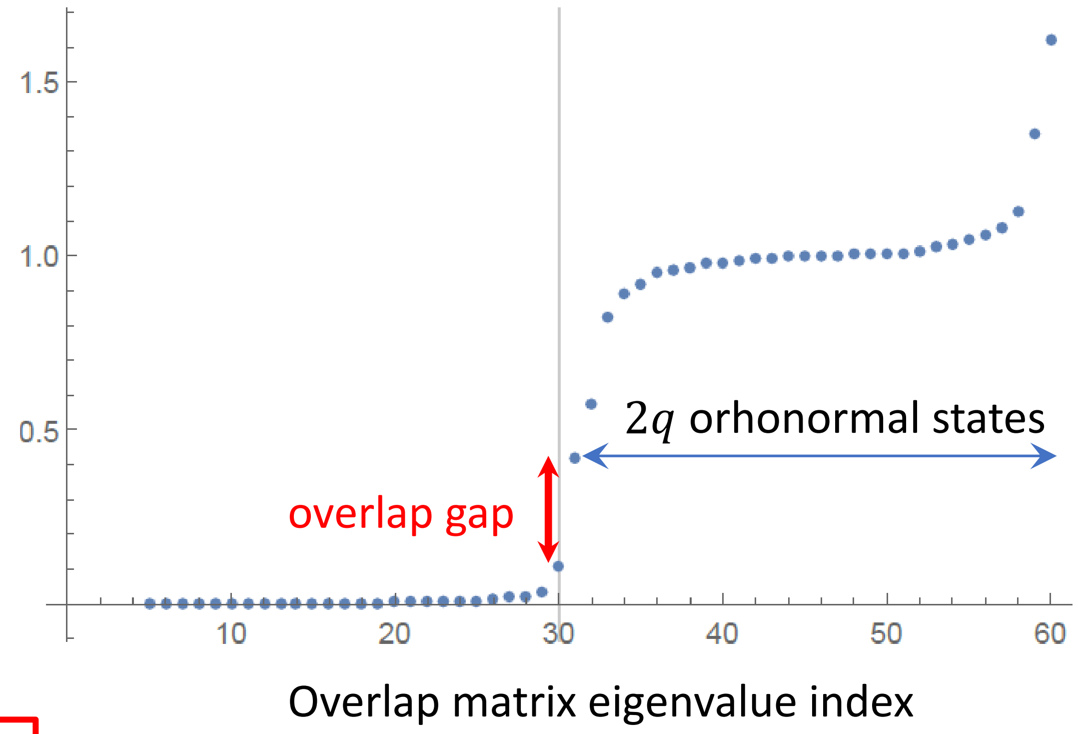

$$\boxed{W_\pm(k_1, k_2; n_0)\rangle \sim \sum_{s=-\infty}^{\infty} e^{2\pi i s k_1} t_{\boldsymbol{L}_1}^s \, |w_\pm(n_0, k_2 \boldsymbol{g}_2)\rangle}$$

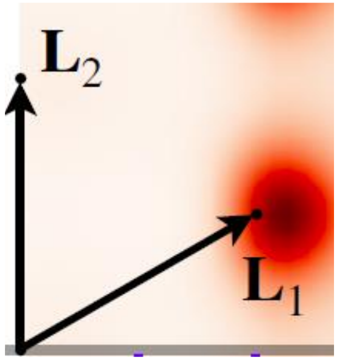

$$t_{L_2}\psi(\boldsymbol{r}) = \psi(\boldsymbol{r} - \boldsymbol{L}_2)$$

$$t_{L_1}\psi(\boldsymbol{r}) = e^{i\frac{eB}{\hbar c}L_{1x}y}\psi(\boldsymbol{r} - \boldsymbol{L}_1)$$

$$\frac{\phi}{\phi_0} = \frac{p}{q}$$

$$\left[t_{\boldsymbol{L}_2}, H_{BM}\left(p_x, p_y - \frac{e}{c}Bx\right)\right] = 0$$

$$\left[t_{\boldsymbol{L}_1}, H_{BM}\left(p_x, p_y - \frac{e}{c}Bx\right)\right] = 0$$

$$\left[t_{\boldsymbol{L}_2}^{q}, t_{\boldsymbol{L}_1}\right] = 0$$

$$\boxed{W_\pm(k_1, k_2; n_0)\rangle \sim \sum_{s=-\infty}^{\infty} e^{2\pi i s k_1} t_{\boldsymbol{L}_1}^{s}\, |w_\pm(n_0, k_2\boldsymbol{g}_2)\rangle}$$

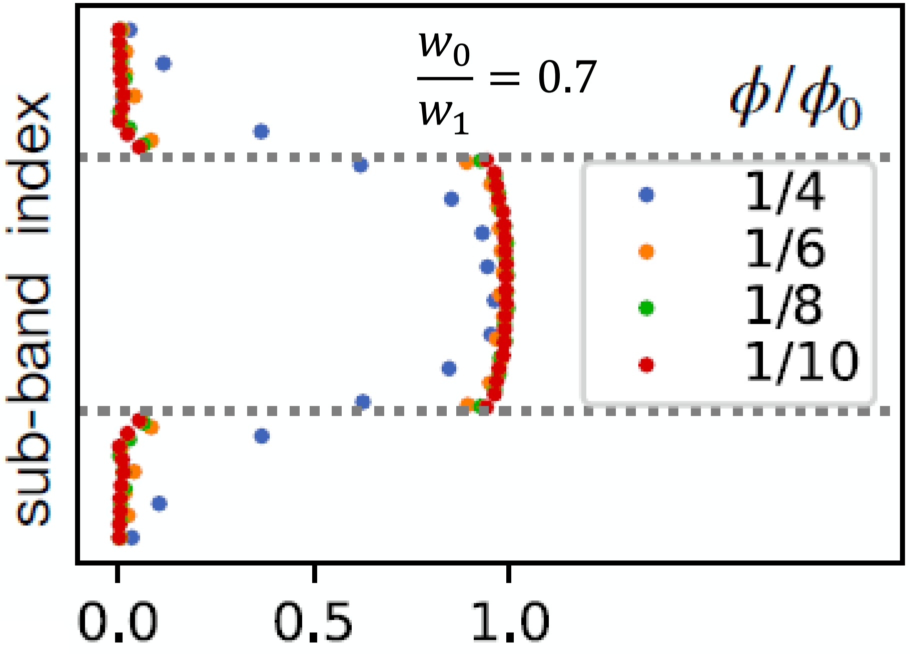

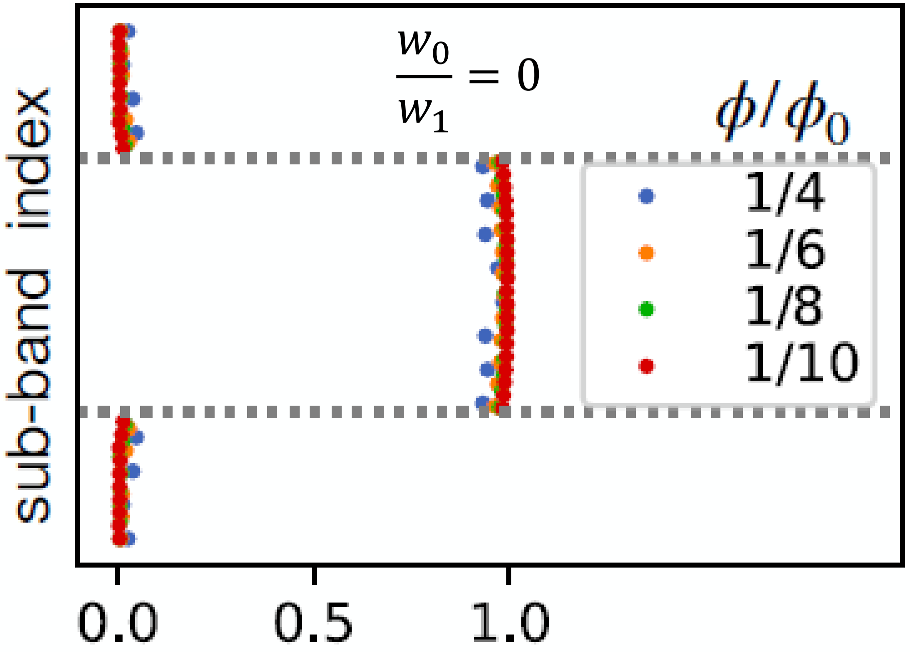

Exact single particle excitation spectrum at CNP in the strong coupling limit at small B-field

$$V_{int}\, X|\Omega\rangle = \frac{1}{2}\int dr\, dr' V(r-r')\big[\delta\varrho(r),[\delta\varrho(r'),X]\big]|\Omega\rangle$$

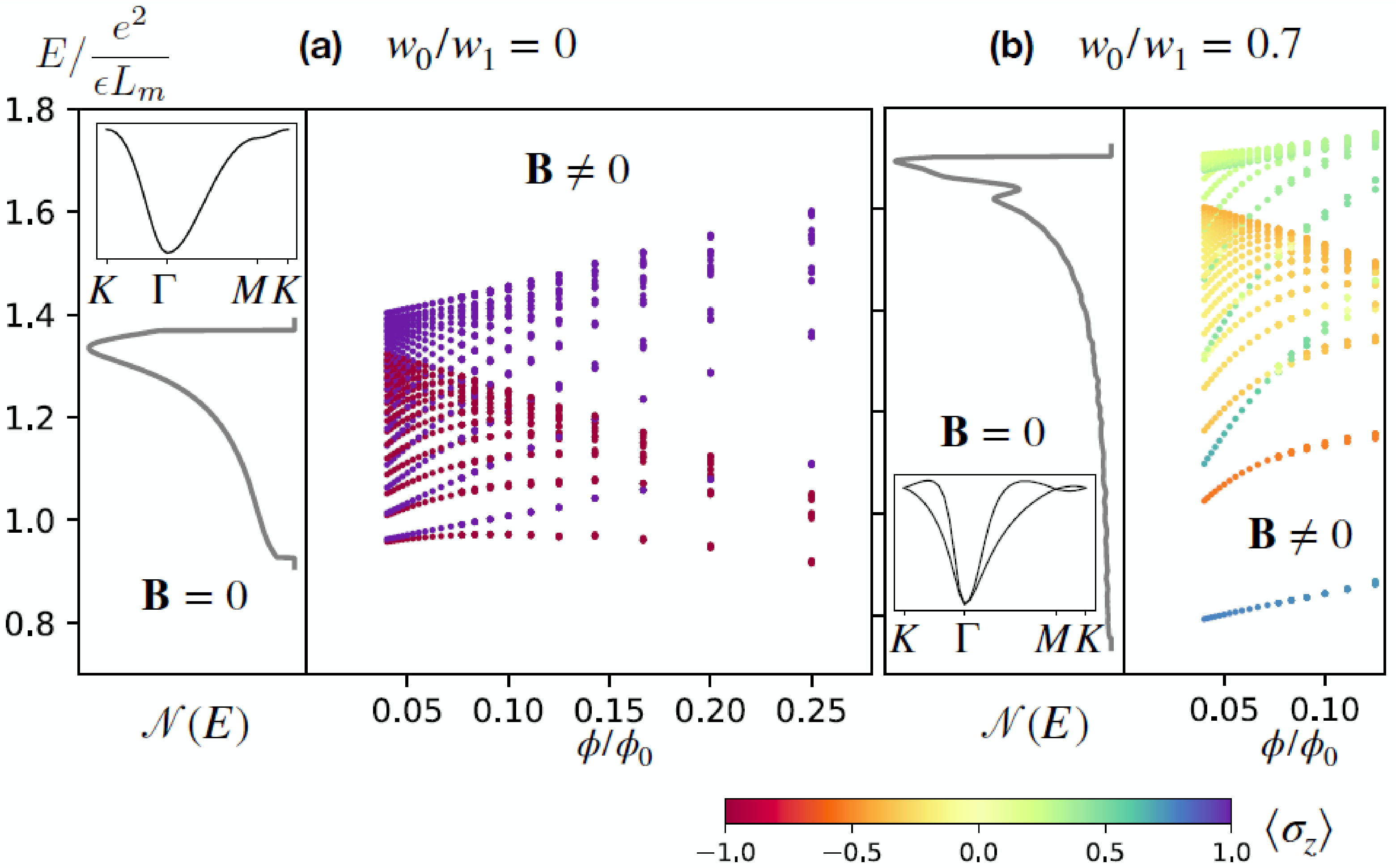

- Landau quantization even in strong coupling
- Imbalance in the sublattice polarization reflects the topology of the bands (blue is subl. A)
- Finite **B**-field causes splitting between the LLs even in the chiral limit due to broken C_2T

X. Wang and OV PRB 106, L121111 (2022)

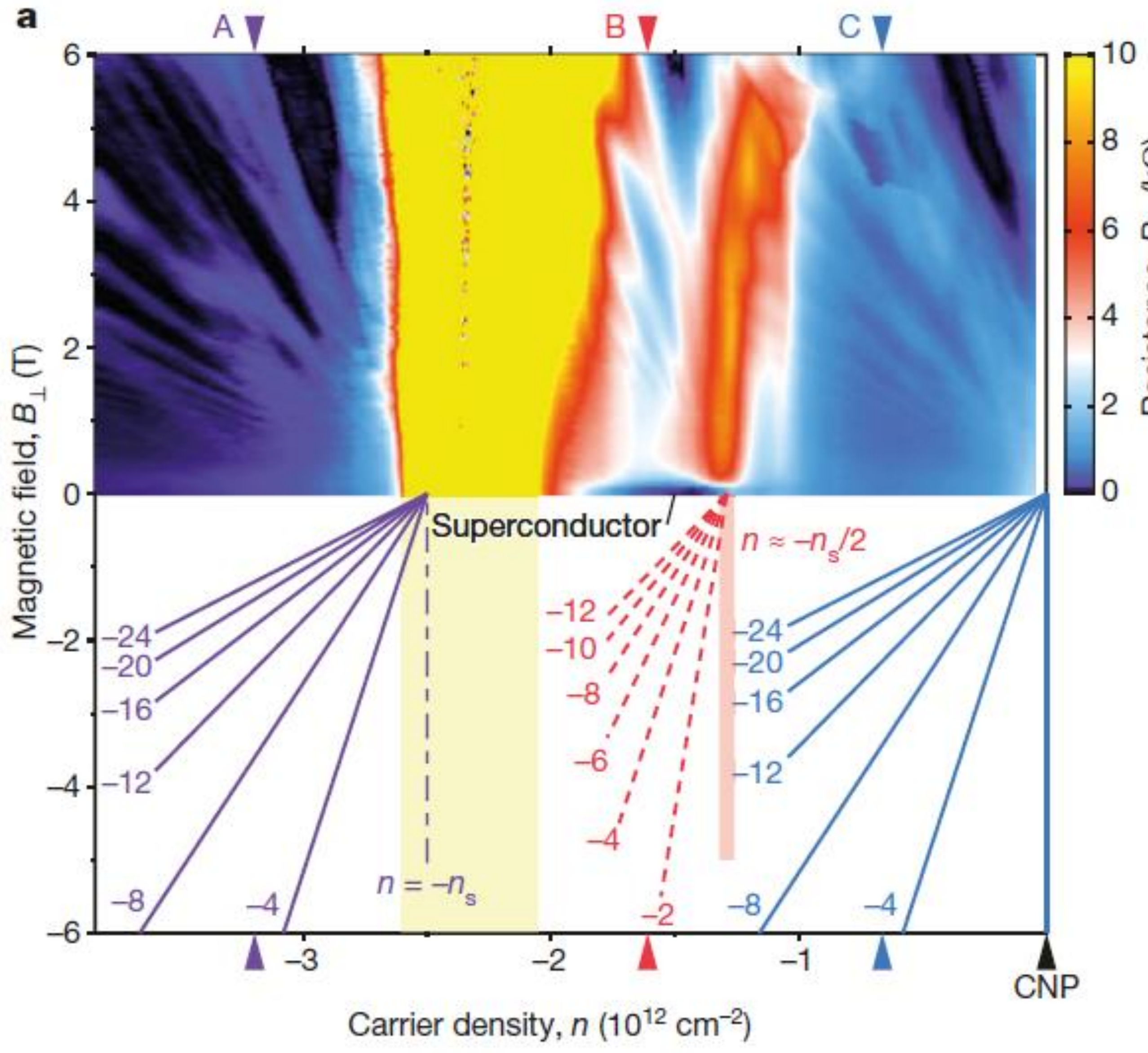

Cao et al, Pablo Jarillo-Herrero Nature 2018

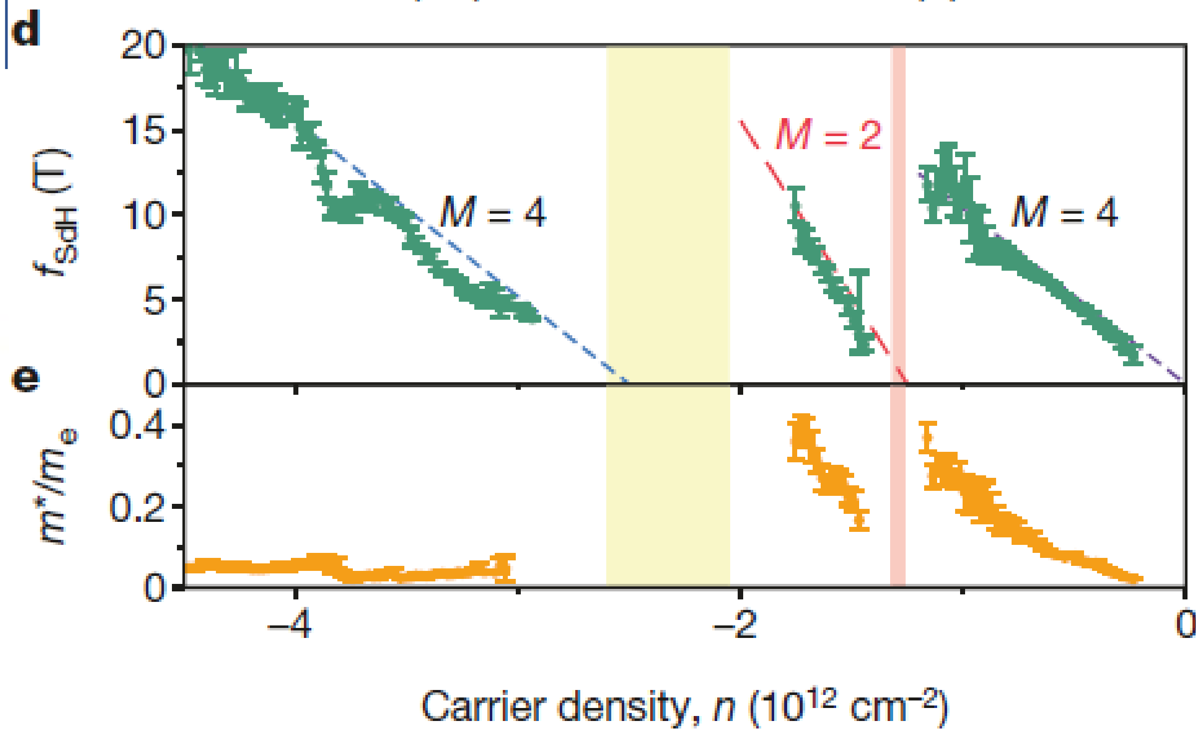

- Naturally explains why Landau fans point away from the CNP

X. Wang and OV PRB 106, L121111 (2022)

PHYSICAL REVIEW LETTERS **129,** 047601 (2022)

Editors' Suggestion Featured in Physics

Magic-Angle Twisted Bilayer Graphene as a Topological Heavy Fermion Problem

Zhi-Da Song[1,2,*] and B. Andrei Bernevig[2,3,4]

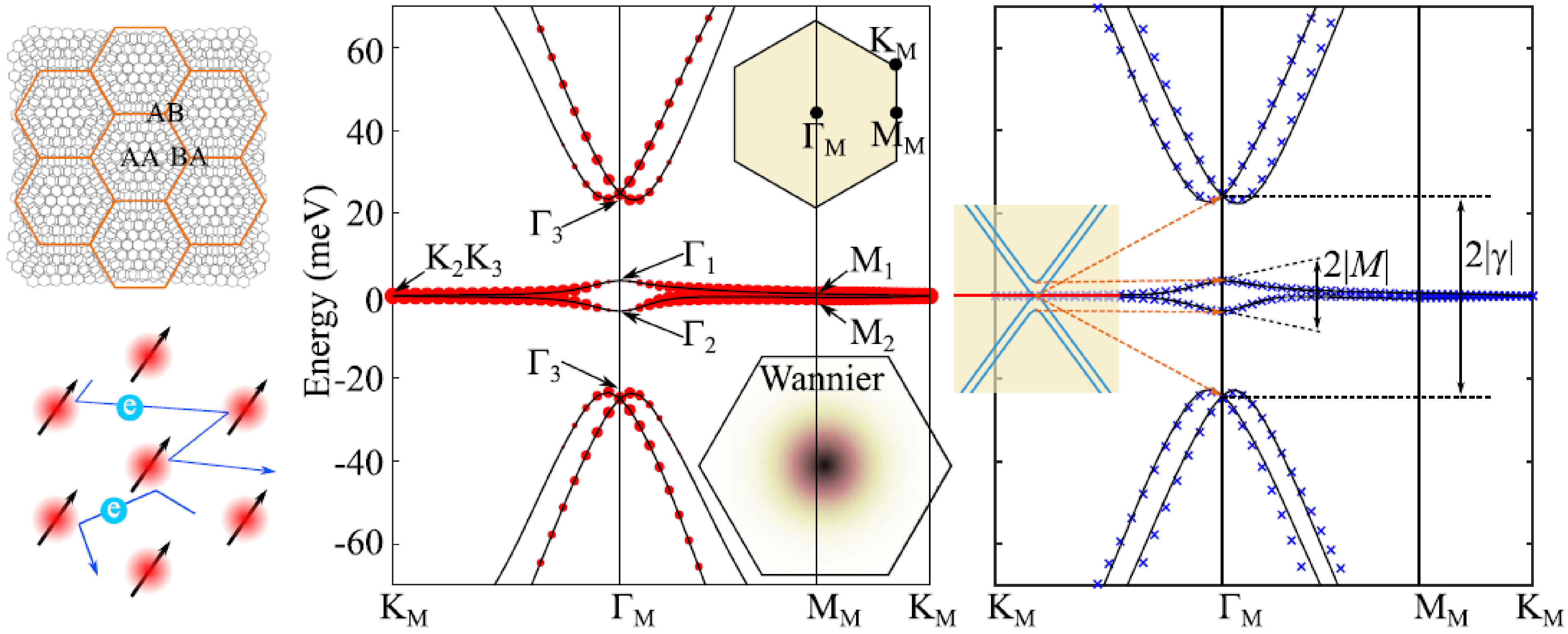

Topological heavy fermions (non-interacting Hamiltonian)

$$\hat{H}_0 = \sum_{|\mathbf{k}|<\Lambda_c} \sum_{\tau s} \sum_{aa'=1}^{4} H_{aa'}^{c,\tau}(\mathbf{k}) \tilde{c}_{\mathbf{k}a\tau s}^\dagger \tilde{c}_{\mathbf{k}a'\tau s} +$$

$$\sum_{|\mathbf{k}|<\Lambda_c} \sum_{\tau s} \sum_{a=1}^{4} \sum_{b=1}^{2} \left(e^{-\frac{1}{2}\mathbf{k}^2\lambda^2} H^{cf,v}(\mathbf{k})_{ab} \tilde{c}_{\mathbf{k}a\tau s}^\dagger \tilde{f}_{\mathbf{k}b\tau s} + \text{h.c.} \right)$$

$$H_{aa'}^{c,\tau}(\mathbf{k}) = \begin{pmatrix} 0_{2\times 2} & v_*(\tau k_x \sigma_0 + i k_y \sigma_z) \\ v_*(\tau k_x \sigma_0 - i k_y \sigma_z) & M\sigma_x \end{pmatrix}$$

$$H_{ab}^{cf,\tau}(\mathbf{k}) = \begin{pmatrix} \gamma\sigma_0 + v_*'(\tau k_x \sigma_x + k_y \sigma_y) \\ 0_{2\times 2} \end{pmatrix}$$

Song and Bernevig PRL2022

``one shot'' Hartree-Fock

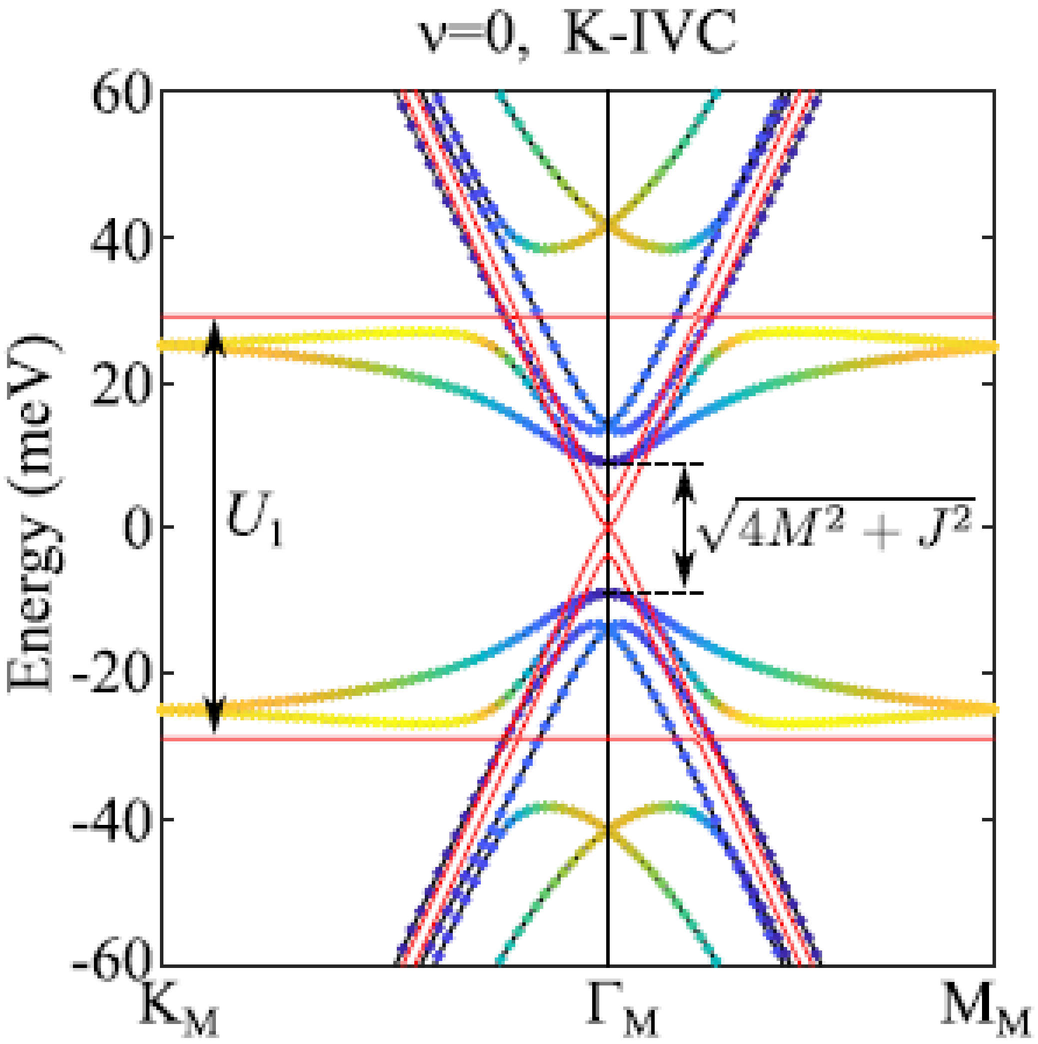

self-consistent Hartree-Fock

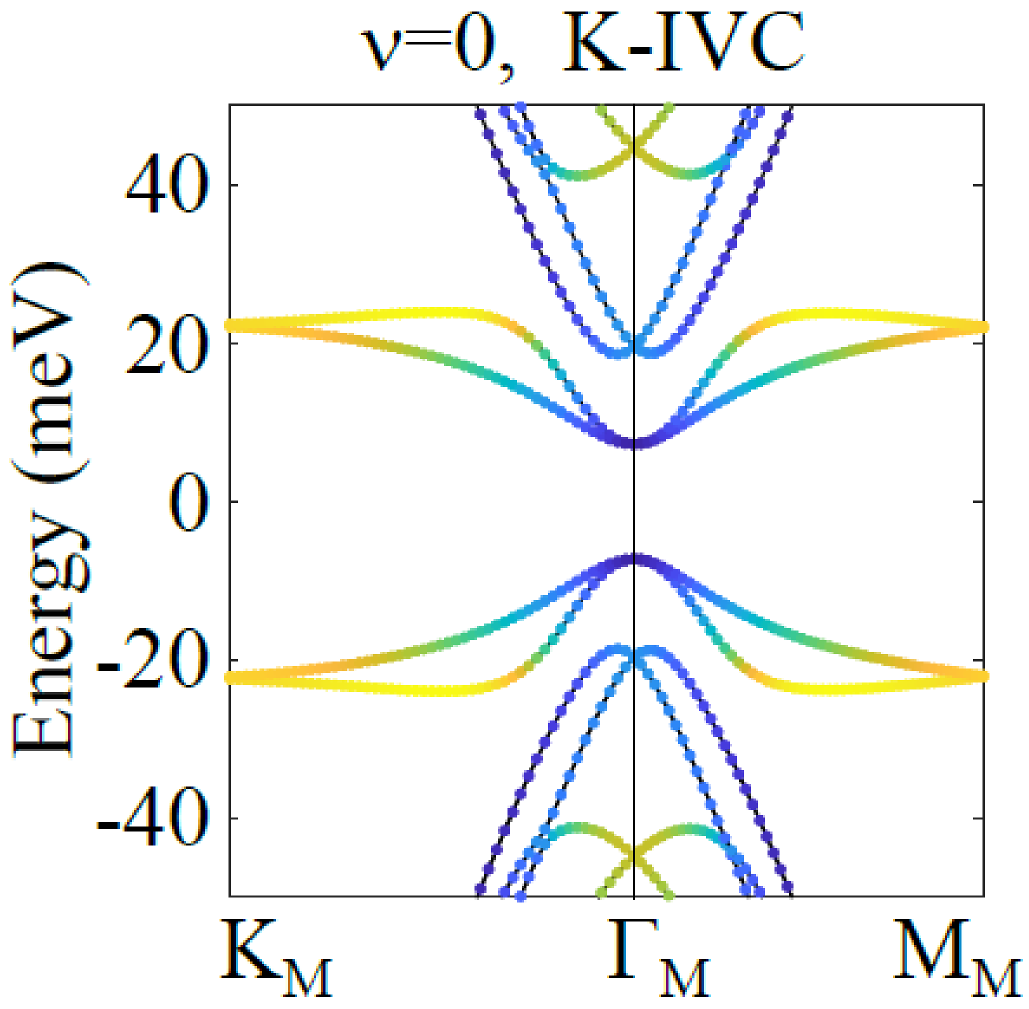

Song and Bernevig PRL2022

Topological heavy fermions in magnetic field

c-f coupling turned off

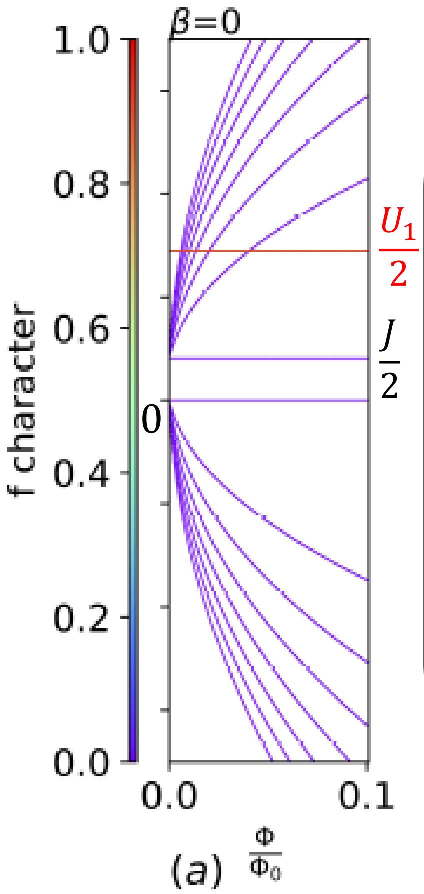

cc

ff

$$\begin{pmatrix} 0 & 0 & -i\sqrt{2}\frac{v_*}{\ell}\hat{a}^\dagger & 0 & \gamma\Sigma(\hat{a}^\dagger\hat{a}) & i\sqrt{2}\frac{v_*'}{\ell}\hat{a}\Sigma(\hat{a}^\dagger\hat{a}) \\ 0 & 0 & 0 & i\sqrt{2}\frac{v_*}{\ell}\hat{a} & -i\sqrt{2}\frac{v_*'}{\ell}\hat{a}^\dagger\Sigma(\hat{a}^\dagger\hat{a}) & \gamma\Sigma(\hat{a}^\dagger\hat{a}) \\ i\sqrt{2}\frac{v_*}{\ell}\hat{a} & 0 & \frac{J}{2} & M & 0 & 0 \\ 0 & -i\sqrt{2}\frac{v_*}{\ell}\hat{a}^\dagger & M & \frac{J}{2} & 0 & 0 \\ \gamma\Sigma(\hat{a}^\dagger\hat{a}) & i\sqrt{2}\frac{v_*'}{\ell}\Sigma(\hat{a}^\dagger\hat{a})\hat{a} & 0 & 0 & \frac{U_1}{2} & 0 \\ -i\sqrt{2}\frac{v_*'}{\ell}\Sigma(\hat{a}^\dagger\hat{a})\hat{a}^\dagger & \gamma\Sigma(\hat{a}^\dagger\hat{a}) & 0 & 0 & 0 & \frac{U_1}{2} \end{pmatrix}$$

$$\Sigma_m = \Sigma(m) \approx 1 - \left(m + \frac{1}{2}\right)\frac{\phi}{\phi_0}\frac{2\pi\lambda^2}{A_{uc}}$$

Keshav Singh, B.A. Bernevig et al, OV arXiv:2305.08171

Topological heavy fermions in magnetic field

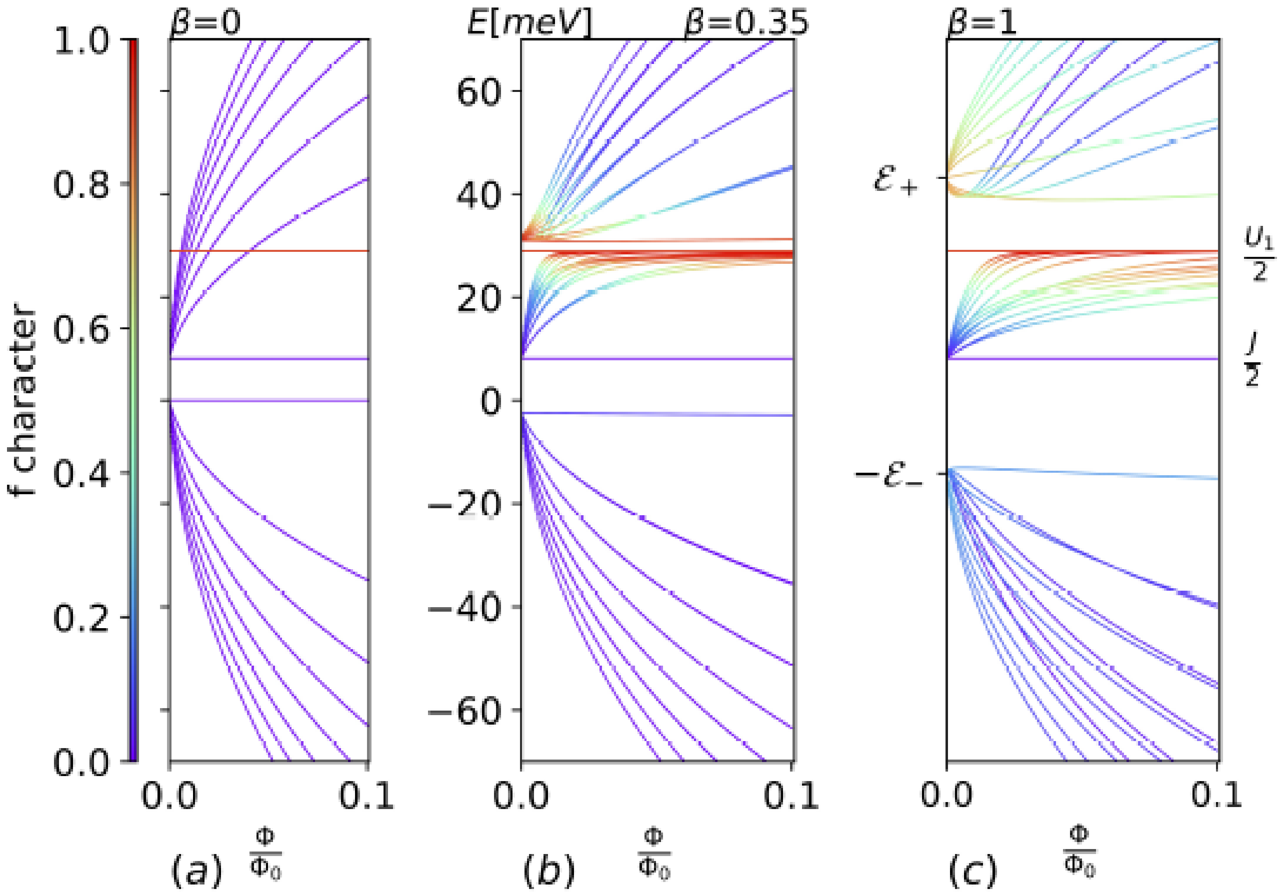

$$\mathcal{E}_{\pm} = \pm\frac{U_1}{4} + \sqrt{\frac{U_1^2}{16} + \gamma^2}$$

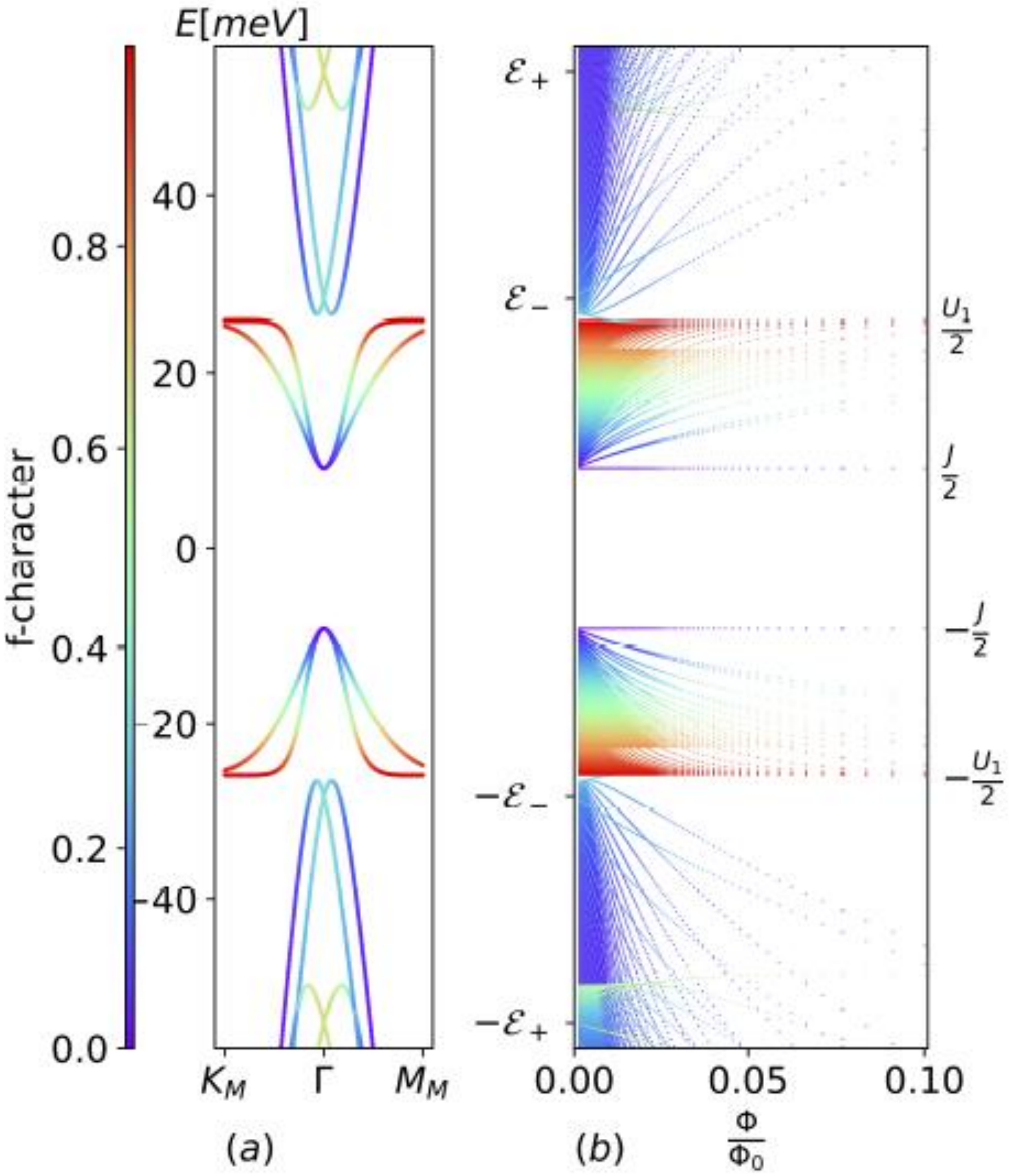

Keshav Singh, B.A. Bernevig et al, OV arXiv:2305.08171

Recovering the non-interacting topological heavy fermions in magnetic field (for M=0)

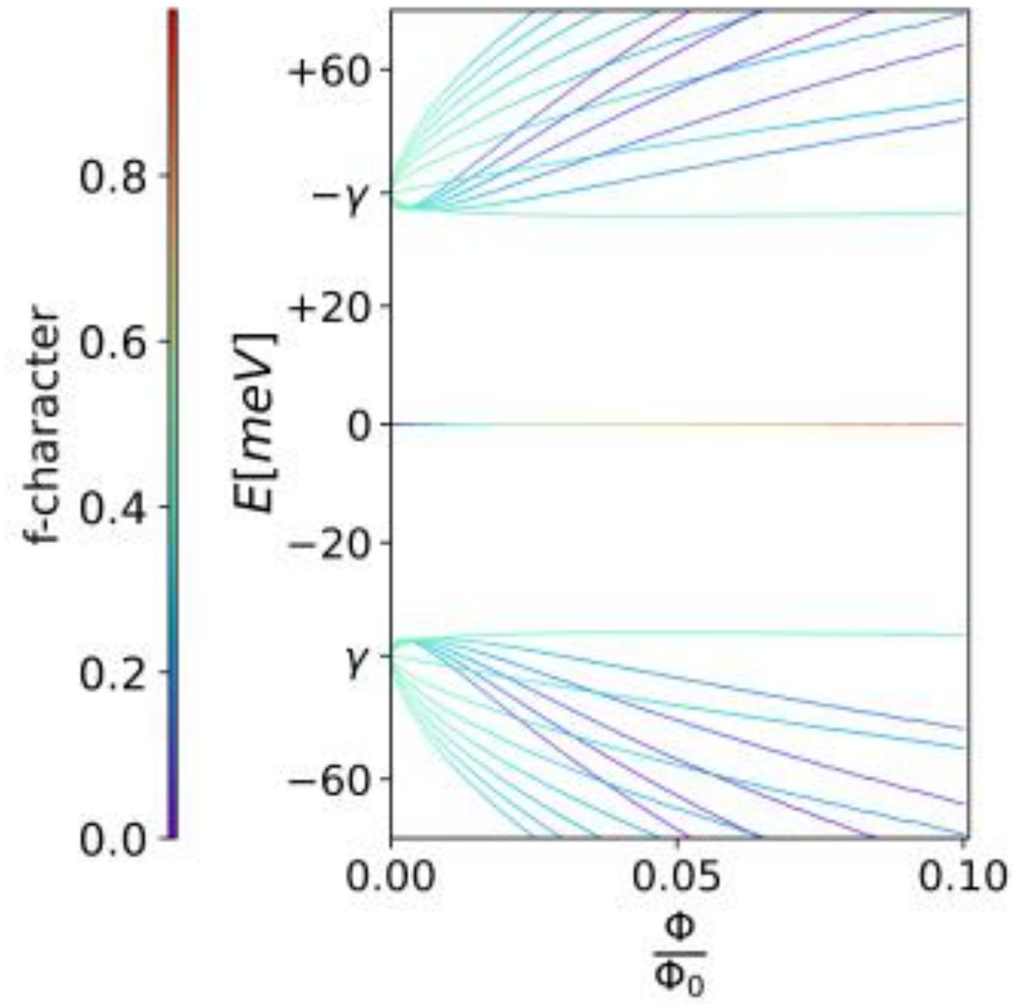

bipartite

$$
\begin{pmatrix}
-i\sqrt{2}\frac{v_*}{\ell}\hat{a}^\dagger & 0 & \gamma\Sigma(\hat{a}^\dagger\hat{a}) & i\sqrt{2}\frac{v_*'}{\ell}\hat{a}\Sigma(\hat{a}^\dagger\hat{a}) \\
0 & i\sqrt{2}\frac{v_*}{\ell}\hat{a} & -i\sqrt{2}\frac{v_*'}{\ell}\hat{a}^\dagger\Sigma(\hat{a}^\dagger\hat{a}) & \gamma\Sigma(\hat{a}^\dagger\hat{a}) \\
0 & 0 & 0 & 0 \\
0 & 0 & 0 & 0 \\
0 & 0 & 0 & 0 \\
0 & 0 & 0 & 0
\end{pmatrix}
$$

coupled zeros *decoupled fs* $\Rightarrow$ *2 per u.c.*

$$\boxed{(2m_{max}+3)} + \boxed{(2q-(2m_{max}+3))} = 2q$$

Keshav Singh, B.A. Bernevig et al, OV arXiv:2305.08171

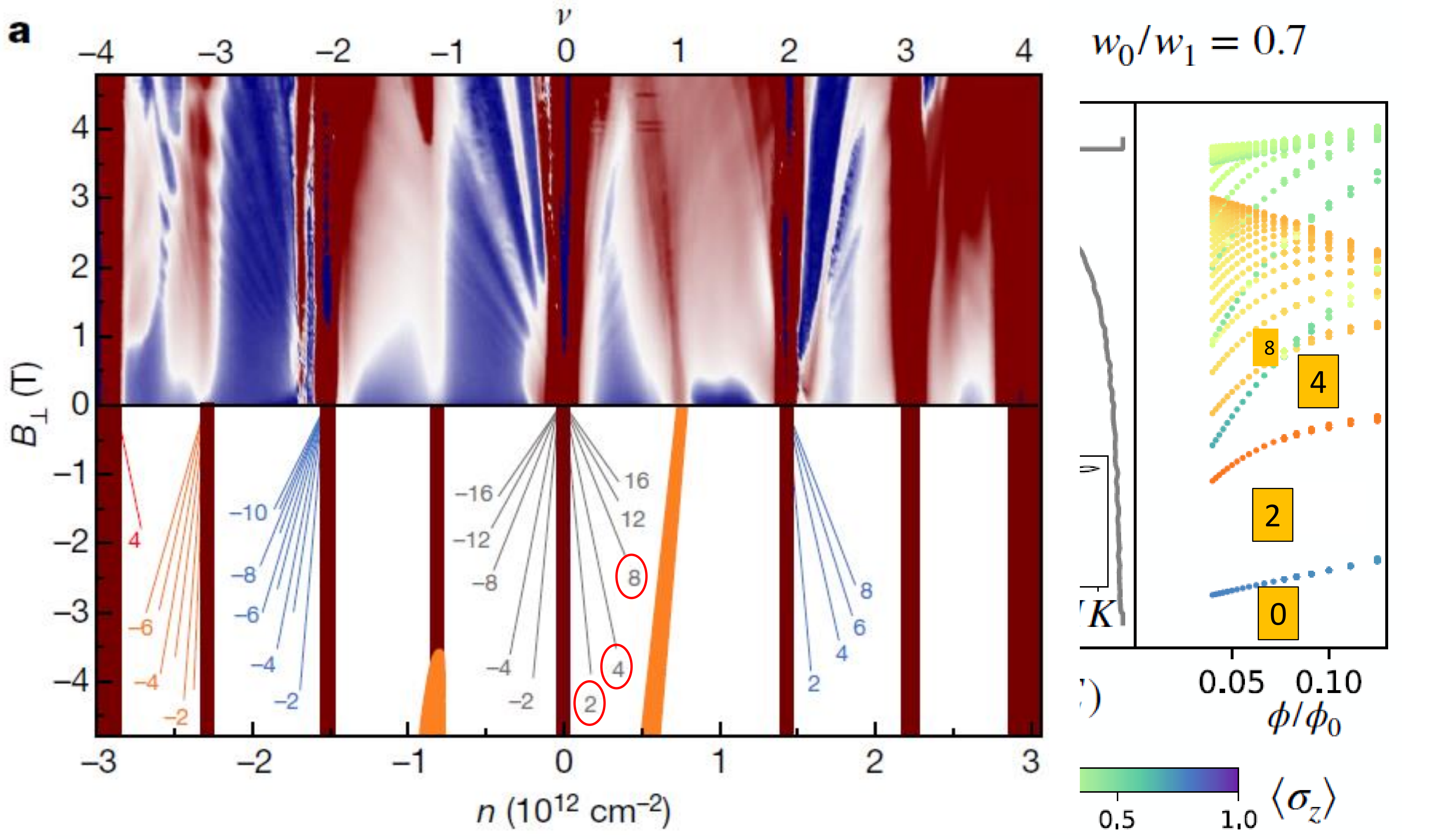
a
ν
−4 −3 −2 −1 0 1 2 3 4
B⊥ (T)
4 3 2 1 0 −1 −2 −3 −4
4
−6 −4 −2
−10 −8 −6 −4 −2
−16 −12 −8 −4 −2
16 12 8 4 2
8 6 4 2
−3 −2 −1 0 1 2 3
n (10^12 cm^−2)
w0/w1 = 0.7
8
4
2
0
K
0.05 0.10
φ/φ0
0.5 1.0
⟨σz⟩

Although it is tempting to make a comparison with the transport data on the device with the gap at CNP, we are not ready to reach any conclusions yet, in part because of the absence of local strain characterization.

In this regard, it would be highly desirable to have the low B Landau level spectroscopy in ultra-low strain device regions where STM reveals a gap at the charge neutrality point without hBN substrate alignment.

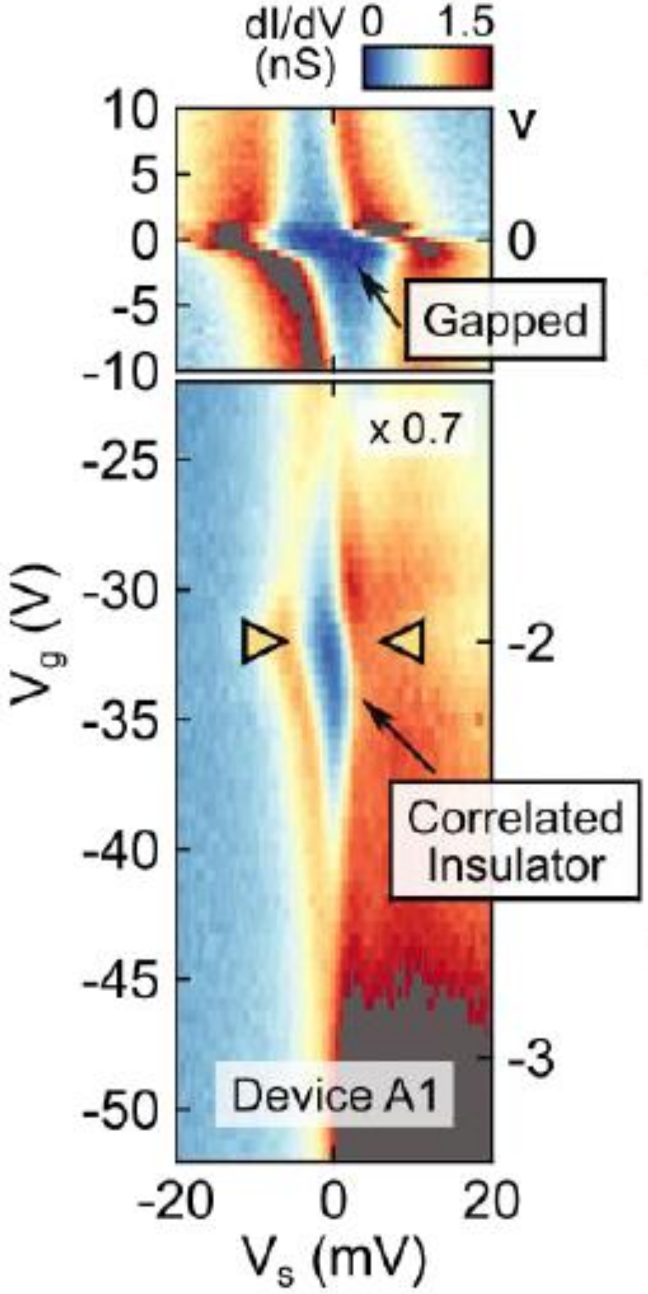

Nuckolls et al, Yazdani 2303.00024

Summary

Itinerancy at the strong coupling and a new approach to the Hofstadter problem

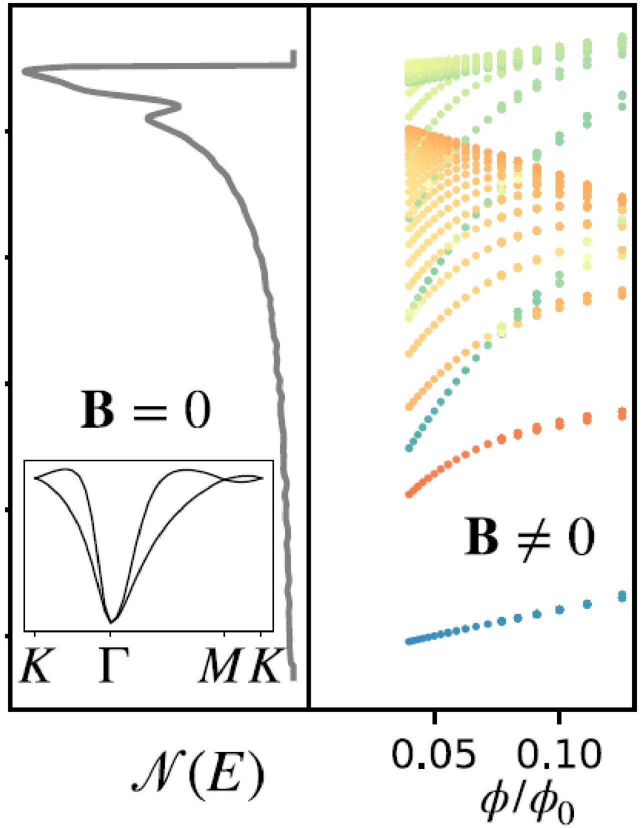

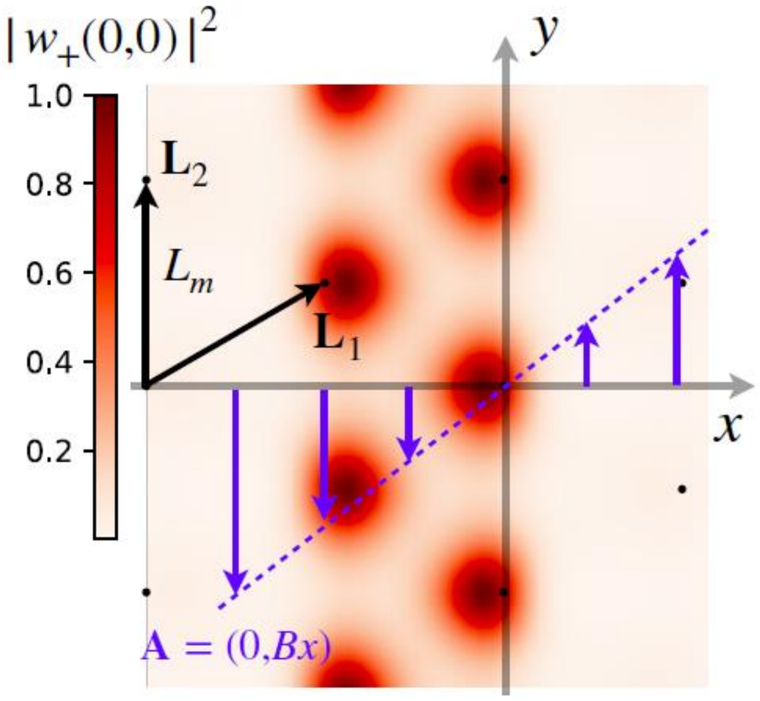

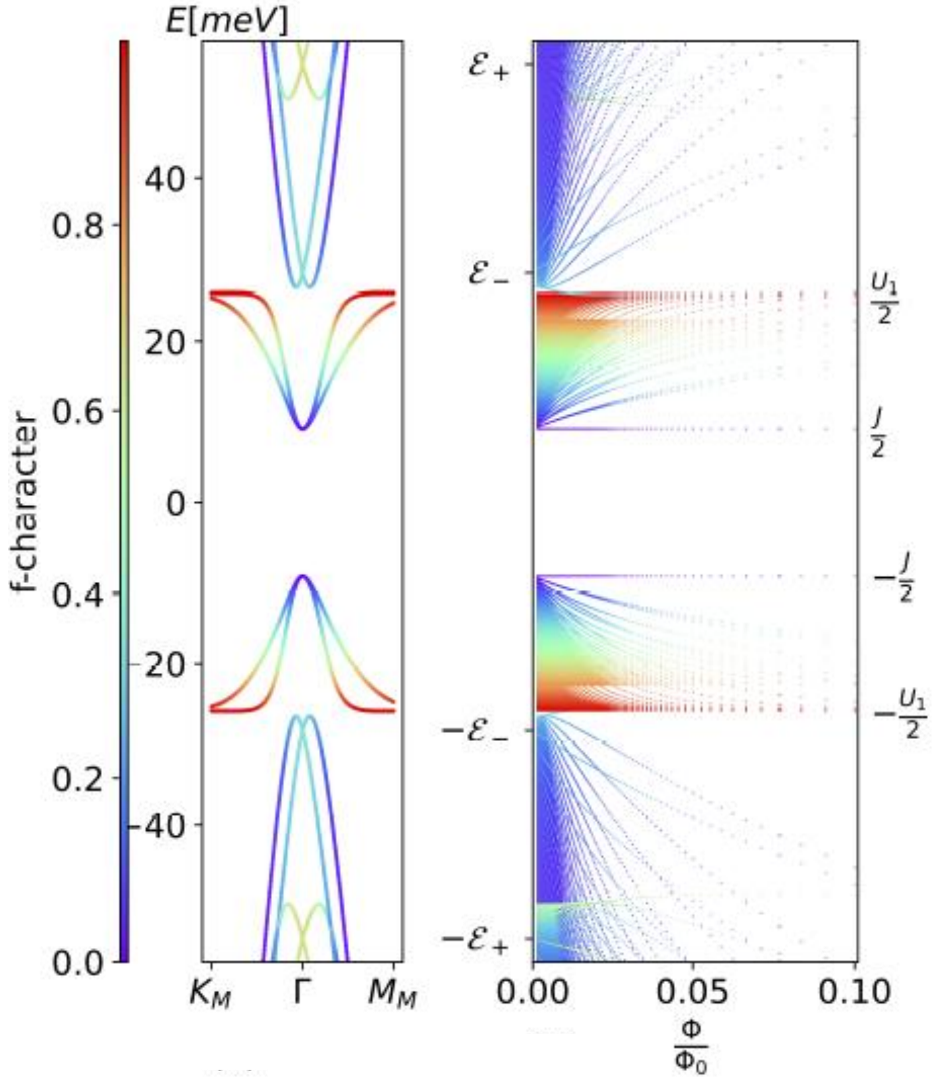

Beyond the minimal continuum model: towards a more accurate description of electronic structure

Near degeneracy among many phases can cause sensitivity to terms in the minimal continuum model which were neglected.

This motivates development of a more accurate continuum theory from microscopic model.

We derived the effective continuum model for graphene bilayers by systematically expanding in real space gradients of the slow fermion fields and the atomic displacements allowing for an arbitrary **inhomogeneous** smooth lattice deformation, including a twist.

OV and Jian Kang, PRB **107** 075123 (2023)
Jian Kang and OV, PRB **107** 075408 (2023)

Beyond the minimal continuum model: towards a more accurate description of electronic structure

Set up a gradient expansion of the slow fermion envelope functions ψ and the atomic displacement field U (in Eulerian coordinates as in Balents SciPost Phys. **7**, 048 (2019))

	intralayer	interlayer
1^{st} order terms:	$\nabla\psi, \nabla U \sim O(200meV)$	contact $w_{0,1} \sim O(100meV)$
2^{nd} order terms:	$(\nabla\psi)^2, \nabla U \nabla\psi, (\nabla U)^2$	$\nabla\psi, \nabla U$

Smaller than 1^{st} order by $\sim |K|a\theta[rad] = 4\pi\theta[rad]/3 = 0.08$ i.e. narrow bandwidth

OV and Jian Kang, PRB **107**, 075123 (2023)
Jian Kang and OV, PRB **107**, 075408 (2023)

Beyond the minimal continuum model: towards a more accurate description of electronic structure

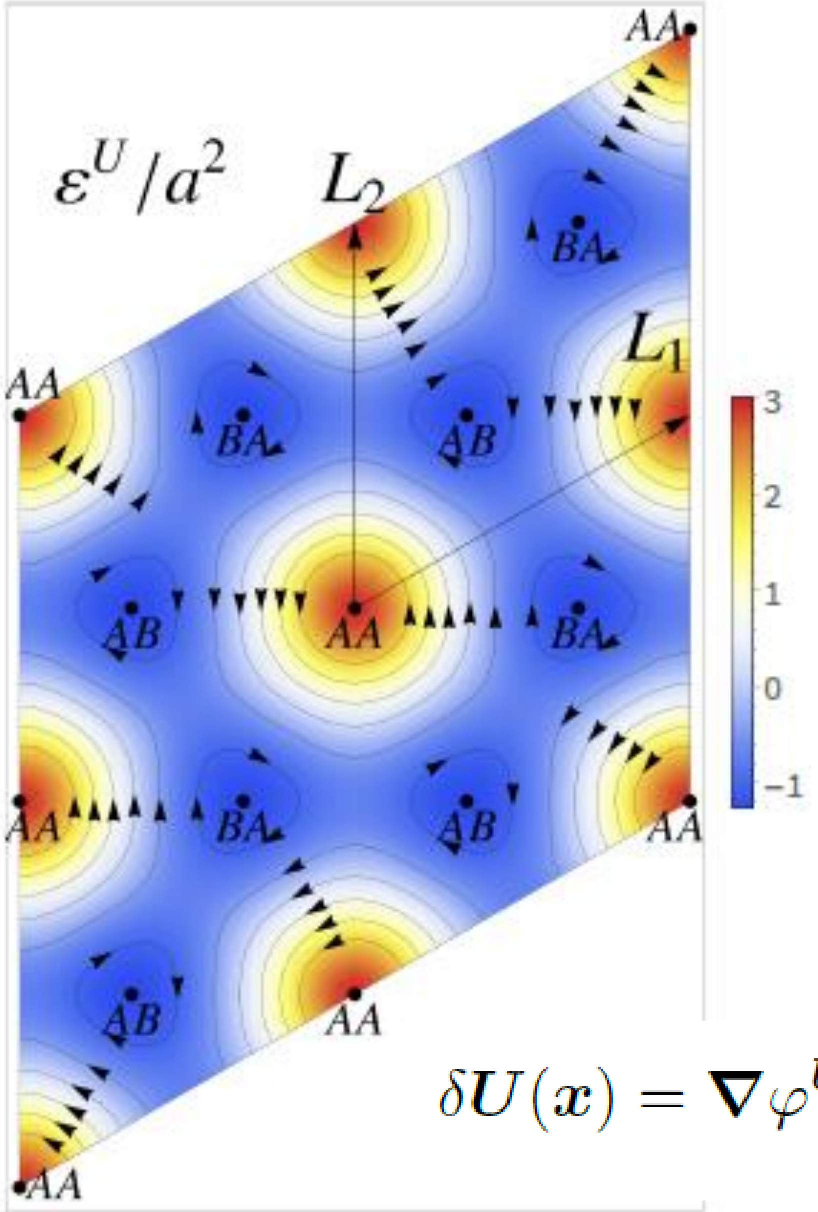

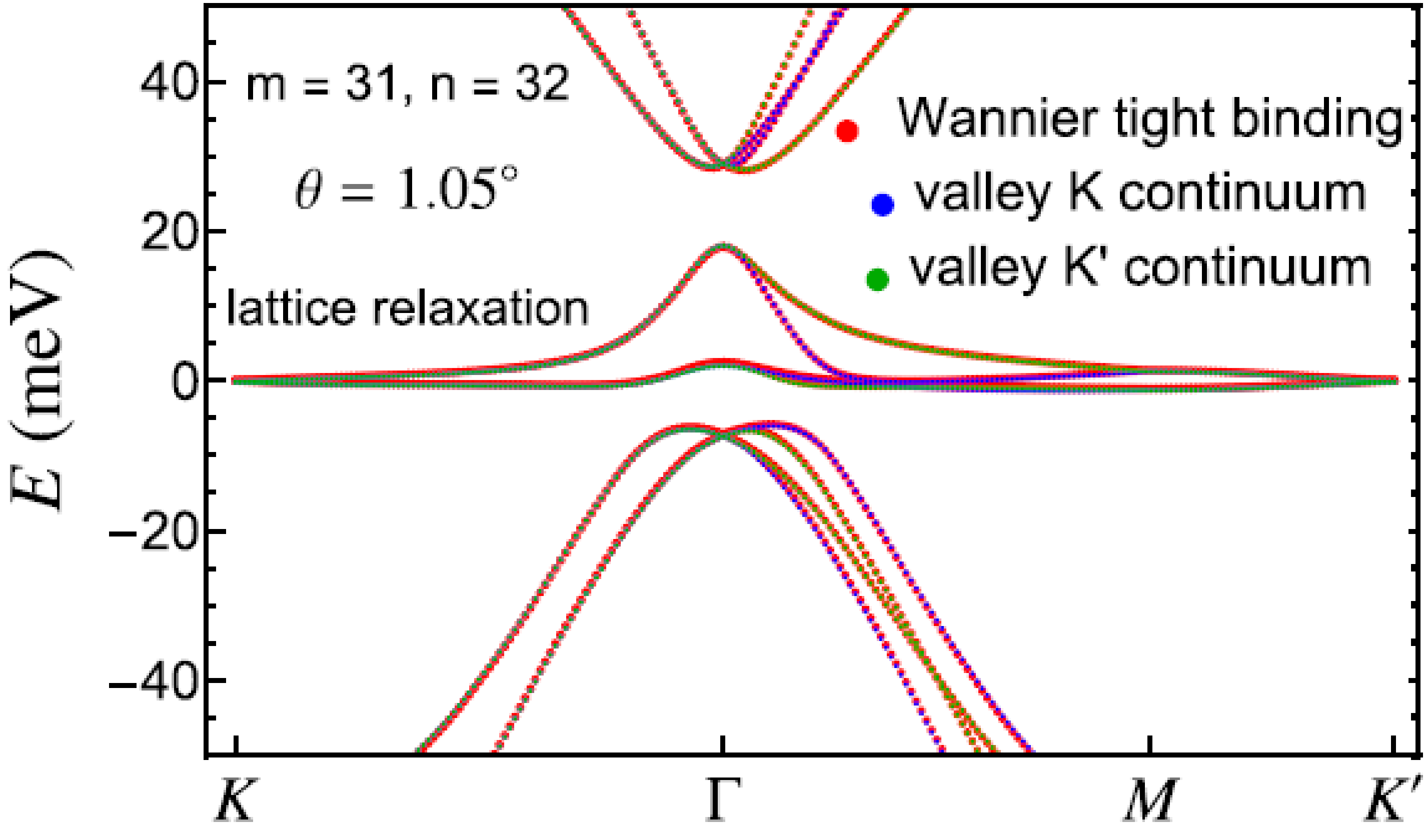

$$\delta \boldsymbol{U}(\boldsymbol{x}) = \boldsymbol{\nabla}\varphi^U(\boldsymbol{x}) + \boldsymbol{\nabla} \times \left(\hat{\boldsymbol{z}}\varepsilon^U(\boldsymbol{x})\right)$$

Jian Kang and OV, PRB **107,** 075408 (2023)

Minimal and next-to-leading order continuum model: spectrum

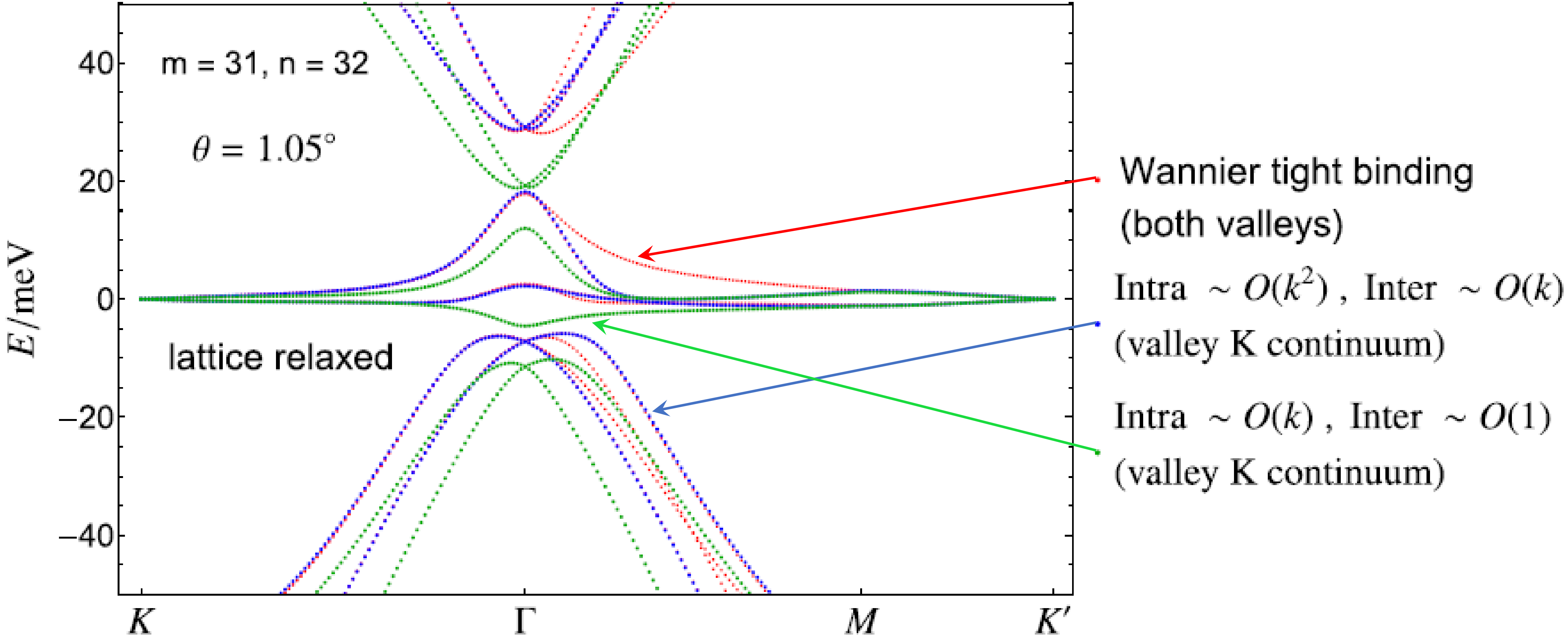

Jian Kang and OV, PRB **107,** 075408 (2023)

Minimal and next-to-leading order continuum model: wavefunctions

Berry curvature distribution further away from chiral limit

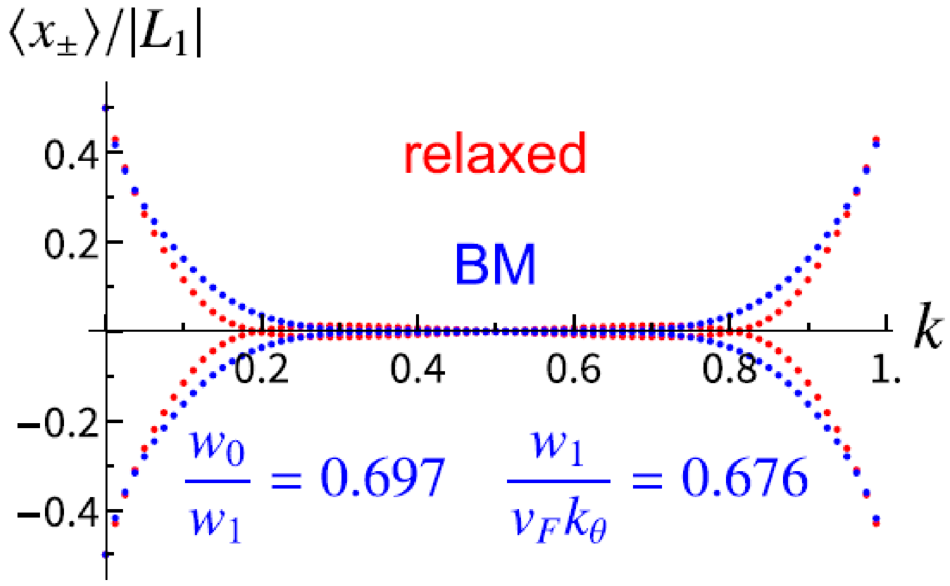

Deviations from 1 measure the p-h asymmetry of the narrow band wavefunctions

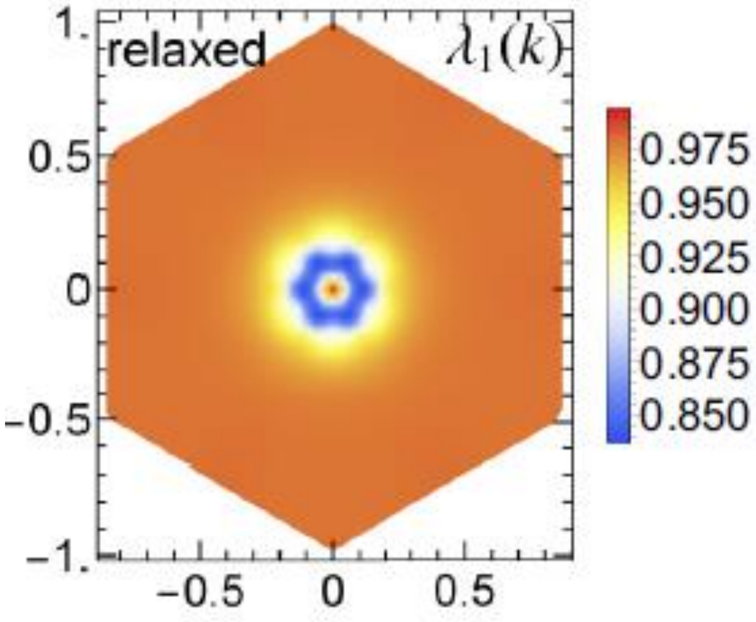

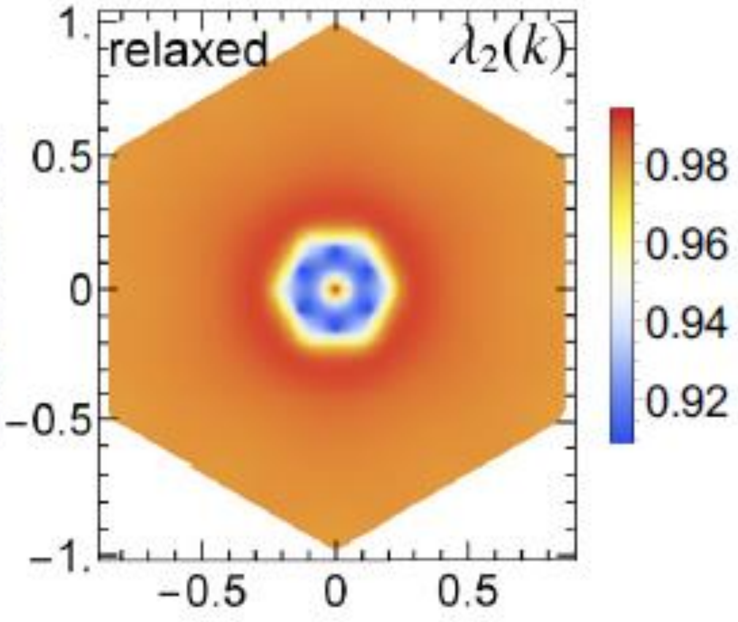

Jian Kang and OV, PRB **107,** 075408 (2023)

Topological heavy fermions in magnetic field

cc

$$
\begin{pmatrix}
0 & 0 & -i\sqrt{2}\frac{v_*}{\ell}\hat{a}^\dagger & 0 & \gamma\Sigma(\hat{a}^\dagger\hat{a}) & i\sqrt{2}\frac{v_*'}{\ell}\hat{a}\Sigma(\hat{a}^\dagger\hat{a}) \\
0 & 0 & 0 & i\sqrt{2}\frac{v_*}{\ell}\hat{a} & -i\sqrt{2}\frac{v_*'}{\ell}\hat{a}^\dagger\Sigma(\hat{a}^\dagger\hat{a}) & \gamma\Sigma(\hat{a}^\dagger\hat{a}) \\
i\sqrt{2}\frac{v_*}{\ell}\hat{a} & 0 & \frac{J}{2} & M\to 0 & 0 & 0 \\
0 & -i\sqrt{2}\frac{v_*}{\ell}\hat{a}^\dagger & M\to 0 & \frac{J}{2} & 0 & 0 \\
\gamma\Sigma(\hat{a}^\dagger\hat{a}) & i\sqrt{2}\frac{v_*'}{\ell}\Sigma(\hat{a}^\dagger\hat{a})\hat{a} & 0 & 0 & \frac{U_1}{2} & 0 \\
-i\sqrt{2}\frac{v_*'}{\ell}\Sigma(\hat{a}^\dagger\hat{a})\hat{a}^\dagger & \gamma\Sigma(\hat{a}^\dagger\hat{a}) & 0 & 0 & 0 & \frac{U_1}{2}
\end{pmatrix}
\begin{pmatrix} 0 \\ 0 \\ 0 \\ |0\rangle \\ 0 \\ 0 \end{pmatrix}
$$

ff

Keshav Singh, B.A. Bernevig et al, OV arXiv:2305.08171

Topological heavy fermions in magnetic field

cc

$$\begin{pmatrix} 0 & 0 & -i\sqrt{2}\frac{v_*}{\ell}\hat{a}^\dagger & 0 & \gamma\Sigma(\hat{a}^\dagger\hat{a}) & i\sqrt{2}\frac{v_*'}{\ell}\hat{a}\Sigma(\hat{a}^\dagger\hat{a}) \\ 0 & 0 & 0 & i\sqrt{2}\frac{v_*}{\ell}\hat{a} & -i\sqrt{2}\frac{v_*'}{\ell}\hat{a}^\dagger\Sigma(\hat{a}^\dagger\hat{a}) & \gamma\Sigma(\hat{a}^\dagger\hat{a}) \\ i\sqrt{2}\frac{v_*}{\ell}\hat{a} & 0 & \frac{J}{2} & M\to 0 & 0 & 0 \\ 0 & -i\sqrt{2}\frac{v_*}{\ell}\hat{a}^\dagger & M\to 0 & \frac{J}{2} & 0 & 0 \\ \gamma\Sigma(\hat{a}^\dagger\hat{a}) & i\sqrt{2}\frac{v_*'}{\ell}\Sigma(\hat{a}^\dagger\hat{a})\hat{a} & 0 & 0 & \frac{U_1}{2} & 0 \\ -i\sqrt{2}\frac{v_*'}{\ell}\Sigma(\hat{a}^\dagger\hat{a})\hat{a}^\dagger & \gamma\Sigma(\hat{a}^\dagger\hat{a}) & 0 & 0 & 0 & \frac{U_1}{2} \end{pmatrix} \begin{pmatrix} 0 \\ c_2^{(3)}|0\rangle \\ 0 \\ c_4^{(3)}|1\rangle \\ 0 \\ c_6^{(3)}|0\rangle \end{pmatrix}$$

ff

Keshav Singh, B.A. Bernevig et al, OV arXiv:2305.08171

Topological heavy fermions in magnetic field

cc

$$\begin{pmatrix} 0 & 0 & -i\sqrt{2}\frac{v_*}{\ell}\hat{a}^\dagger & 0 & \gamma\Sigma(\hat{a}^\dagger\hat{a}) & i\sqrt{2}\frac{v_*'}{\ell}\hat{a}\Sigma(\hat{a}^\dagger\hat{a}) \\ 0 & 0 & 0 & i\sqrt{2}\frac{v_*}{\ell}\hat{a} & -i\sqrt{2}\frac{v_*'}{\ell}\hat{a}^\dagger\Sigma(\hat{a}^\dagger\hat{a}) & \gamma\Sigma(\hat{a}^\dagger\hat{a}) \\ i\sqrt{2}\frac{v_*}{\ell}\hat{a} & 0 & \frac{J}{2} & M\to 0 & 0 & 0 \\ 0 & -i\sqrt{2}\frac{v_*}{\ell}\hat{a}^\dagger & M\to 0 & \frac{J}{2} & 0 & 0 \\ \gamma\Sigma(\hat{a}^\dagger\hat{a}) & i\sqrt{2}\frac{v_*'}{\ell}\Sigma(\hat{a}^\dagger\hat{a})\hat{a} & 0 & 0 & \frac{U_1}{2} & 0 \\ -i\sqrt{2}\frac{v_*'}{\ell}\Sigma(\hat{a}^\dagger\hat{a})\hat{a}^\dagger & \gamma\Sigma(\hat{a}^\dagger\hat{a}) & 0 & 0 & 0 & \frac{U_1}{2} \end{pmatrix} \begin{pmatrix} c_1^{(5)}|0\rangle \\ c_2^{(5)}|1\rangle \\ 0 \\ c_4^{(5)}|2\rangle \\ c_5^{(5)}|0\rangle \\ c_6^{(5)}|1\rangle \end{pmatrix}$$

ff

Keshav Singh, B.A. Bernevig et al, OV arXiv:2305.08171

Topological heavy fermions in magnetic field

cc

ff

$$
\begin{pmatrix}
0 & 0 & -i\sqrt{2}\frac{v_*}{\ell}\hat{a}^\dagger & 0 & \gamma\Sigma(\hat{a}^\dagger\hat{a}) & i\sqrt{2}\frac{v_*'}{\ell}\hat{a}\Sigma(\hat{a}^\dagger\hat{a}) \\
0 & 0 & 0 & i\sqrt{2}\frac{v_*}{\ell}\hat{a} & -i\sqrt{2}\frac{v_*'}{\ell}\hat{a}^\dagger\Sigma(\hat{a}^\dagger\hat{a}) & \gamma\Sigma(\hat{a}^\dagger\hat{a}) \\
i\sqrt{2}\frac{v_*}{\ell}\hat{a} & 0 & \frac{J}{2} & M\to 0 & 0 & 0 \\
0 & -i\sqrt{2}\frac{v_*}{\ell}\hat{a}^\dagger & M\to 0 & \frac{J}{2} & 0 & 0 \\
\gamma\Sigma(\hat{a}^\dagger\hat{a}) & i\sqrt{2}\frac{v_*'}{\ell}\Sigma(\hat{a}^\dagger\hat{a})\hat{a} & 0 & 0 & \frac{U_1}{2} & 0 \\
-i\sqrt{2}\frac{v_*'}{\ell}\Sigma(\hat{a}^\dagger\hat{a})\hat{a}^\dagger & \gamma\Sigma(\hat{a}^\dagger\hat{a}) & 0 & 0 & 0 & \frac{U_1}{2}
\end{pmatrix}
\begin{pmatrix}
c_1^{(6m)}|m-1\rangle \\
c_2^{(6m)}|m\rangle \\
c_2^{(6m)}|m-2\rangle \\
c_4^{(6m)}|m+1\rangle \\
c_5^{(6m)}|m-1\rangle \\
c_6^{(6m)}|m\rangle
\end{pmatrix}
$$

Keshav Singh, B.A. Bernevig et al, OV arXiv:2305.08171

Strong coupling limit magic angle

Parameter choices:

$$\frac{w_1}{v_F k_\theta} = 0.586, \frac{w_0}{w_1} = 0.7, V_q = \frac{2\pi}{\epsilon_r q}\tanh\frac{q\xi}{2}, \xi = L_m, \epsilon_r = 15$$

Dropping small angle rotation of Pauli matrices

Hartree Fock density matrix: $P_{\alpha\beta}(k) \equiv \langle d^+_{\alpha k} d_{\beta k}\rangle$, where α, β labels valley, spin, and 2q bands

Strong coupling limit and finite field Hartree Fock at flux $\frac{\phi}{\phi_0} = \frac{1}{4}$:

(s,t) = (0,0)

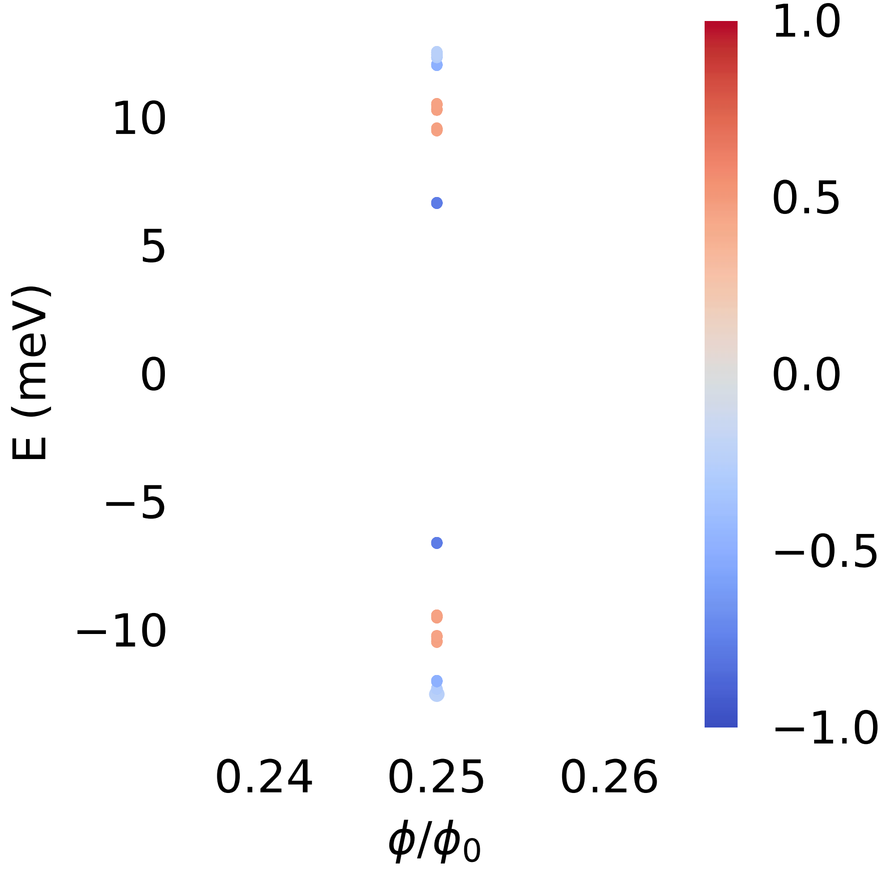

$\Delta \approx 13.23\text{meV}$

Density matrix in BM eigen basis;
U(4) valley spin rotation symmetry

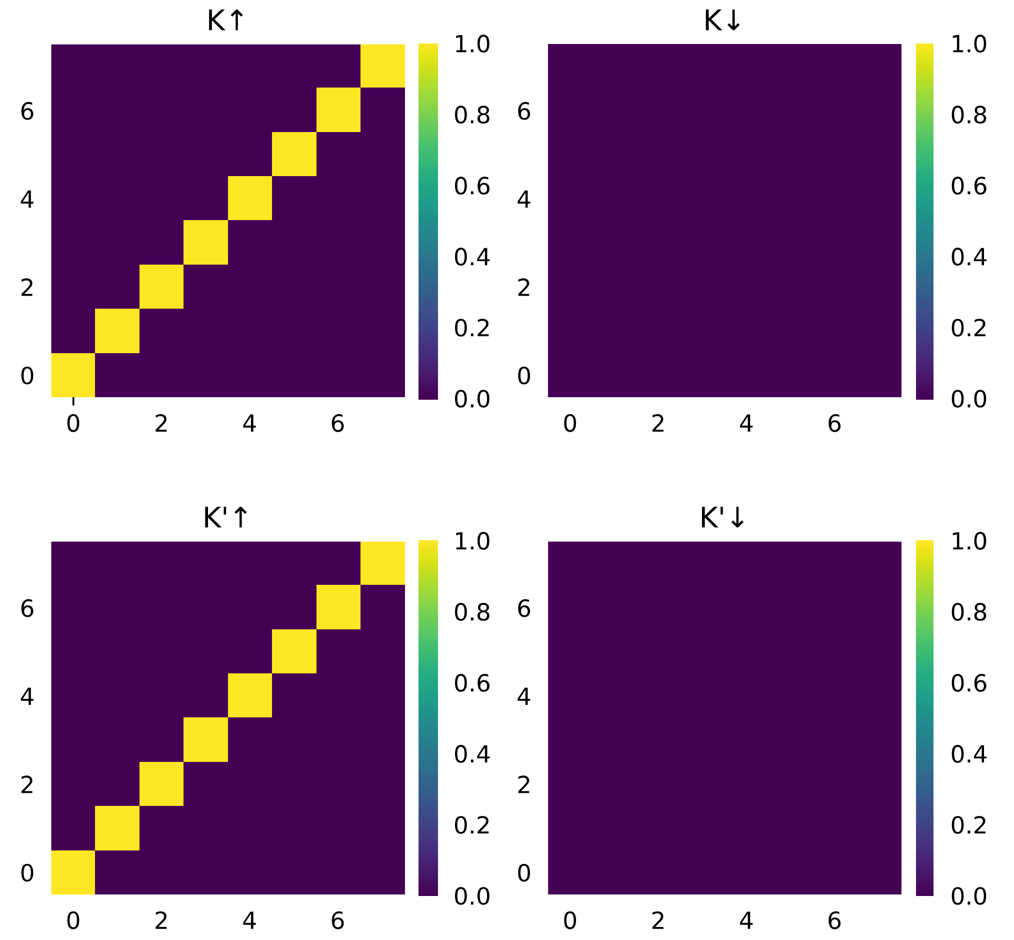

Strong coupling limit and finite field Hartree Fock at flux $\frac{\phi}{\phi_0} = \frac{1}{4}$:

At low densities, Hartree-Fock spectrum corresponds to populating lowest energy strong coupling spectrum

Quantum Hall ferromagnetism at (s,t) = (0,1)

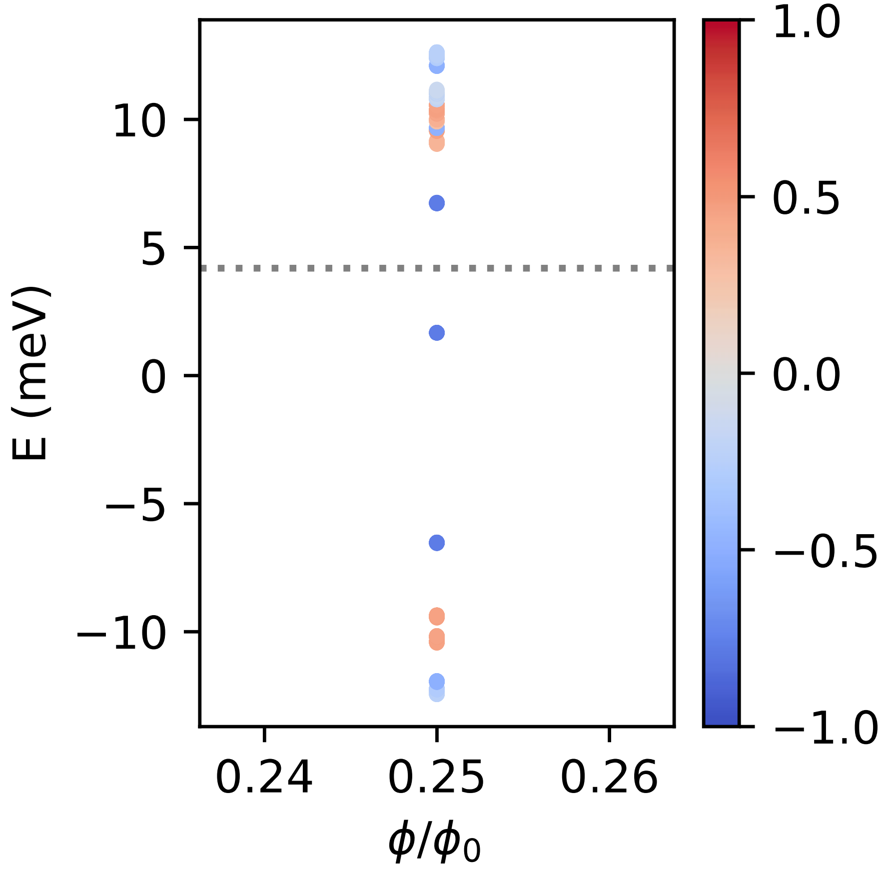

$\Delta \approx 5.05\text{meV}$

Density matrix in strong coupling basis

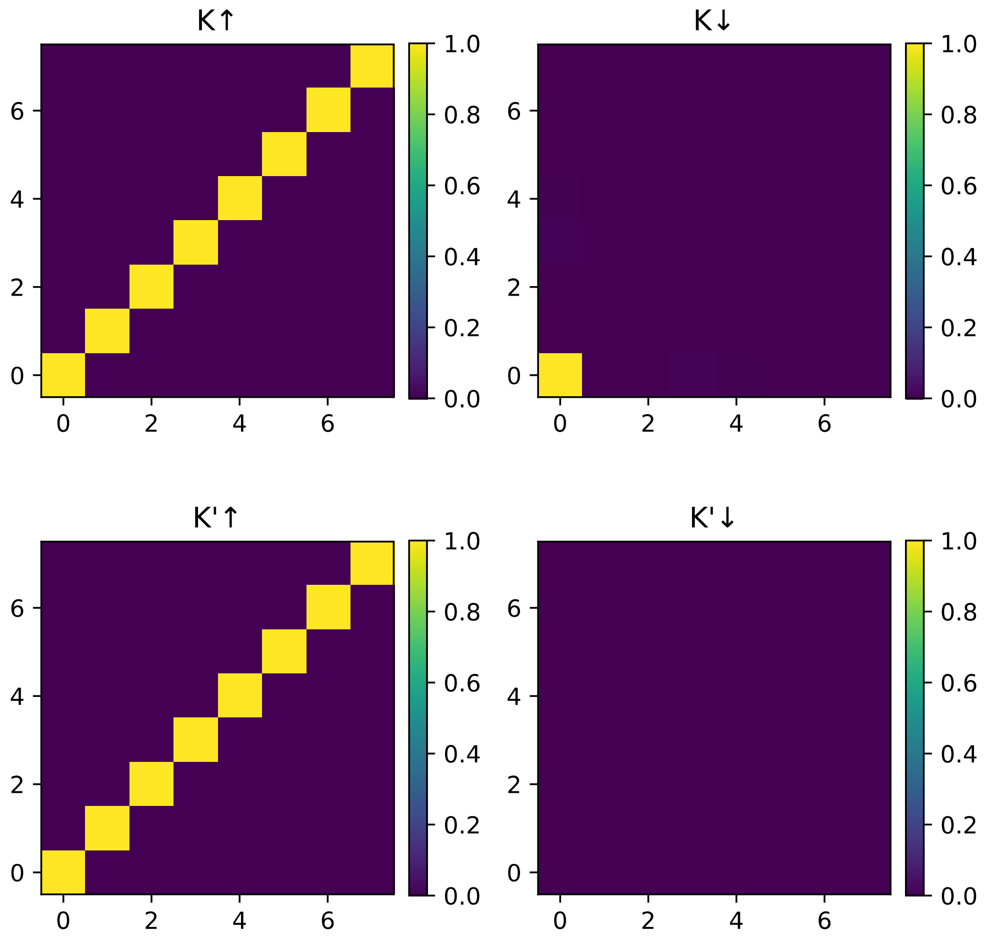

Strong coupling limit and finite field Hartree Fock at flux $\frac{\phi}{\phi_0} = \frac{1}{4}$:

At low densities, Hartree-Fock spectrum corresponds to populating lowest energy strong coupling spectrum

(s,t) = (0,2)

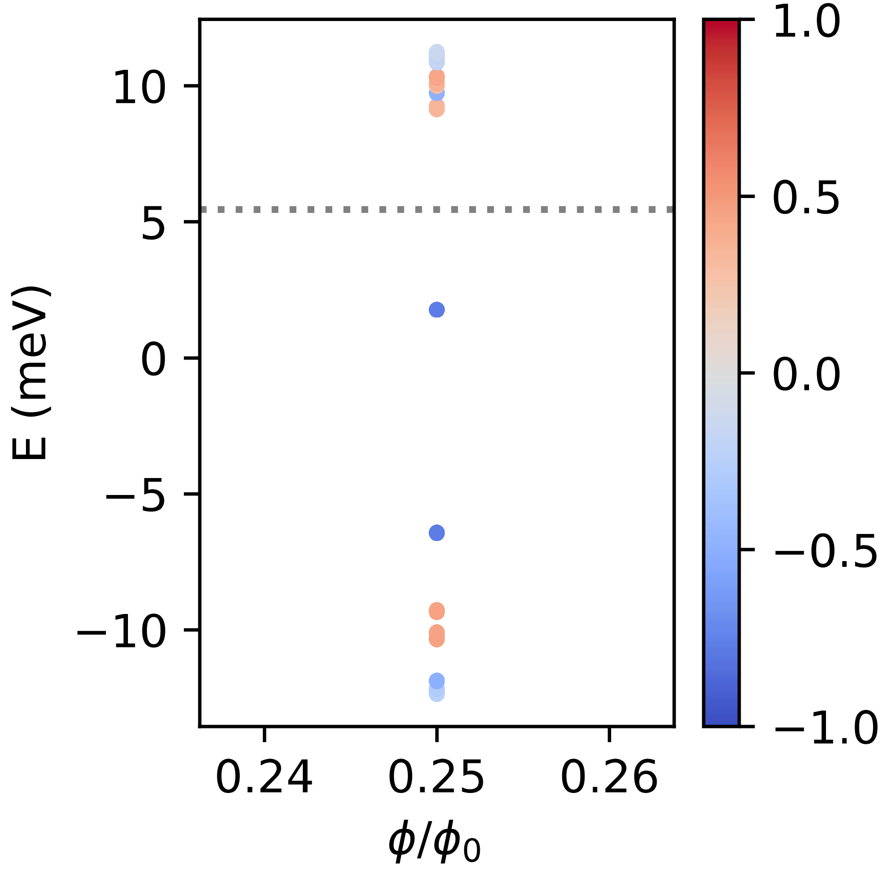

$\Delta \approx 7.36\text{meV}$

Density matrix in strong coupling basis

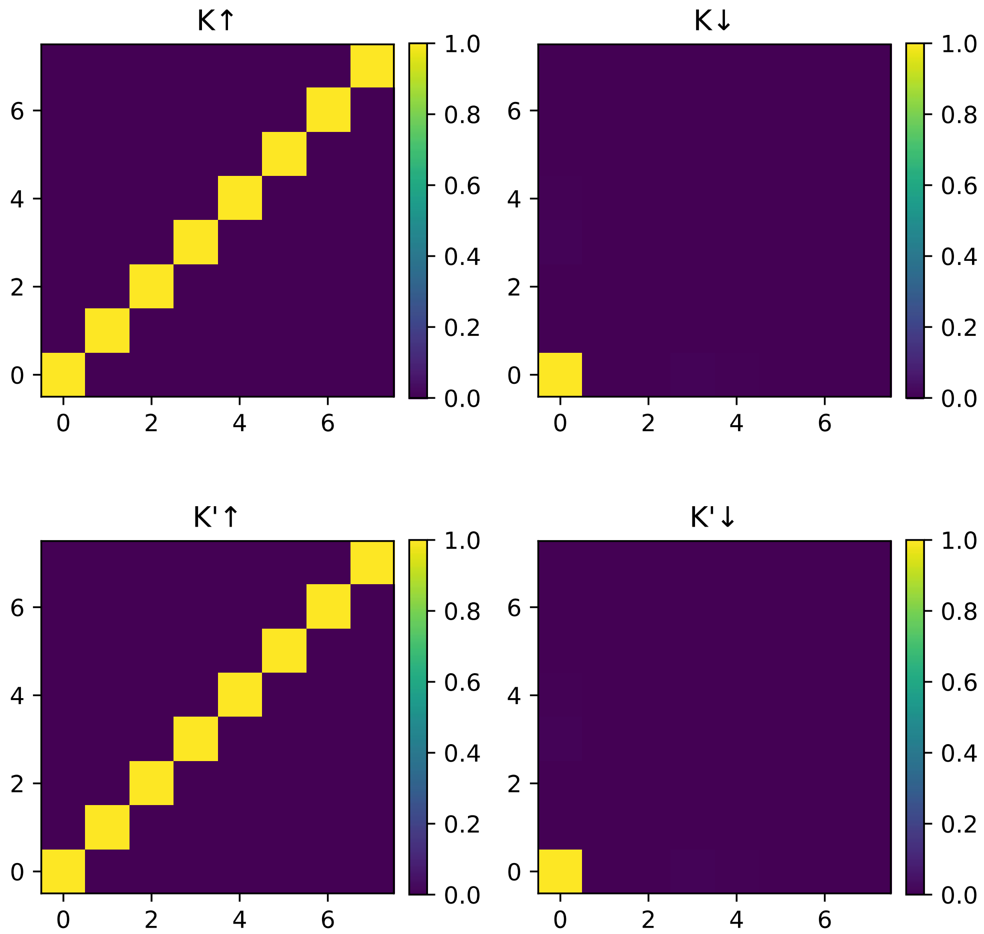

Strong coupling limit and finite field Hartree Fock at flux $\frac{\phi}{\phi_0} = \frac{1}{4}$:

At higher densities, Hartree-Fock reorganizes the wavefunctions from CNP

Spectrum indicative of a first order phase transition near (s,t) = (0,3)

Heavy part of the spectrum gets brought down in energy instead of light ones

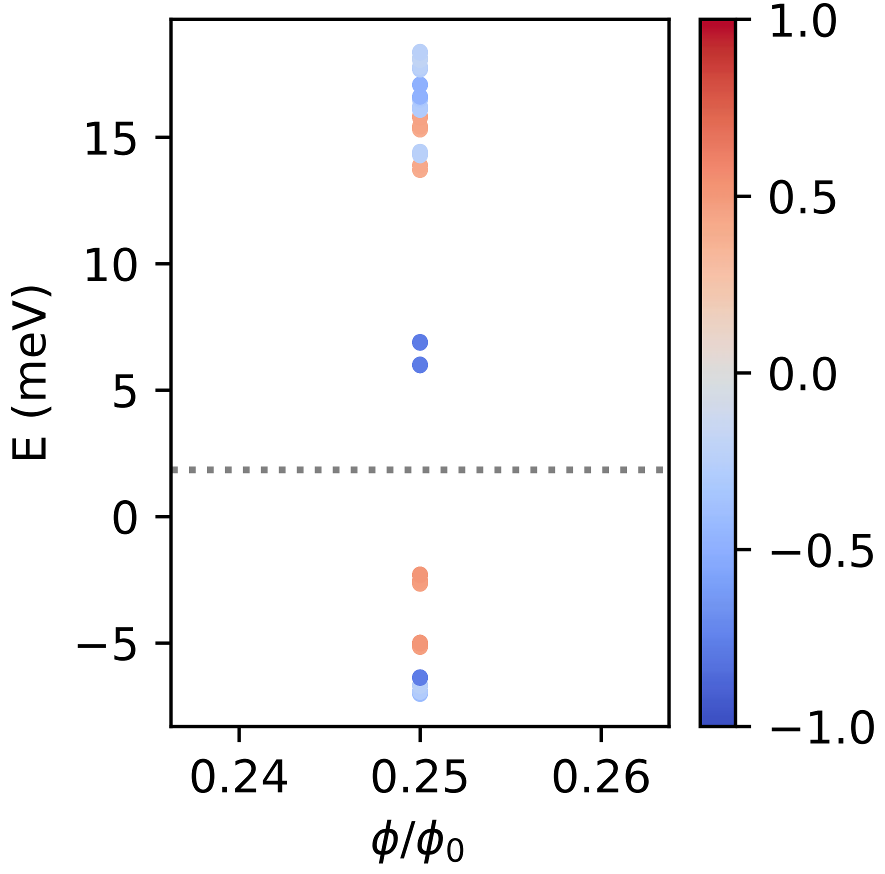

$\Delta \approx 8.26\text{meV}$

Density matrix in strong coupling basis

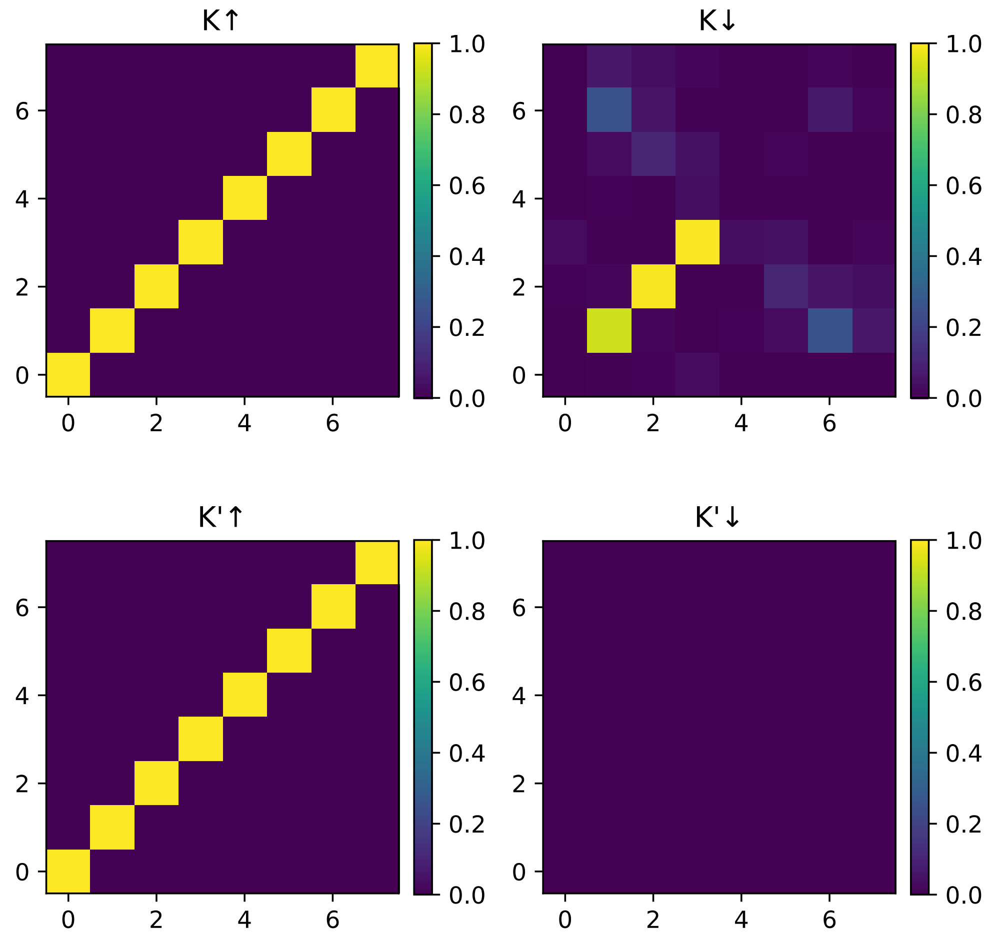

Strong coupling limit and finite field Hartree Fock at flux $\frac{\phi}{\phi_0} = \frac{1}{4}$:

At higher densities, Hartree-Fock reorganizes the wavefunctions from CNP

(s,t) = (0,4)

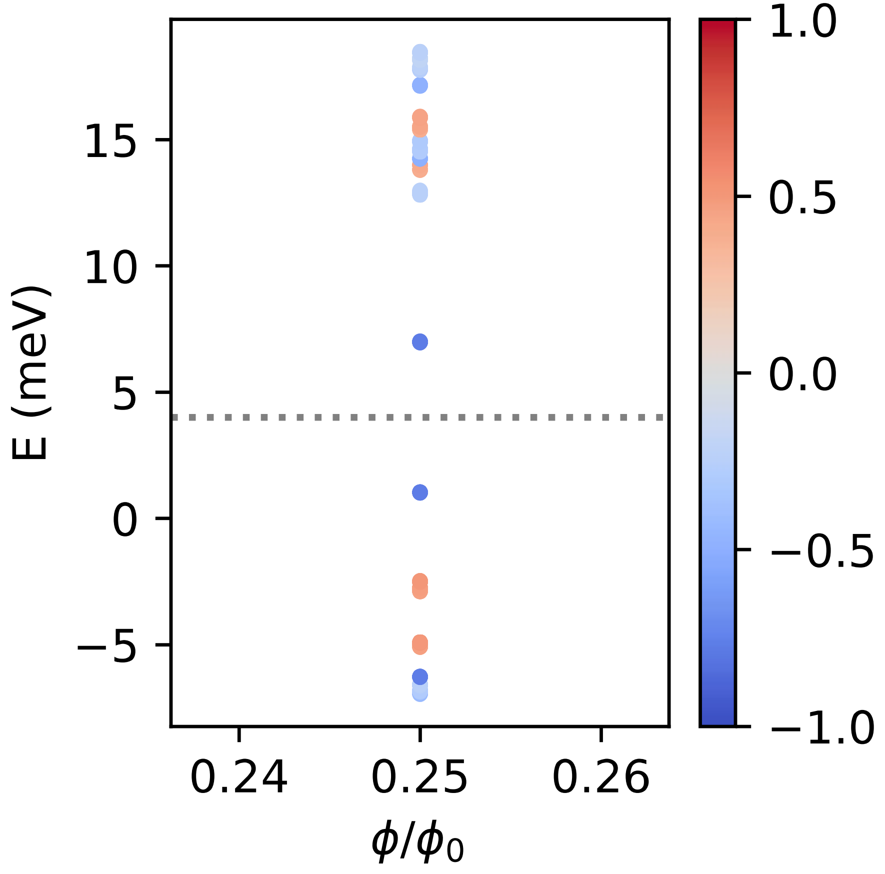

$\Delta \approx 5.92\text{meV}$

Density matrix in strong coupling basis

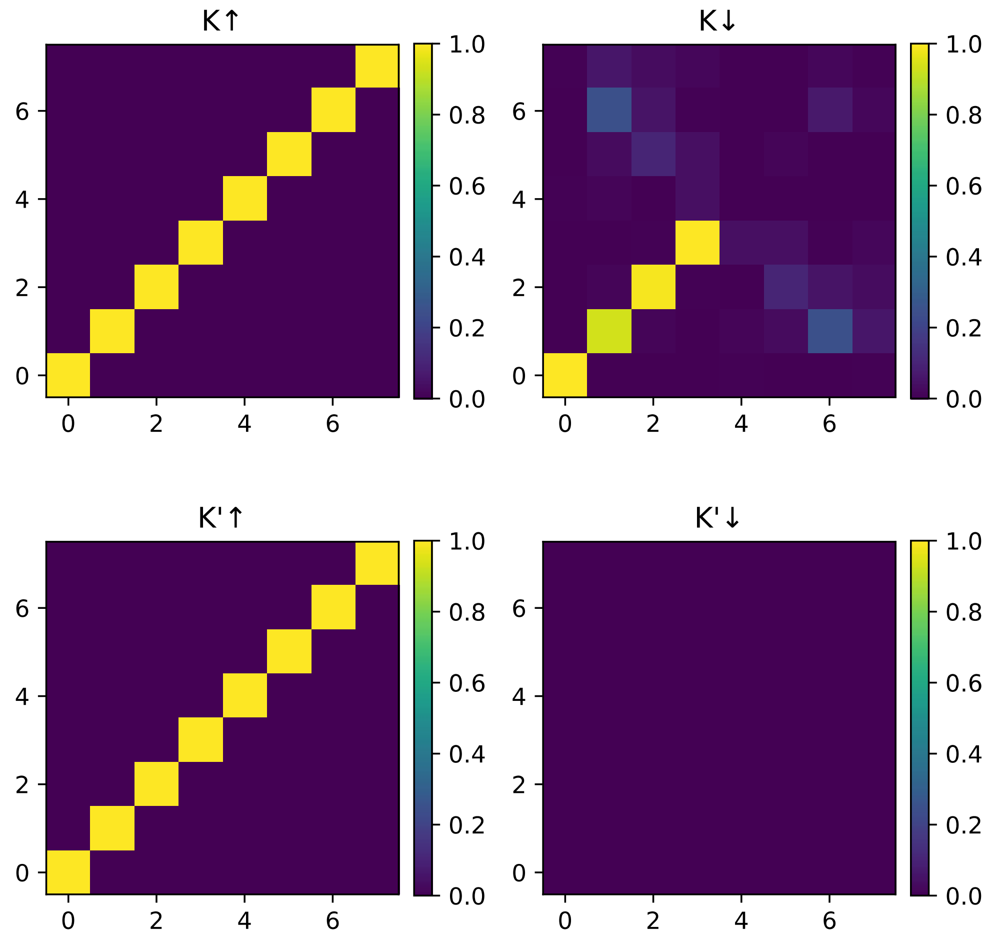

Strong coupling limit and finite field Hartree Fock at flux $\frac{\phi}{\phi_0} = \frac{1}{4}$:

Heavy-light dichotomy at (s,t) = (2,0)

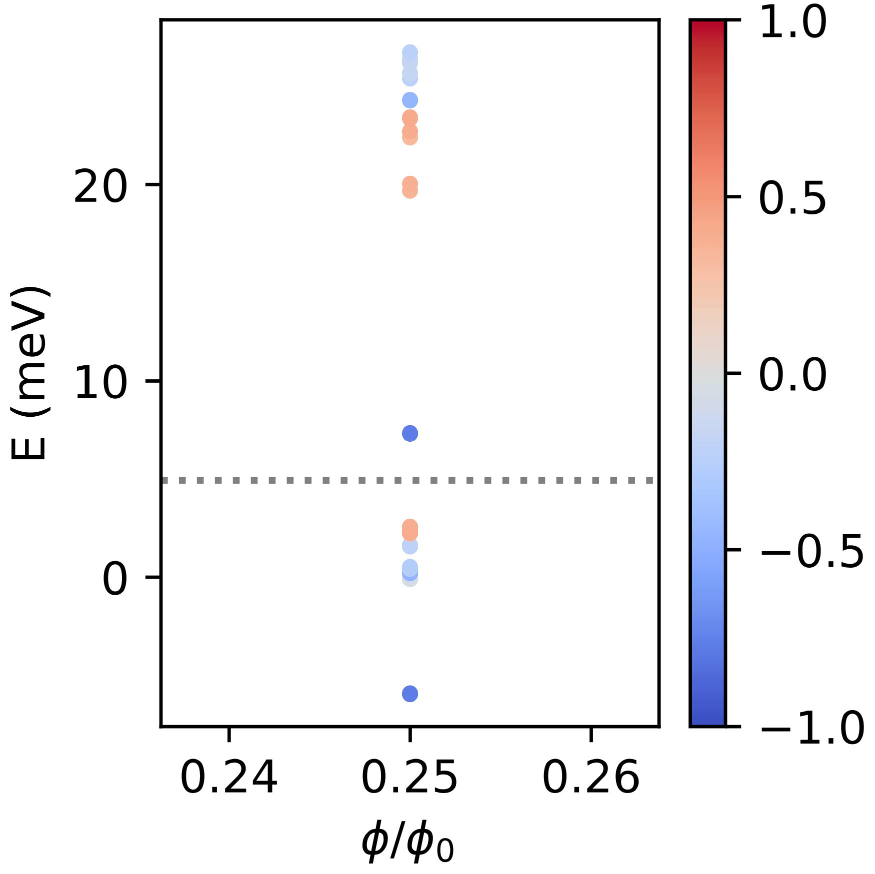

$\Delta \approx 4.72\text{meV}$

Density matrix in BM eigen basis;
U(4) valley spin rotation symmetry

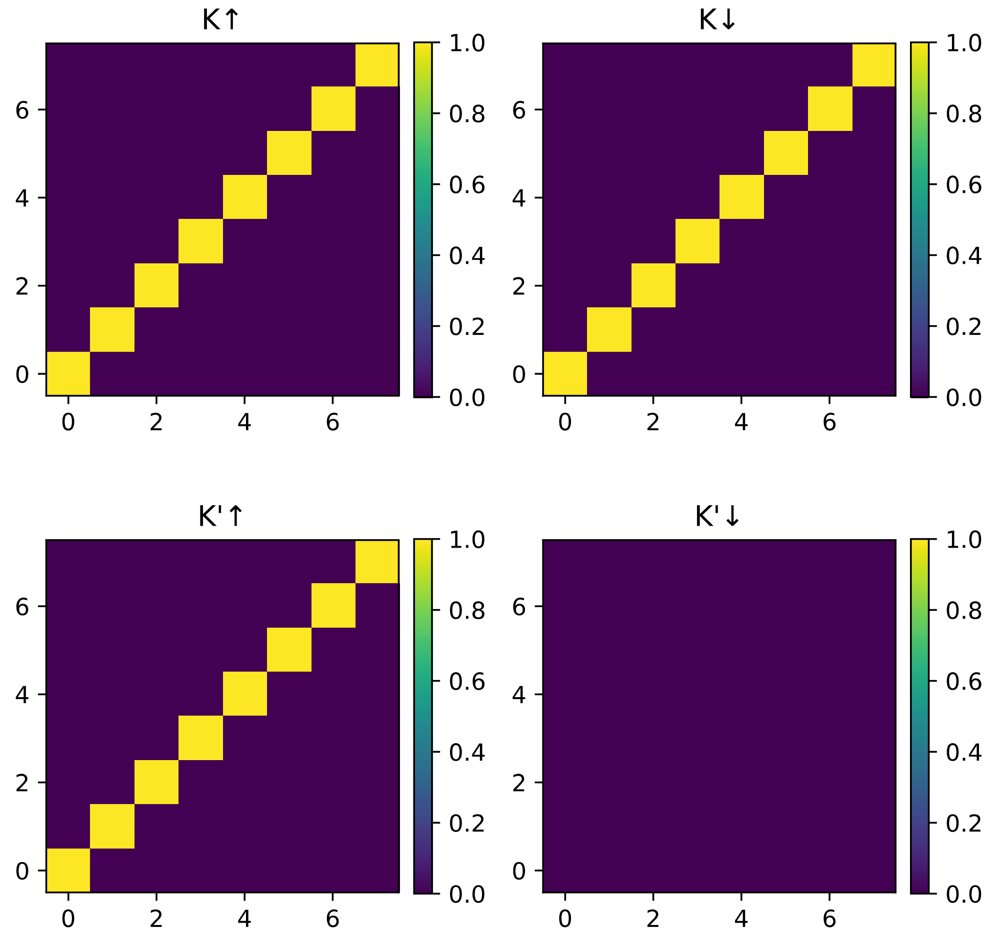

Strong coupling limit and finite field Hartree Fock at flux $\frac{\phi}{\phi_0} = \frac{1}{4}$:

At low densities, Hartree-Fock spectrum corresponds to populating lowest energy strong coupling spectrum

(s,t) = (2,1)

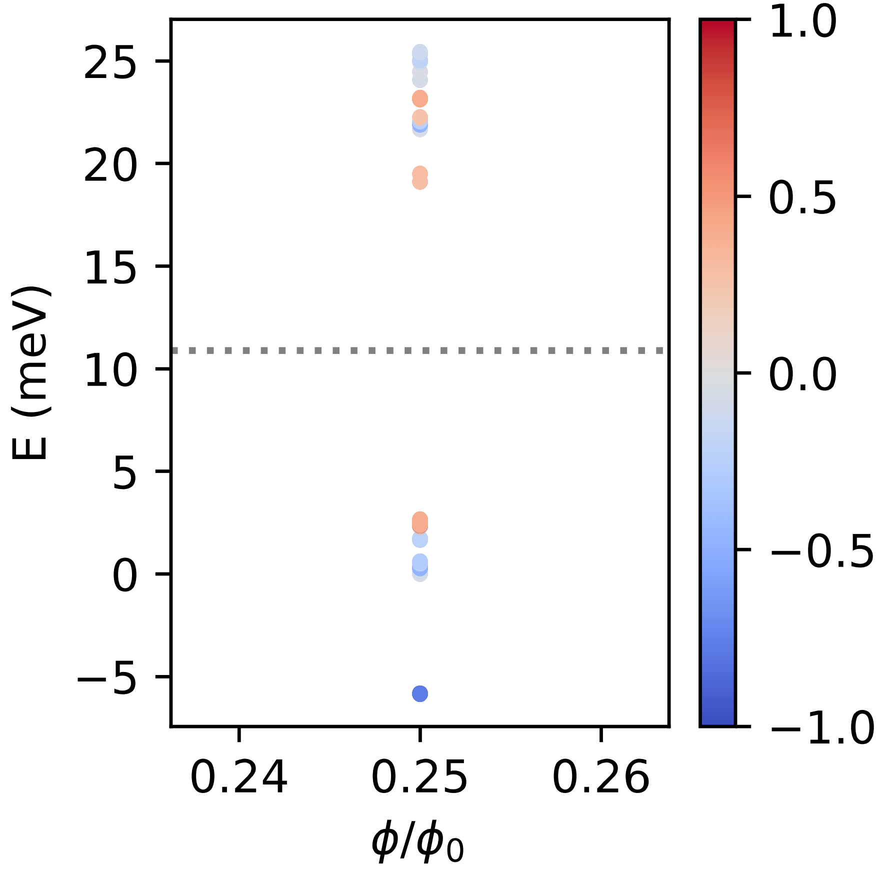

$\Delta \approx 16.44\text{meV}$

Density matrix in strong coupling basis

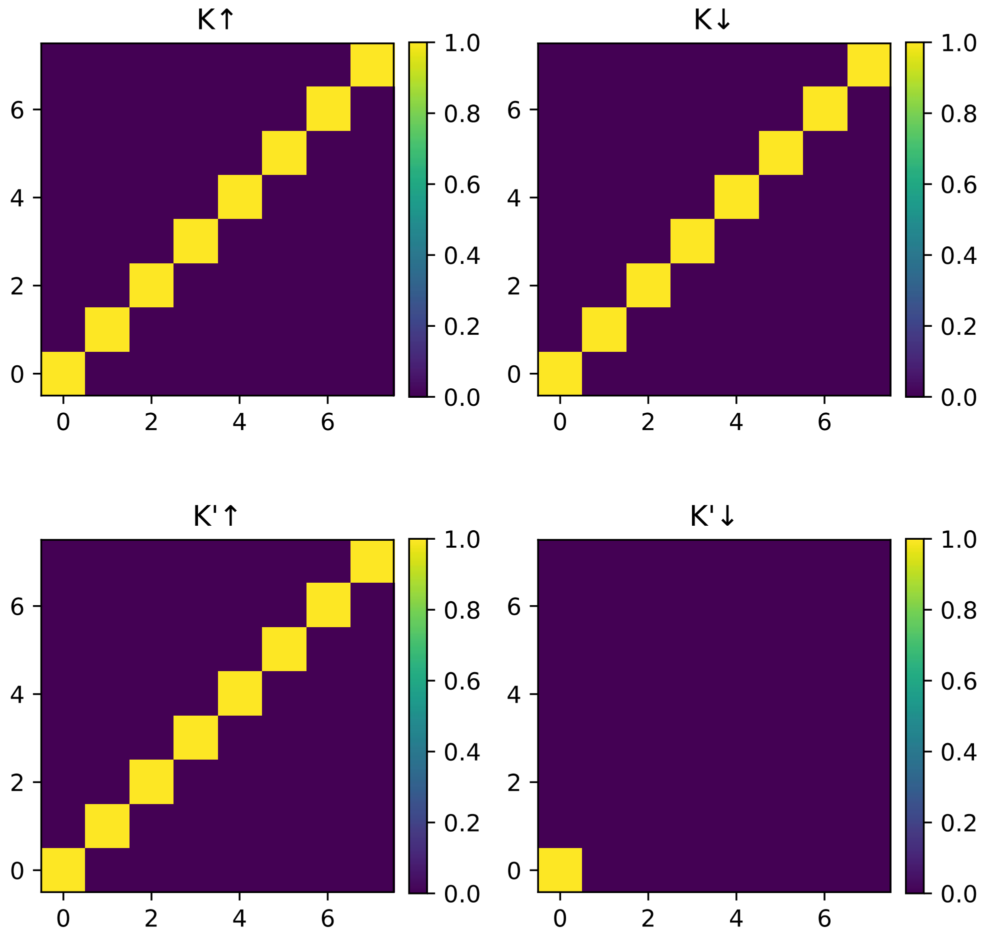

Strong coupling limit and finite field Hartree Fock at flux $\frac{\phi}{\phi_0} = \frac{1}{4}$:

At low densities, Hartree-Fock spectrum corresponds to populating lowest energy strong coupling spectrum

(s,t) = (2,2)

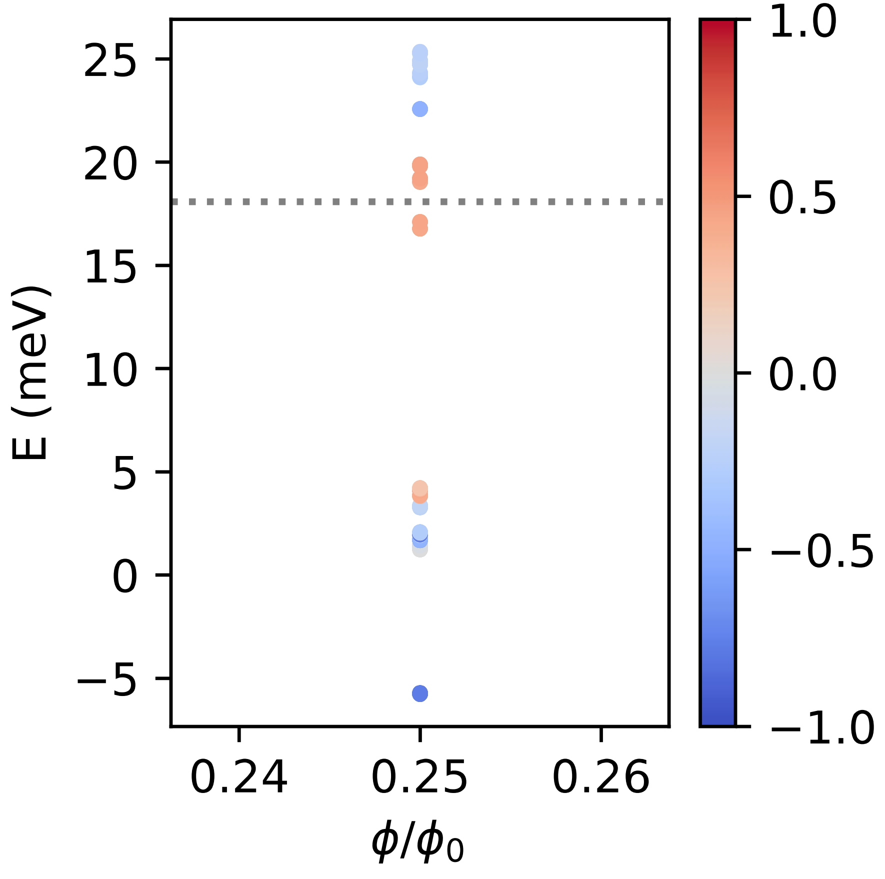

$\Delta \approx 1.92\text{meV}$

Density matrix in strong coupling basis

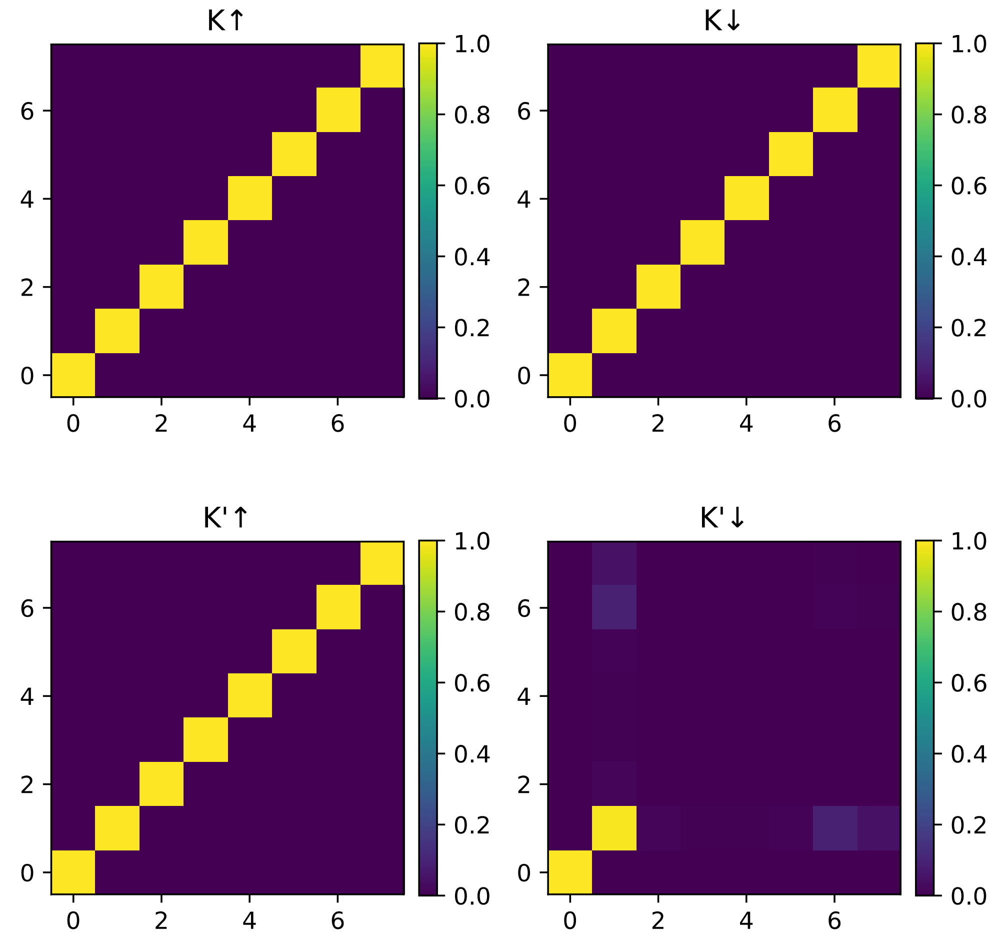

Strong coupling limit and finite field Hartree Fock at flux $\frac{\phi}{\phi_0} = \frac{1}{4}$:

A highly energetically competitive state at (s,t) = (2,2) is maximum Chern polarization

HF energy (chern): ≈ -4.36meV per u.c.
HF energy (flavor): ≈ -4.54meV per u.c.

Can tip the energetic favor with w0/w1, screening length etc.

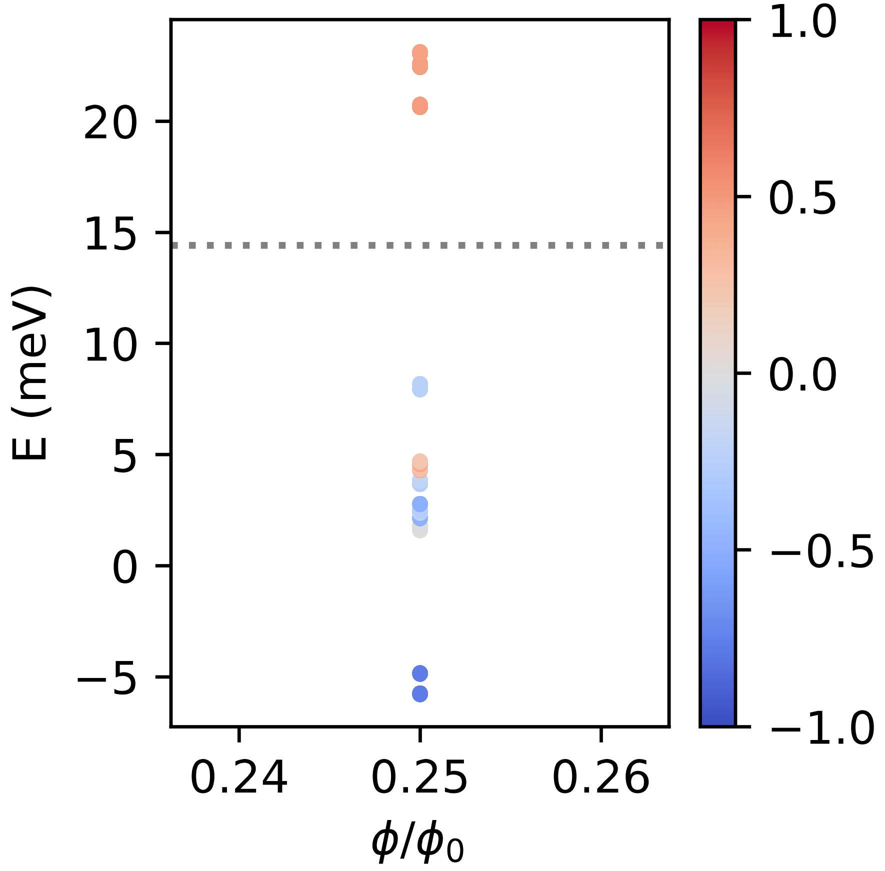

$\Delta \approx 12.44$meV

Density matrix in sublattice x valley τ_z eigenbasis;
U(4) valley spin rotation symmetry

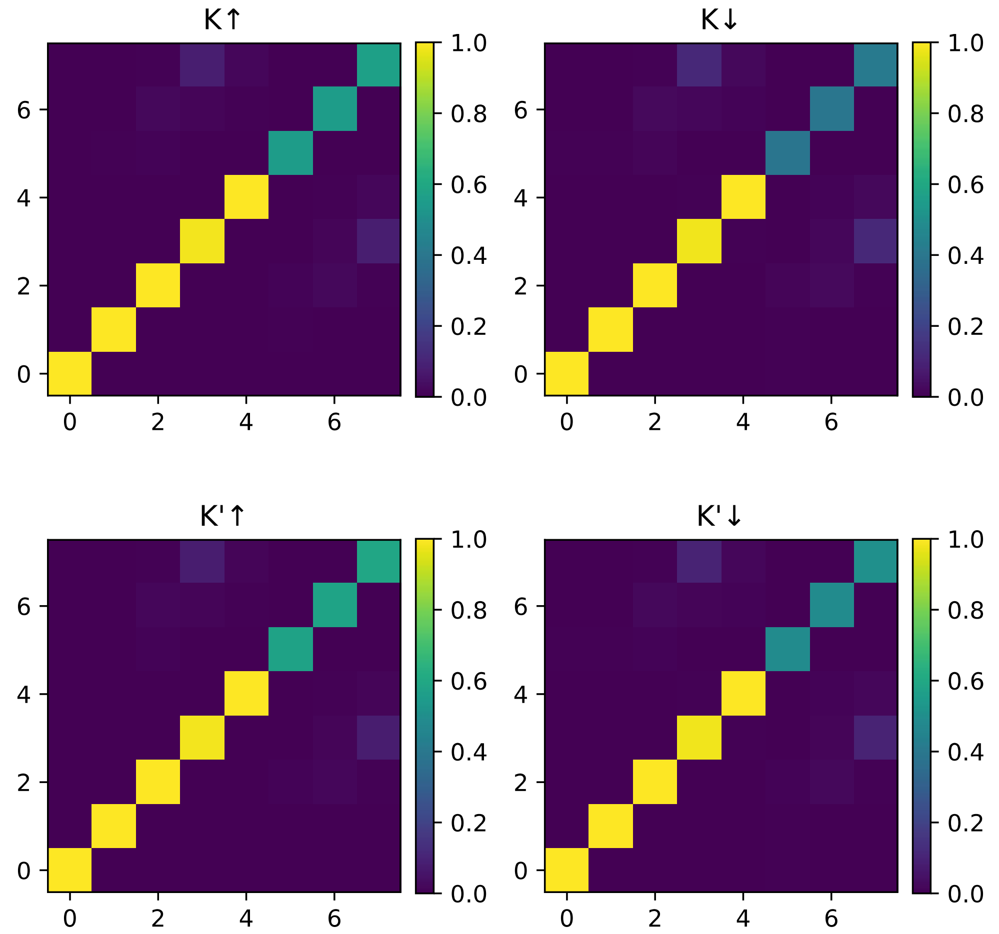

Hartree Fock spectral gaps on various Streda lines at flux 1/4

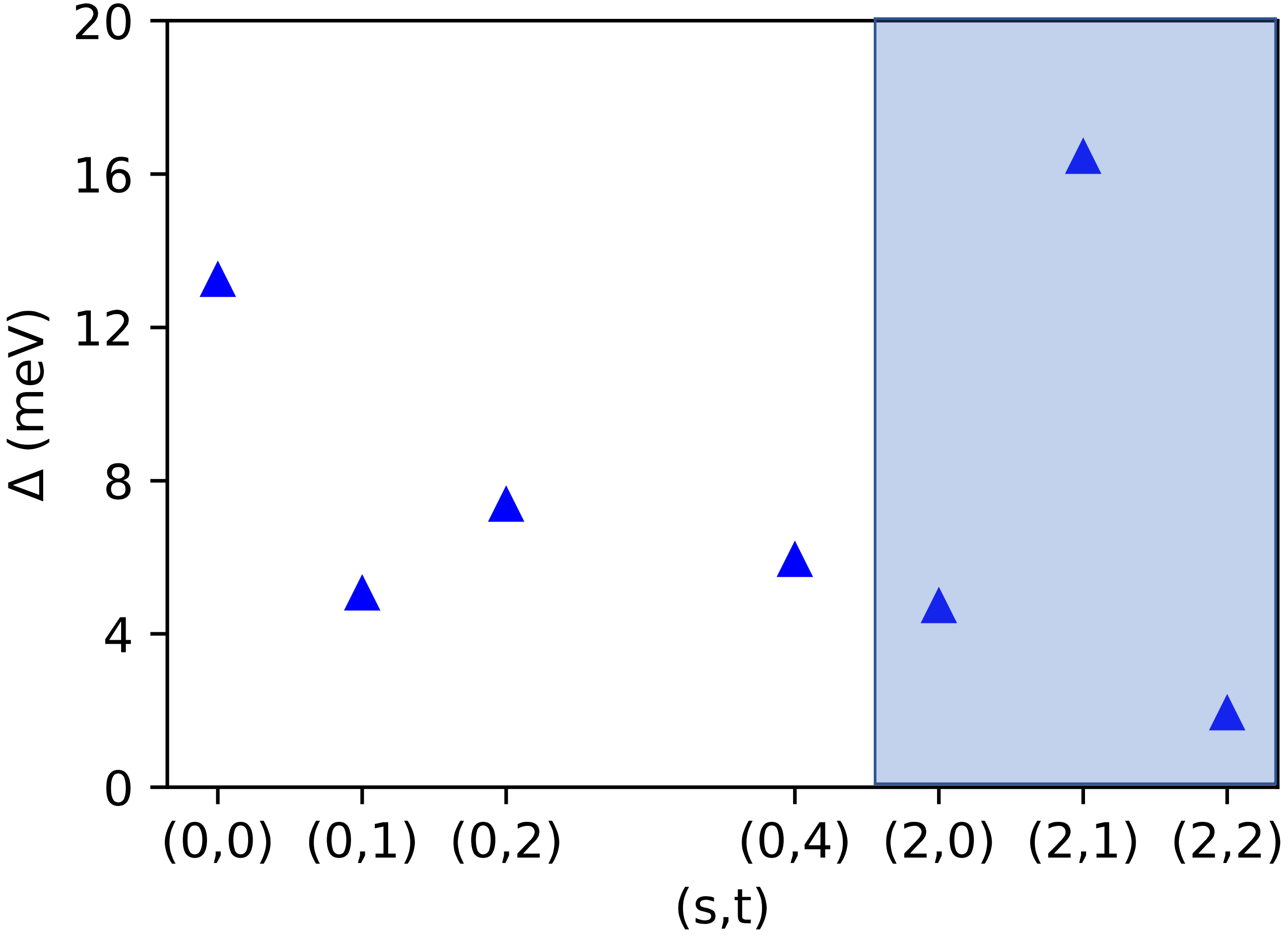

Analytic construction of exact zero modes at $\boldsymbol{B} \neq 0$ in the chiral limit: anomaly and the index theorem

$$H_{BM} = \begin{pmatrix} v_F \sigma \cdot (\boldsymbol{p} - \frac{e}{c}\boldsymbol{A}) & T(\boldsymbol{r}) e^{i\boldsymbol{q}_1 \cdot \boldsymbol{r}} \\ e^{-i\boldsymbol{q}_1 \cdot \boldsymbol{r}} T^\dagger(\boldsymbol{r}) & v_F \sigma \cdot (\boldsymbol{p} + \boldsymbol{q}_1 - \frac{e}{c}\boldsymbol{A}) \end{pmatrix}$$

Laughlin gauge: $\boldsymbol{A} = \frac{1}{2} B(-y, x)$

Let $\begin{pmatrix} A_{top} \\ B_{top} \\ A_{bot} \\ B_{bot} \end{pmatrix} \longrightarrow \begin{pmatrix} A_{top} \\ A_{bot} \\ B_{top} \\ B_{bot} \end{pmatrix}$ then $H_{BM} \longrightarrow \begin{pmatrix} 0 & D^\dagger \\ D & 0 \end{pmatrix}$

$$D = \begin{pmatrix} -iv_F \left(2\frac{\partial}{\partial \bar{z}} + \frac{z}{2\ell_B^2} \right) & w_1 U(\boldsymbol{r}) e^{i\boldsymbol{q}_1 \cdot \boldsymbol{r}} \\ w_1 U(-\boldsymbol{r}) e^{-i\boldsymbol{q}_1 \cdot \boldsymbol{r}} & -iv_F \left(2\frac{\partial}{\partial \bar{z}} + k_\theta + \frac{z}{2\ell_B^2} \right) \end{pmatrix}$$

Unlike at $\boldsymbol{B} = 0$, there is no normalizable state on B-sublattice

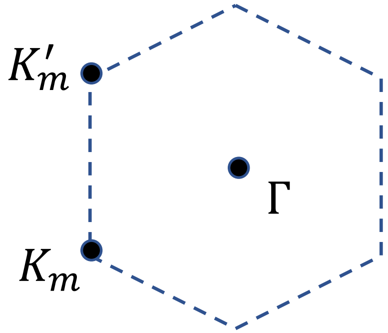

$$f(z) e^{-\bar{z}z/4\ell_B^2} \begin{pmatrix} \Psi_{K_m}^{\boldsymbol{B}=0}(\boldsymbol{r}) \\ 0 \end{pmatrix}$$

$$f(z) e^{-\bar{z}z/4\ell_B^2} \begin{pmatrix} \Psi_{K_m'}^{\boldsymbol{B}=0}(\boldsymbol{r}) \\ 0 \end{pmatrix}$$

Popov and Milekhin PRB2021, Sheffer and Stern PRB2021; X. Wang and OV arXiv:2112.08620

Analytic construction of exact zero modes at $\boldsymbol{B} \neq 0$ in the chiral limit: anomaly and the index theorem

$\boldsymbol{B} = 0$ zero energy states at K_m and K'_m have an opposite parity under $PC_{2y}T$

Laughlin gauge: $\boldsymbol{A} = \frac{1}{2}B(-y, x)$

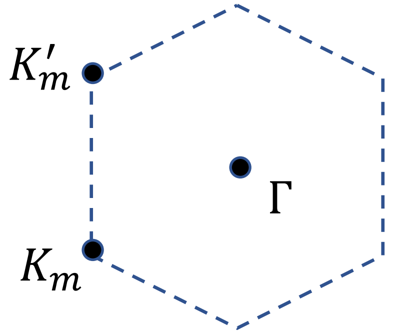

Letting $f(z) = (1, z, z^2, \ldots, z^{N-1})$ we therefore prove linear independence of 2Landau levels worth of exact zero energy states living on A sublattice

So for each $k_1 \in (0,1)$ and $k_2 \in (0, \frac{1}{q})$ we have $2p$ zero modes

$$f(z)e^{-\bar{z}z/4\ell_B^2}\begin{pmatrix}\Psi_{K_m}^{B=0}(\boldsymbol{r}) \\ 0\end{pmatrix}$$

$$f(z)e^{-\bar{z}z/4\ell_B^2}\begin{pmatrix}\Psi_{K'_m}^{B=0}(\boldsymbol{r}) \\ 0\end{pmatrix}$$

Because $\{H_{BM}, \sigma_z\} = 0$, by index theorem we must have

$$Tr\langle\sigma_z\rangle = n_+ - n_- = 2p$$

At $\boldsymbol{B} = 0, Tr\langle\sigma_z\rangle = 0.$
Therefore $Tr\langle\sigma_z\rangle$ is *discontinuous* at $\boldsymbol{B} = 0$

Popov and Milekhin PRB2021, Sheffer and Stern PRB2021; X. Wang and OV arXiv:2112.08620

Exact single particle excitation spectrum at CNP in the strong coupling limit at small B-field at a single k_1, k_2

$$\frac{w_0}{w_1} = 0$$

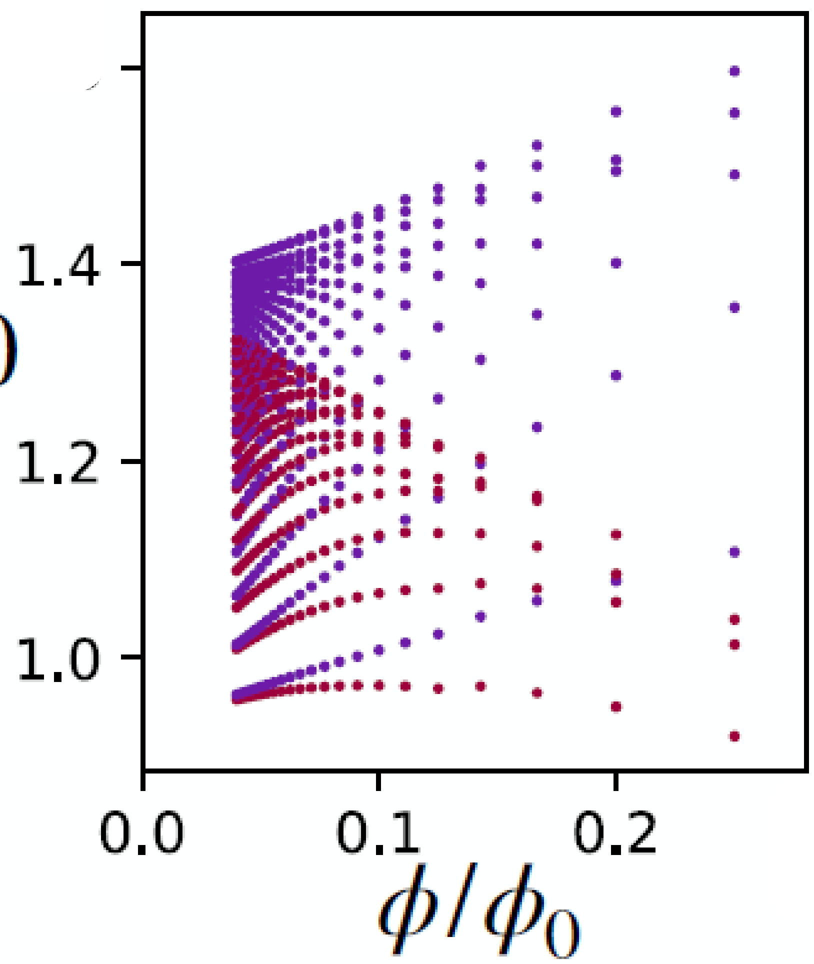

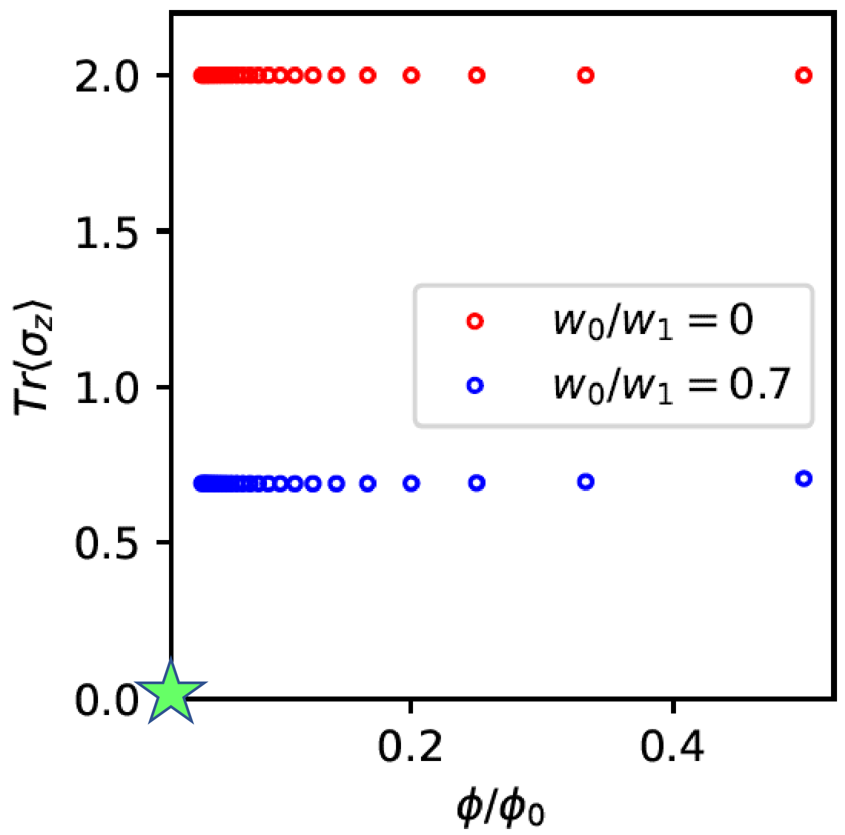

Evolution of the dispersion with interaction at $\nu = -4$ from weak to intermediate coupling

$\theta = 1.38°$

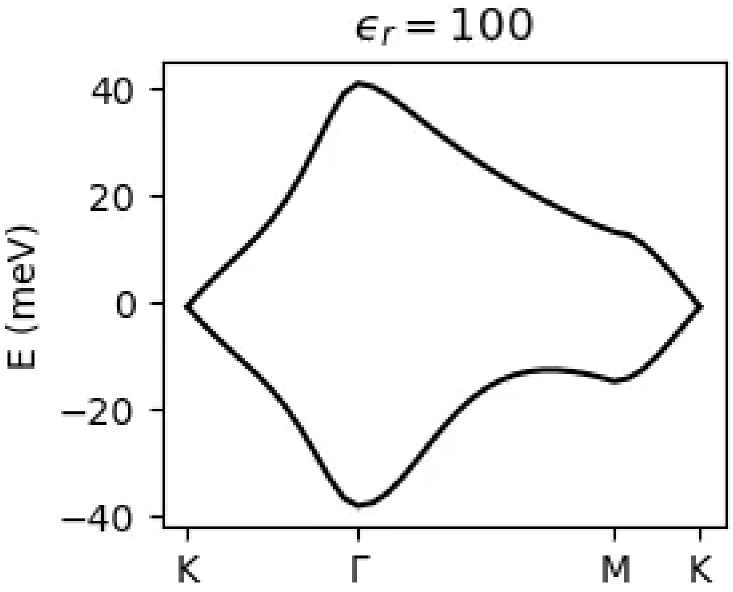

$$V_q = \frac{2\pi e^2}{\epsilon_r} \frac{\tanh(\frac{q\xi}{2})}{q}$$

$$\xi = L_m$$

$$\nu = -4$$

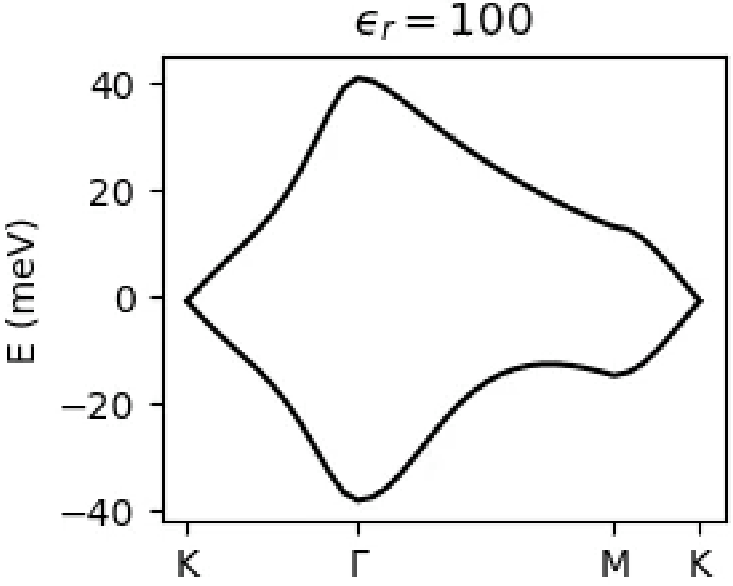

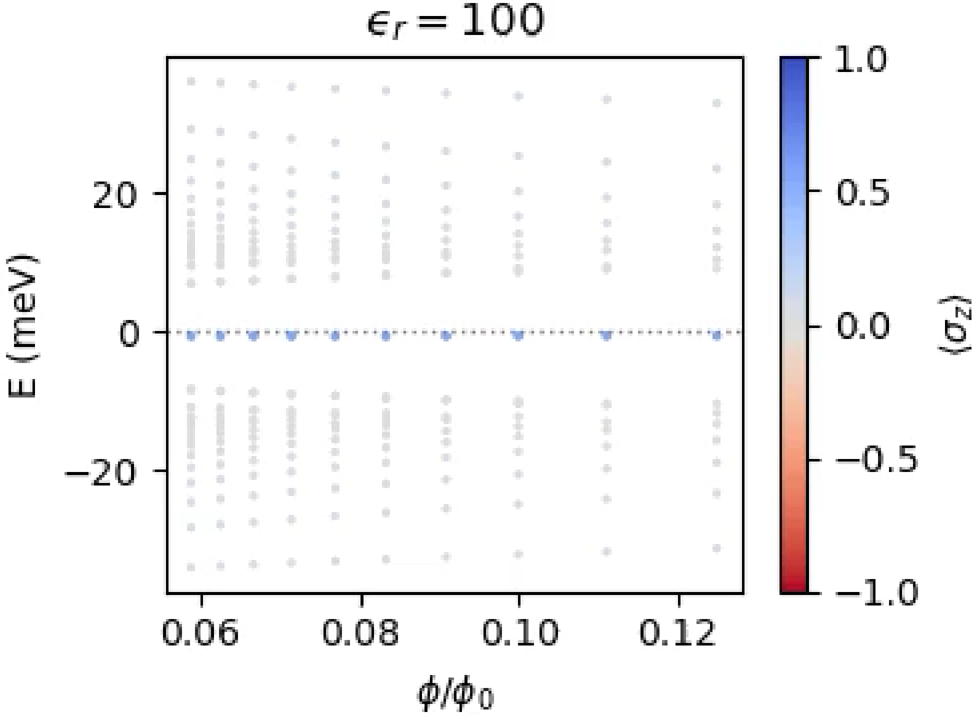

$$\theta = 1.38°$$

$$V_q = \frac{2\pi e^2}{\epsilon_r}\frac{\tanh(\frac{q\xi}{2})}{q}, \xi = L_m$$

X. Wang and OV unpublished

Correlated electron physics in the narrow bands: RG perspective

Stage 1:
Coulomb interaction and interlayer tunneling are **perturbative**

Stage 2:
Coulomb interaction **perturbative**, interlayer tunneling **non-perturbative**

Final step:
Coulomb interaction **non-perturbative**: strong coupling

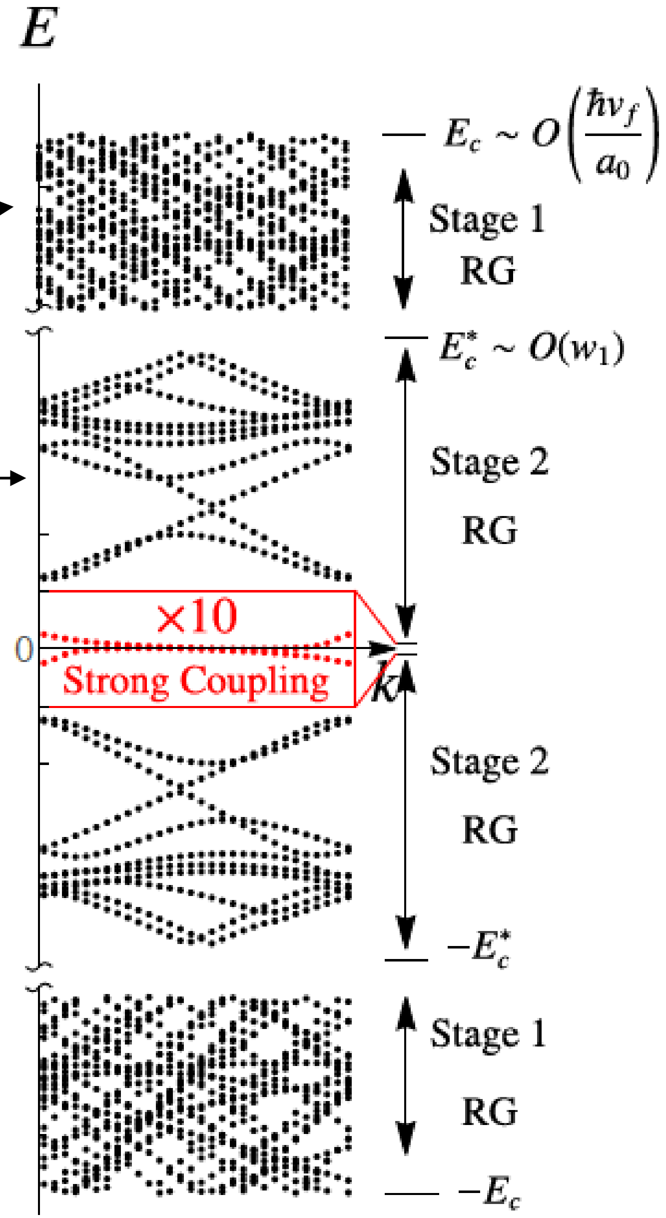

OV and J. Kang PRL2020

Exact (neutral) collective modes in the strong coupling limit at CNP

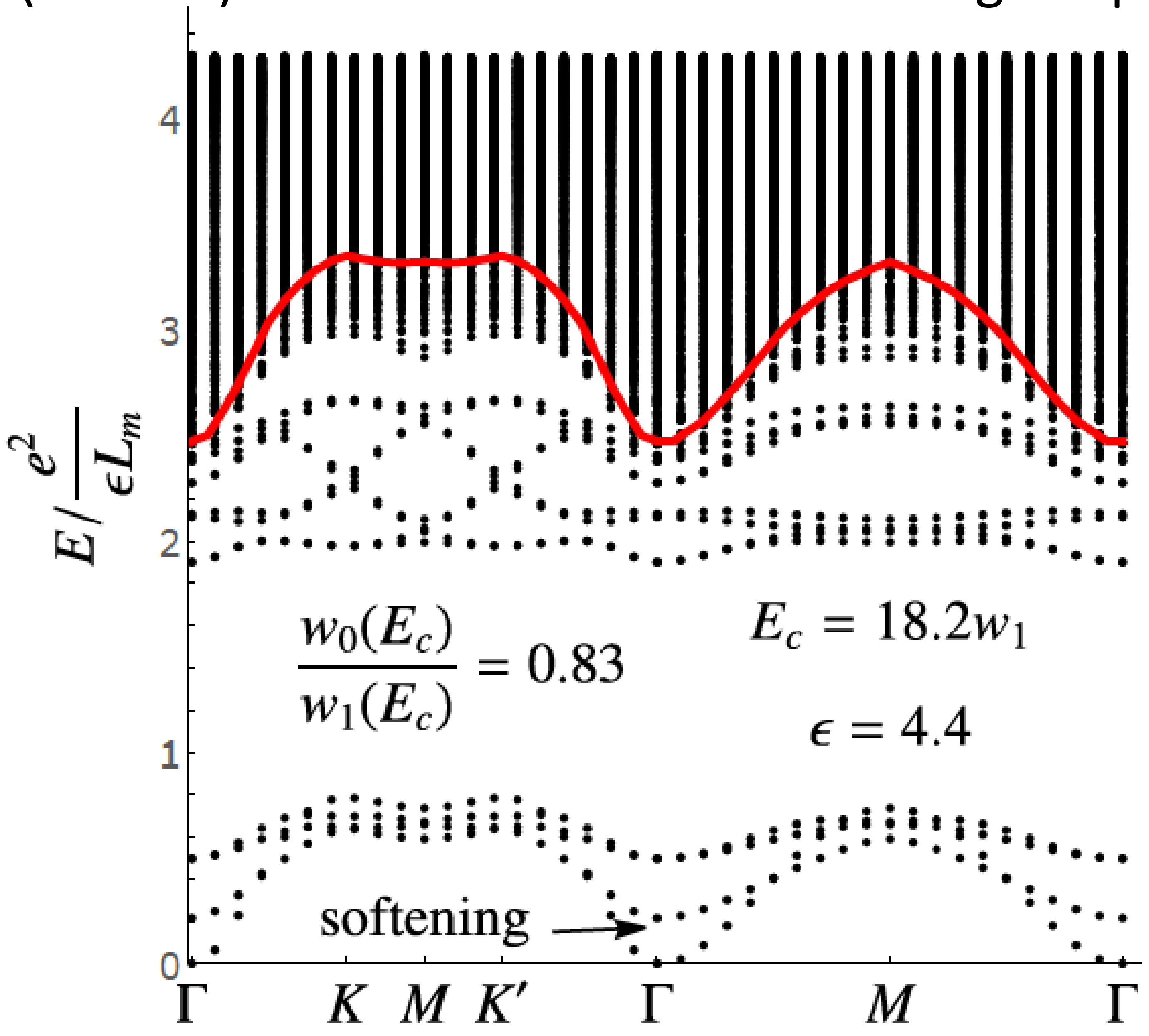

OV and Jian Kang, PRL 2020

Justification for the strong coupling approach

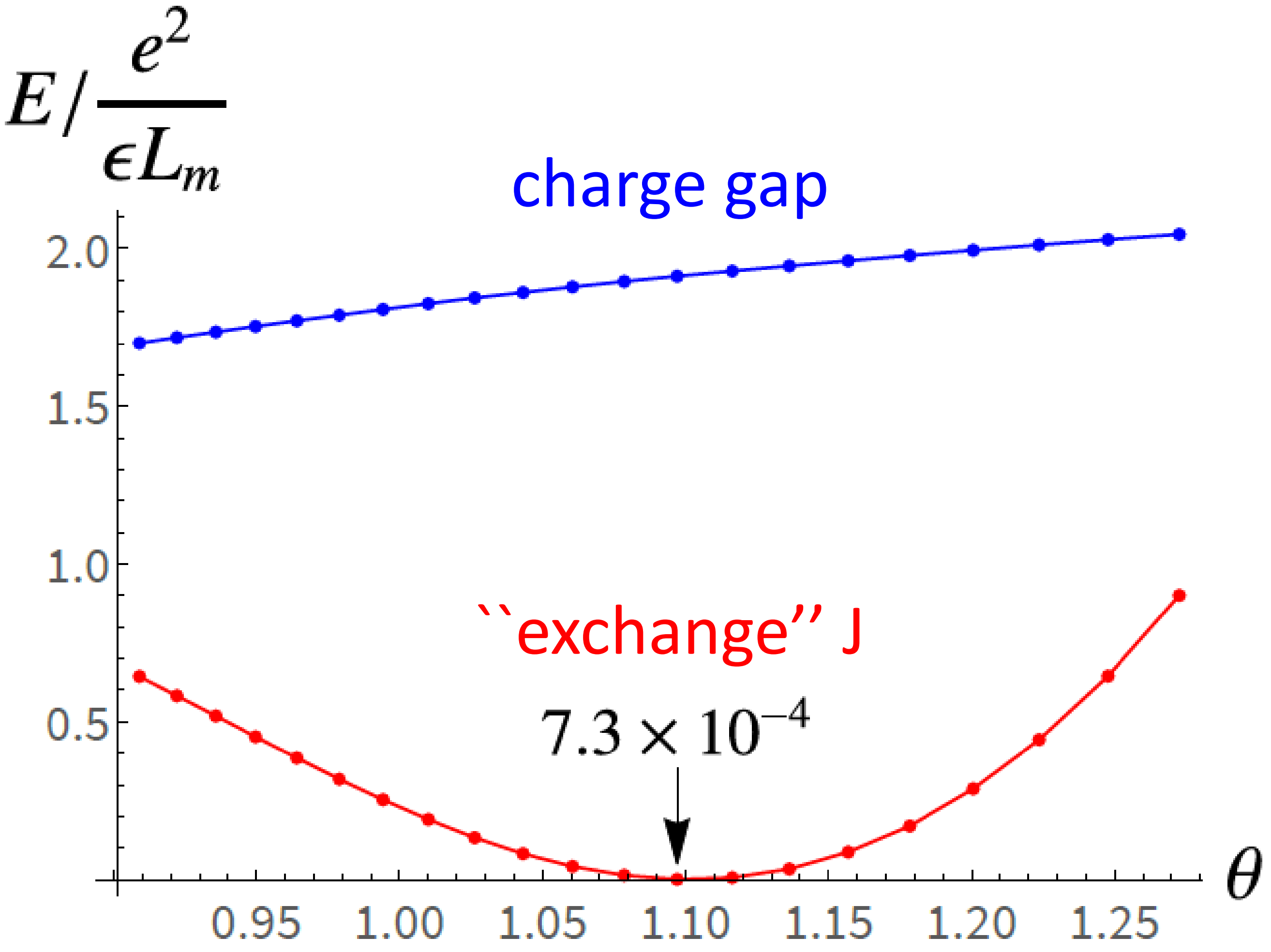

Jian Kang and OV (unpublished)